

# **INVESTIGATION OF SPACE BASED SOLID STATE COHERENT LIDAR**

**CONTRACT No. NCC8-146**

**Period of Performance:**

**October 2, 1997 – November 30, 2001**

**Submitted To:**

**NASA/MSFC  
Marshall Space Flight Center, AL 35812**

**Prepared By:**

**Farzin Amzajerdian**

**June 10, 2002**

**Center for Applied Optics  
University of Alabama In Huntsville  
Huntsville, AL 35899**

## ACKNOWLEDGMENTS

The author wishes to acknowledge the dedication and hard work of UAH/CAO Lidar team members: Timothy Blackwell, Dr. Bruce Peters, Dr. Patrick Reardon, Darrell Engelhaupt, Gary Spiers, Ye Li, and Deborah R. Bailey. This work was performed with close collaboration with NASA/MSFC scientists and engineers. The contributions and guidance of Roy Young and Tim Miller of NASA/MSFC were particularly instrumental in completion of this work. The author would also like to acknowledge the other members of The Center for Applied Optics at UAH, in particular, Dr. John O. Dimmock and Freya W. Bailey for their support and valuable assistance.

## TABLE OF CONTENT

Introduction	3
System Requirements	3
Operational And Performance Analyses	3
Sparcle Instrument Description	4
Optical Design And Analysis	5
Lidar Opto-Mechanical Design And Analysis	6
Telescope Integration And Test	7
Optical Subsystem Integration And Test	7
Optical Subsystem Requirements Of Major Components	8
Sparcle Optical Subsystem Design And Analyses	14
Optical Subsystem Interfaces	25
Telescope Fabrication Process	32
Sparcle Telescope Performance	38
Wide Bandwidth Heterodyne Photoreceiver	44
Optical Integration Plan	48
Appendix - Publications	52

## INTRODUCTION

This report describes the work performed under NASA contract NCC8-146, over the period of October 1, 1997 through March 31, 2001. Under this contract, UAH/CAO participated in defining and designing the SPace Readiness Coherent Lidar Experiment (SPARCLE) mission, and developed the instrument's optical subsystem. This work was performed in collaborative fashion with NASA/MSFC engineers at both UAH/CAO and NASA/MSFC facilities.

Earlier work by the UAH/CAO had produced a preliminary top-level system design for the Shuttle lidar instrument meeting the proposed mission performance requirements and the Space Shuttle Hitchhiker canister volume constraints. The UAH/CAO system design efforts had concentrated on the optical and mechanical designs of the instrument. The instrument electronics were also addressed, and the major electronic components and their interfaces defined. The instrument design concept was mainly based on the state of the transmitter and local oscillator laser development at NASA Langley Research Center and Jet Propulsion Laboratory, and utilized several lidar-related technologies that were either developed or evaluated by the NASA/MSFC and UAH/CAO scientists. UAH/CAO has developed a comprehensive coherent lidar numerical model capable of analyzing the performance of different instrument and mission concepts. This model uses the instrument configuration, atmospheric conditions and current velocity estimation theory to provide prediction of instrument performance during different phases of operation. This model can also optimize the design parameters of the instrument.

## SYSTEM REQUIREMENTS

UAH/CAO scientists and engineers actively participated in generating the system requirements document for the development of SPARCLE. Based on an instrument system concept developed earlier, the system design was analyzed in detail and the instrument optical and mechanical interfaces between various subsystems were specified. These subsystems include the transmitter laser, local oscillator laser, beam expanding telescope, scanner, transmitter/receiver optical train, beam misalignment compensator, and optical receiver. UAH/CAO team also participated in defining the instrument control and data processing electronics. This task was performed with close interaction with NASA/MSFC personnel to ensure that the system requirements are in compliance with the mission objectives and the Hitchhiker accommodation requirements.

## OPERATIONAL AND PERFORMANCE ANALYSES

Using a coherent lidar numerical model, the performance of the instrument was fully analyzed using different atmospheric models over different mission operating modes. The results of these analyses played a critical role in defining the requirements of the instrument electronic receiver, and data acquisition/processing system. These analyses were also critical for defining the instrument inertial reference data and pointing control requirements, command and control format specifications, and data down-link and up-link requirements. Furthermore, the operational and performance analyses helped the development of the mission operational modes.

The following charts describes the instrument design and top level specifications.

# SPARCLE INSTRUMENT DESCRIPTION

CAO

## Coherent Lidar Program

SPARCLE was a technology demonstration Shuttle mission with the following key objectives:

- Demonstrate coherent lidar technology capability of measuring atmospheric winds from space
- Validate coherent lidar wind measurement performance prediction models to confirm scalability to follow-on missions
- Characterize atmospheric winds, aerosol backscatter, wind turbulence, cloud effects, and surface reflectance for optimization of future science and operational missions



UAH

CAO

## Coherent Lidar Program

### UAH/CAO SPARCLE Responsibilities and Tasks

1. System Requirements
2. Operational and Performance Analyses
3. Optical Design and Analyses
4. Opt-mechanical Design and Analysis
5. Optical Characterization Facility at MSFC
6. Design, Analyses, Fabrication, and Test of Optical Subsystem:
  - Telescope
  - Scanner Element
  - Optical Window
  - Alignment Stages
7. Optical Subsystem Integration and Test
8. Wideband Heterodyne Photodetector
9. Mission Operational Plan
10. Instrument Optical Integration and Test

UAH

CAO

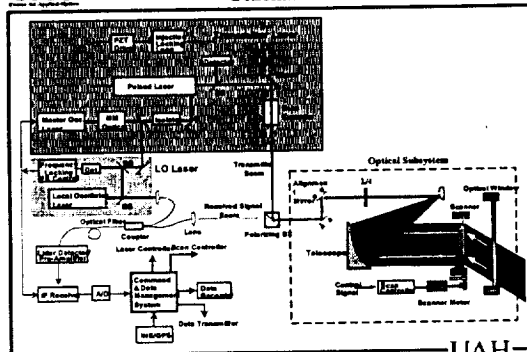
## SPARCLE System Specifications

Transmitter Laser Energy Per Pulse	100 mJ
Pulse Repetition Rate	6 Hz
Transmitter Pulse Width	200 nsec
Aperture Diameter	23.3 cm
Maximum Scanner Speed	45°/sec
Scan Full Angle	60°
Wavelength	2.05 $\mu$ m
Receiver Bandwidth	500 MHz
Trans./Rec. Boresight Alignment Budget	7.2 $\mu$ rad over pulse round trip time
Transmitter Beam Pointing Knowledge Accuracy	90 $\mu$ rad
Vertical Range Resolution	250 m
Optical Subsystem Efficiency	0.1
Receiver Subsystem Efficiency	0.25

UAH

CAO

## Space-based Coherent Lidar System Schematic



UAH

CAO

## SPARCLE Concept

- Developed system design concept and defined system specifications based on:
  - Existing hardware, designs, and technologies
    - Compact, Metallic Telescope
    - Silicon Wedge Scanner
    - 75  $\mu$ m diameter InGaAs detectors
    - LaRC, JPL, MSFC 2-micron Laser Development
  - Step-Stare Scanning
  - Simple Receiver Optical Train (No De-rotator or LAC)
  - Utilize NASA/Hitchhiker Program for Space Shuttle accommodation
- Performed System Performance and Operational Analyses

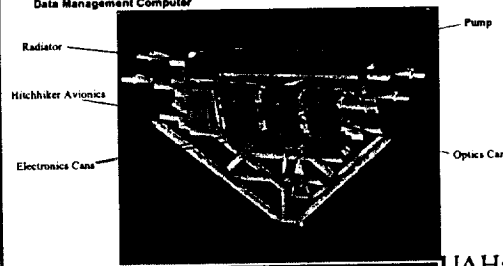


UAH

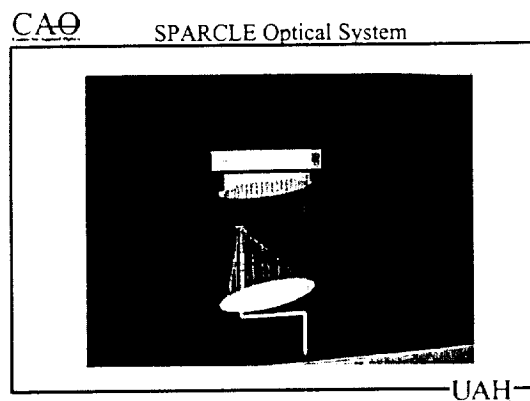
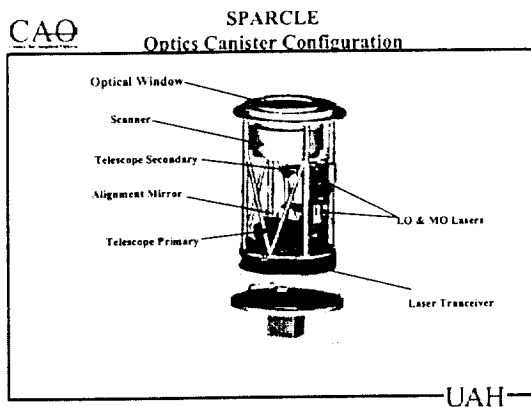
CAO

## SPARCLE Instrument

- SPARCLE instrument was designed to be housed in Hitchhiker Canisters:
  - The optics can contains the lidar transceiver, telescope, scan motor/encoder, and scan element
  - The electronics cans contain all associated electronics including the Command and Data Management Computer



UAH



## OPTICAL DESIGN AND ANALYSIS

The lidar optical subsystem has two major functions: first, it expands the laser beam and directs it toward the atmosphere in a conical scan pattern. Second, it receives the backscattered radiation, compensates for the scanner and spacecraft motions, and directs it toward the lidar photodetector to be effectively mixed with the optical local oscillator. The optical subsystem consists of a large-aperture telescope, a laser beam scanner, an optical window, and beam routing and conditioning optics.

Earlier work had produced a preliminary optical subsystem design based on the general requirements of a coherent lidar system considering the requirements specific to operating from a space-based platform such as long pulse round trip times, and the high platform velocity. Based on the UAH optical design and specifications, several prototype components of the optical subsystems had already been acquired by MSFC. These components include a wedge scanning element, a compact telescope (developed by UAH/CAO), polarizing beam splitter, laser beam collimator, quarter-wave plates, mirrors, lenses, and optical mounts.

Early in the project, a complete optical analysis was performed on the optical subsystem to specify the spatial properties of the transmitter and local oscillator beams. Optimization of these optical elements is particularly critical for efficient optical heterodyne detection of the return signal. A complete set of optical drawings was produced specifying all the instrument optical elements and their positions.

The optical window, providing environmental isolation for the SPARCLE instrument, was analyzed based on instrument performance and physical requirements such as effective optical transmission, and operating temperature and pressure. The optical window was to maintain a high degree of wavefront quality under a harsh space environment. The optical window required a high optical quality while under considerable stress caused by the extreme temperature and pressure differences between the sealed instrument canister and space. The instrument canister

was to operate at about 15°C and one half of the atmospheric pressure. Additional description of the window's opto-mechanical analysis is provided in the following section. Based on these analyses, a complete set of specifications (including both optical and mechanical specifications) for the optical window was generated.

After completion of the design and analysis of the beam routing and conditioning optical train, an end-to-end optical analysis was performed to quantify the performance of the instrument optical subsystem including the optical window, optical wedge scanner, and the telescope. This analysis included wavefront quality and polarization tracing for both transmitter and receiver optical paths.

### **LIDAR OPTO-MECHANICAL DESIGN AND ANALYSIS**

The opto-mechanical design and analysis of the optical telescope subsystem had two areas of emphasis: athermalization (maintaining optical alignment in the presence of thermal gradients) and dynamic load integrity (maintaining optical alignment through shuttle launch). The overall system performance was the driver on the opto-mechanical design. Therefore, the thermal and structural issues were investigated in parallel since both factors are linked. For example, component masses affect the thermal equilibrium of the optical system (larger masses take longer to come to equilibrium and allow for greater thermal gradients within the system) and dynamic stability (larger masses will aid in dampening vibrations) and as such, a change to improve one aspect could worsen another. Both of these areas are best addressed through a detailed thermal and structural finite element analysis. In order to maximize productivity by sharing analysis tools, UAH/CAO worked with Sverdrup, who had the task of performing a structural dynamic analysis of the canister, to enhance their NASTRAN model to include optical surfaces and increase the fidelity of the analysis. The areas that were investigation regarding the thermal and structural analysis are described below.

Temperature effects, most notably the potential for thermal irradiation effects through the window on the top of the canister containing the telescope optics, was investigated. The potential for cyclic heating and cooling as the space shuttle moves in and out of the earth's shadow may cause thermal gradients within the canister. These gradients and their variation over time may lead to differential expansions of the telescope elements creating slight defocus. This effect combined with the thermal gradient effects produced by the heat generated by the laser system and the scanner motor was a serious concern. The athermalization of the telescope design and optical structure by the use of similar materials with equivalent coefficients of thermal expansion and careful mounting of the optical components mitigated any deleterious defocus of the telescope. Therefore, a high fidelity structural finite element analysis incorporating thermal loading conditions was performed to predict the potential severity of the thermal gradient induced telescope misalignments in order to determine whether any special adjustment to the optical system was needed. That was not the case, since the telescope design incorporates all similar materials for the optical components and mounting structures resulting in a very athermal design.

Thermal shock of the optical system was not a concern except for the canister window. The window, once the canister lid is opened, would have been exposed to the thermal environment of

the shuttle bay and depending on the conditions, it may experience a rapid and significant temperature drop on the exterior surface. While this would not cause any concern to the window integrity, it could have caused some slight temporary "lensing" due to thermal gradients until the window reaches thermal equilibrium. This effect was shown to be minimal and did not impact the optical performance.

Static loading of the telescope and its support structure were not a concern to its operation in orbit, during assembly on the ground or during transport. The goal with regards to the structure was to reduce the weight while maintaining stiffness and increasing ease of assembly. The concern with regards to vibration and dynamic shock was that the system might experience severe part dislocations during shuttle launch that would permanently impair optical alignment of the more fragile components. This effect was evaluated through the use of finite element analysis incorporating the expected g-force acceleration that is present during launch. The large mass of the primary mirror works in the favor of the optical system because the mass will help to dampen vibration.

### **TELESCOPE INTEGRATION AND TEST**

Under an earlier NASA/MSFC sponsored work, a novel compact lidar telescope was designed and fabricated and its merits for a space-based coherent lidar system were demonstrated. The optical and mechanical designs of this telescope were upgraded for SPARCLE in order to further reduce the telescope mass while maintaining its alignment robustness in the space environment. These design upgrades were based on the results of the telescope performance measurements, analysis of heterodyne detection efficiency, and the analyses of the Shuttle vibration and thermal specifications.

The telescope structure design was modified in order to withstand the Shuttle launch load and temperature variations. Its optical design was modified to eliminate the telescope's tertiary element for easier integration with lidar transceiver. The tertiary component was used in the demonstrator unit to provide variable focusing and a wide field of view not needed for SPARCLE. A complete set of fabrication drawings were then generated and all the optical and mechanical components were fabricated. Upon completion of the telescope structure fabrication and testing of the mirrors, the telescope was assembled and characterized. Two telescope units were assembled and tested. The telescope characterization was performed at the 2-micron Receiver Characterization Facility, developed earlier by UAH/CAO personnel, and the 18" Zygo Interferometer at NASA/MSFC. The telescopes were then subjected to a series of thermal and vibration tested. The following sections describe the telescope design, fabrication process, assembly, performance, and environmental tests.

### **OPTICAL SUBSYSTEM INTEGRATION AND TEST**

UAH/CAO personnel were responsible for assembling the optical subsystem and characterizing its performance. The Optical subsystem included the optical window, scanner, telescope, beam routing and conditioning optics. For some of the characterization tests, a continuous wave (CW) 2-micron lasers was used to measure parameters such as transmission, polarization, and transmissive wavefront quality. A detailed test plan was produced for performing environmental



testing (thermal and vibration) and analyzing the results to predict the instrument operation in space.

## OPTICAL SUBSYSTEM

### REQUIREMENTS OF MAJOR COMPONENTS

The optical subsystem has two major functions: first, it expands the laser beam and directs it toward the atmosphere in a conical scan. Second, it receives the backscattered radiation and directs it toward the lidar photodetector to be effectively mixed with the optical local oscillator. The SPARCLE optical subsystem consists of a large-aperture telescope, a scanning element, an optical window, and beam routing/alignment optics. The optical layout of the optical subsystem, with the relative positions of its major components, is shown in figure 1.

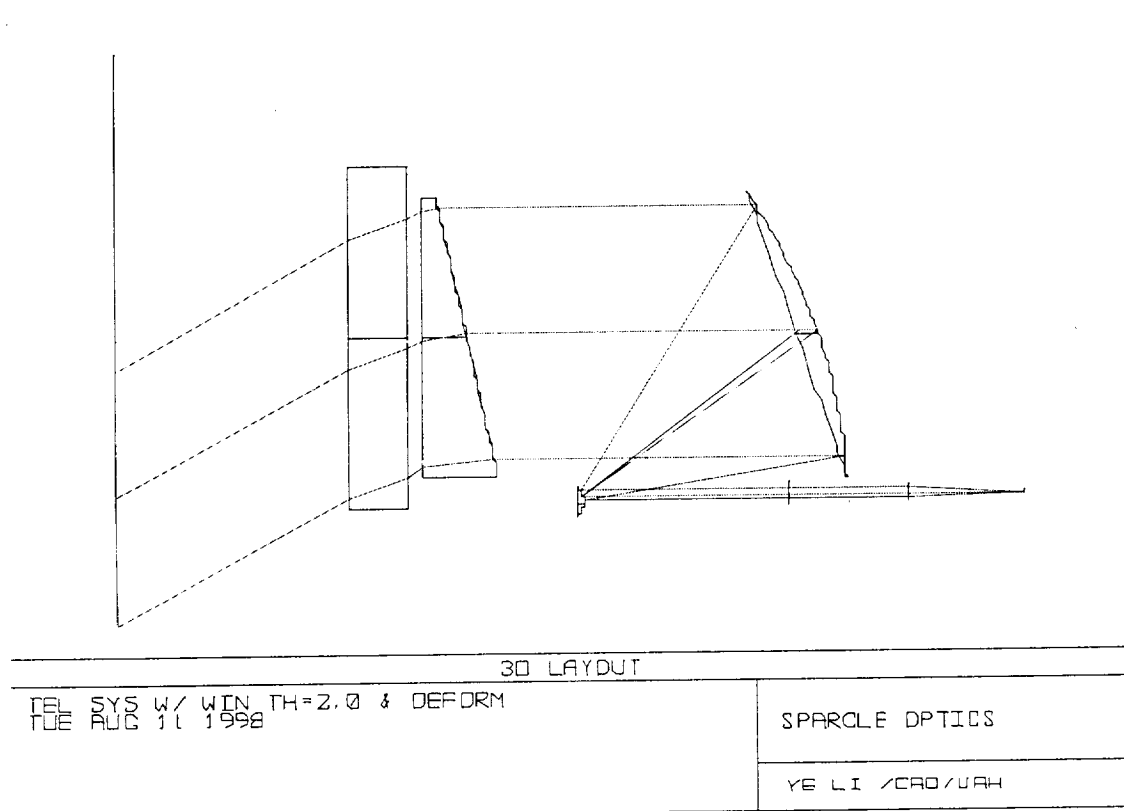


Figure 1. Optical Subsystem Layout

#### 1. Telescope

The Telescope is a compact, afocal beam expander used for both transmitting the laser beam and collecting the return radiation. The Telescope expand the transmitter beam from the transceiver subsystem and direct it toward the scanner. The Telescope shall accept linearly polarized light

from the transceiver subsystem and shall convert it to circular polarization. The Telescope shall also collect the reflected laser radiation, after passing through the optical window and the scanner, and compressed it to a small beam to be routed to the signal detector. The Telescope shall also convert the polarization of the received radiation to a linear polarization which is orthogonal to the polarization of transmitter beam generated by the transceiver subsystem.

## Requirements

Beam Expansion Ratio	25:1
Single Pass Wavefront Quality wavelength over full clear aperture	1/15 wave RMS at 2.0 $\mu\text{m}$
Single Pass Optical Transmission	0.85 at 2.0 $\mu\text{m}$ wavelength
Input Clear Aperture Diameter	0.92 centimeter
Output Clear Aperture Diameter	23.3 centimeter
Total Backscattering Coefficient	TBD
Vibrational Integrity	as per CARS/HHG-730-1503-07
Maximum Permitted Envelope	38 (dia.) x 43 (height) centimeters
Survivability Temperature	-40°C to 60°C
Operating Temperature	0°C to 25°C
Maximum Operating Temperature Gradient	8°C

## 2. Beam Routing/Alignment Optics

The Beam Routing/Alignment Optics shall provide for alignment at the interface between the optical subsystem and the transceiver subsystem. The Beam Routing/Alignment Optics consist of high reflective mirrors and alignment mounts. The Beam Routing/Alignment Optics shall provide the routing and pre-flight fine-alignment of the transmitter laser beam and return signal beam.

## Requirements

Single Pass Wavefront Quality wavelength over full clear aperture	1/30 wave RMS at 2.0 $\mu\text{m}$
Single Pass Optical Transmission	0.95
Polarization Efficiency	less than 4% difference in transmission between S & P polarization
Tilt range along x and y axes	> 0.1 rad
Tilt resolution	50 microradians
Effective Clear Aperture	1.5 cm
Maximum Diameter	5.0 cm
Survivability Temperature	-40 °C to 60 °C
Operating Temperature	0 °C to 25 °C

### 3. Scanner Optical Element

The Scanner Subsystem provides step-stare, conical scanning of the transmitted laser beam and receiver field of view. The scanner consists of a motor/encoder and an optical element. The motor/encoder shall provide the controlled rotation and stop of the optical element. The optical element is a silicon wedge which deflects the transmitted beam by 30 degrees. When the silicon wedge rotated about an axis perpendicular to one of its faces, it permits conical scanning of the lidar. The Scanner Subsystem shall mount to the top plate of the can at three attachment points. The specifications for the scanner motor/encoder, including its mechanical and electrical interfaces, have been defined in the Scanner Component Specification Document. The specifications for the scanner optical element are as following.

#### Optical Wedge Requirements

Material	Silicon
Deflection Angle	$30 \pm 1.0$ degrees
Wedge Angle	$11.7 \text{ deg.} \pm 10 \text{ min.}$
Thickness at Center of Substrate	37.785 mm
Surface Figure	1/60 wave RMS at $2.0 \text{ } \mu\text{m}$ or 1/6 wave p-v@0.633 micron on each of the two surfaces
Surface Quality	60-40 scratch-dig on each of the two surfaces
Polarization Efficiency	less than 5% difference in transmission between S & P polarization
Optical Transmission	0.9 at $2.0 \text{ } \mu\text{m}$ at required incident angle
Transmission Bandwidth	greater than 8 nm centered at 2051 nm for 30 degrees incidence angle on incidence on wedged surface
normal surface and 11.7 degrees	
Single Pass Wavefront Quality	1/30 wave RMS at $2.0 \text{ } \mu\text{m}$ over full clear aperture
Total Solar Reflection	greater than 65% integrated reflectance from 0.2 to 3.0 microns wavelength at normal and 75 deg. incident angles as defined in attachment (1). Solar reflection coating shall be applied to the top surface.
Totla IR Reflection	greater than 48% integrated

	reflectance over 7.0-20.0 microns region of spectrum at normal incidence as defined in attachment (2).
Clear Aperture Diameter	22.8±0.2 centimeter
Physical Diameter	24.71+0.00-0.06 centimeter
Edge Finish	Ground edge, break all sharp edges
Survivability Temperature	-40 °C to 60 °C
Operating Temperature	0 °C to 25 °C
Vibrational Integrity	as per CARS/HHG-730-1503-07

#### 4. Window

The window shall provide the separation between the vacuum and internal optic can. The Window permits the transmission of the laser pulse and reception of the reflected laser signal, respectively. It is mounted on the Top Plate and forms a vacuum seal to it.

Material	Fused Silica
Maximum Differential Pressure Deflection	less than 2.5 µm at the center of window due to 0.5 atm differential pressure
Parallelism of Surfaces	better than 1 min.
Surface Figure	1/60 wave RMS at 2.0 µm on each of the two surfaces
Surface Quality	60-40 scratch-dig on each of the two surfaces
Polarization Efficiency	less than 5% difference in transmission between S & P polarization
Optical Transmission	0.88 at 2.052 µm normal and 30 degrees incidence angles
Transmission Bandwidth	greater than 8 nm centered at 2051 Signle
Pass Wavefront Quality	1/30 wave RMS at 2.0 µm over full clear aperture
Total Solar Reflection	greater than 80% integrated reflectance from 0.2 to 3.0 microns wavelength at normal and 75 deg. incident angles as defined in attachment (1). Solar reflection coating shall be applied to either outer surface or both surfaces.
Totla IR Reflection	greater than 18% integrated reflectance over 7.0-20.0 microns

	region of spectrum at normal incidence as defined in attachment (2).
Homogeneity	less than $4 \times 10^{-6}$ variation in index of refraction
Relative Temperature Coefficient of Refractive Index	$10^{-6} \text{ K}^{-1}$
Clear Aperture Diameter	Greater than 29.79 centimeter
Substrate Diameter	31.385+000-0.1 centimeter
Substrate Edge Finish	Ground edge, break all sharp edges
Substrate Thickness	5.08+0.1-0.0 centimeter
Survivability Temperature	-40 °C to 60 °C
Operating Temperature	0 °C to 25 °C
Vibrational Integrity	as per CARS/HHG-730-1503-07

### **Definition of Integrated Solar Reflectance**

The integrated solar reflectance is defined by the following equation:

$$R_{\text{Solar}} = \frac{\int_{0.2}^{2.0} E(\lambda) \cdot R(\lambda) d\lambda}{\int_{0.2}^{2.0} E(\lambda) d\lambda}$$

where  $R_{\text{Solar}}$  is the solar reflectance per surface,  $R(\lambda)$  is the reflectance of the coating as a function of wavelength,  $\lambda$ , and  $E(\lambda)$  is the solar irradiance spectrum based on Plank's law with a black body radiation temperature of 5560 Kelvin,

$$E(\lambda) = \frac{A}{\lambda^5} \frac{1}{e^{B/\lambda} - 1},$$

where  $A$  is the radiation constant and  $B = 2.58775 \times 10^{-6} \text{ m}$ . The calculation of  $R_{\text{Solar}}$  can be approximated numerically by the following expression:

$$R_{\text{Solar}} = \frac{\sum_{\lambda_i} E(\lambda_i) \cdot R(\lambda_i)}{\sum_{\lambda_i} E(\lambda_i)},$$

$R_{\text{Solar}}$  shall be calculated with a wavelength resolution of no larger than 50 nm over the range of 0.2 to 3.0  $\mu\text{m}$ , i.e.,  $\lambda_{i+1} - \lambda_i \leq 50 \text{ nm}$ .

### Definition of Integrated IR Reflectance

The integrated IR reflectance is defined by the following equation:

$$R_{IR} = \frac{\int E(\lambda) \cdot R(\lambda) d\lambda}{\int E(\lambda) d\lambda}$$

where  $R_{IR}$  is the IR reflectance per surface,  $R(\lambda)$  is the reflectance of the coating as a function of wavelength,  $\lambda$ , and  $E(\lambda)$  is the IR irradiance spectrum based on Plank's law with a black body radiation temperature of 300 Kelvin,

$$E(\lambda) = \frac{A}{\lambda^5} \frac{1}{e^{B/\lambda} - 1},$$


where  $A$  is the radiation constant and  $B=4.79596 \times 10^{-5}$  m. The calculation of  $R_{IR}$  can be approximated numerically by the following expression:

$$R_{IR} = \frac{\sum_{\lambda_i} E(\lambda_i) \cdot R(\lambda_i)}{\sum_{\lambda_i} E(\lambda_i)},$$


$R_{IR}$  shall be calculated with a wavelength resolution of no larger than 50 nm over the range of 7.0 to 20.0  $\mu\text{m}$ , i.e.,  $\lambda_{i+1} - \lambda_i \leq 50$  nm.

# SPARCLE OPTICAL SUBSYSTEM




## Design and Analyses




### General Optical System Requirements




Output Clear Aperture Diameter	22.6 cm
Output Beam Diameter	18.5 cm $1/e^2$
Beam Expansion Ratio	25:1
Field Of View	80 $\mu$ rad
Wavefront Quality	1/10 Wave RMS
Optical Transmission	64%
Beam Pointing Stability	4 $\mu$ rad/3 msec
Beam Pointing Error	28 $\mu$ rad in nadir and azimuth
Polarization	10% diff. between S and P transmissions
Scan Angle	30 degrees
Maximum Scanner Speed	45°/sec
Maximum Permitted Envelope	38 (dia.) x 43 (height) cm
Survivability Temperature	-40C to 60C
Operating Temperature	0C to 25C
Operating Temperature Gradients	8C
Pressure	0.5 atm






### Beam Expanding Telescope



**SPARCLE telescope design was based on the prototype system**

- Modified optical and opto-mechanical designs to comply with the thermal environment of the Hitchhiker canister without a complex mechanical design
- Design modifications took advantage of relaxed requirements resulting from selection of step-stare over continuous scanning for SPARCLE
- Followed the same mirror fabrication method as before
- Telescope consists of two parabolic mirrors as opposed to earlier system that uses a parabolic primary mirror, hyperbolic secondary mirror, and a tertiary negative lens

Telescope design utilizes the experience and lessons learned from the fabrication and assembly of the demonstrator system

- Utilized optical measurements data to further optimize the optical design
- Incorporated alignment lessons into the opto-mechanical design
- Accommodated the thermal environment of the Optics canister
- Addressed the integration issues with the Transceiver

**Advantages Over the demonstrator system**

- Greater efficiency without lens
- No  $dn/dT$  effects from lens to defocus telescope
- Easier to align and test (Visible HeNe beam and ZYGO interferometer can be directly used)



**Optical Design Description**

- Off-axis two confocal parabola mirrors configuration
- Magnification = 25X
- Primary Aperture = 10" with 5.9" de-center
- Two mirrors spacing = 8.9" (225mm)
- Full field of view = 80  $^{\circ}$ rad
- Primary mirror F# = 0.9 of parent F# = 0.4
- Strehl Ratio = 99 %
- Wavefront Quality = better than  $\lambda/15$  RMS over all operational conditions in space
- Mirrors Surface Roughness = less than 50 Angstroms RMS





Design Attributes

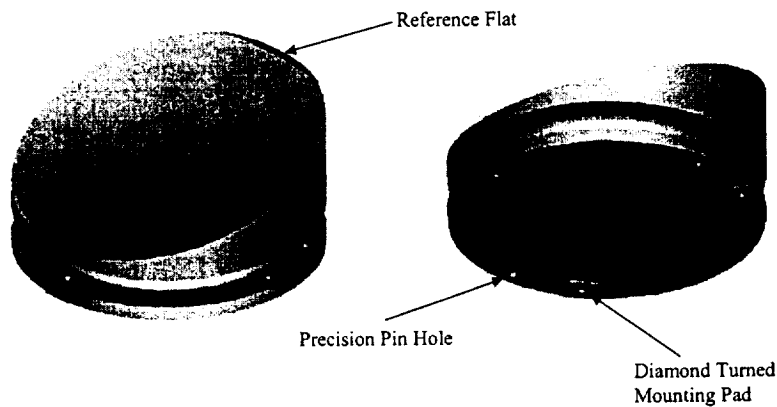
- Athermal Design
  - Telescope mirrors and support structure are all made of the same Aluminum material
  - The thermal expansion of the support structure are perfectly balanced by the changes in radius of curvature and thickness of the mirrors to maintain the system alignment
- Optical baseplate is diamond turned to serve as the optical reference surface for telescope assembly and alignment
- Built-in alignment and assembly reference surfaces into mirrors
- Precision machined alignment pin holes into the mirrors and optical baseplate for ease of assembly
- Two alignment mirrors with 5 degrees of freedom (total) for interfacing with the lidar transceiver



**SPARCLE**

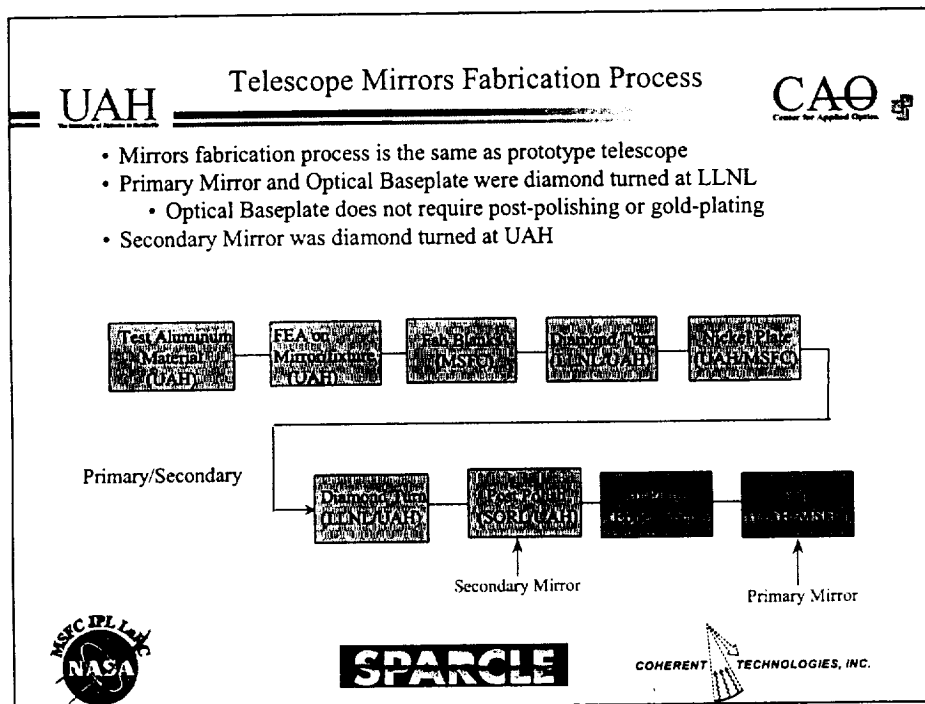
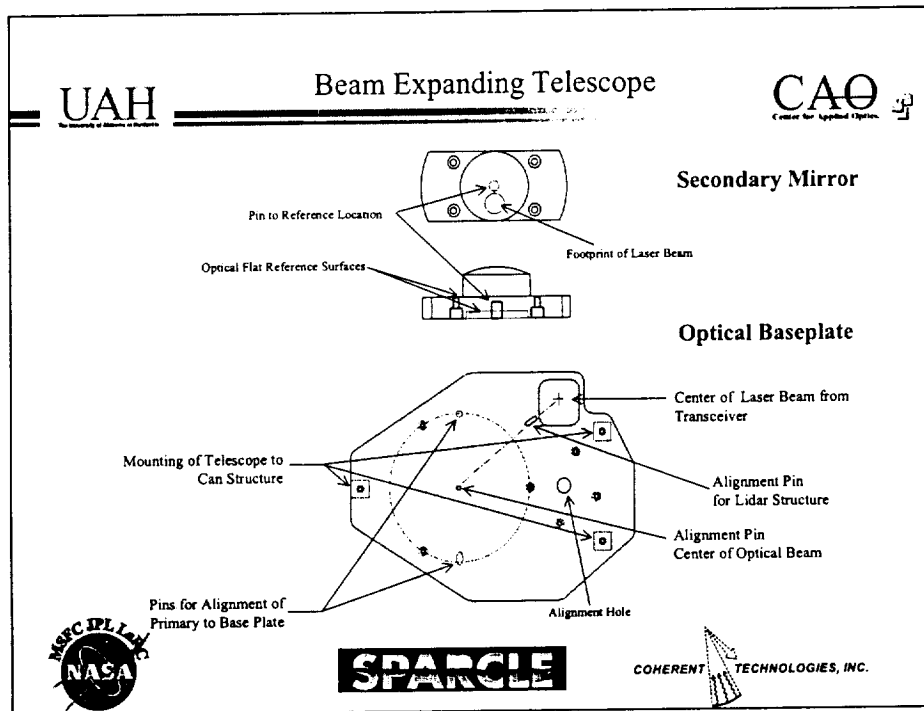


Primary Mirror



**SPARCLE**



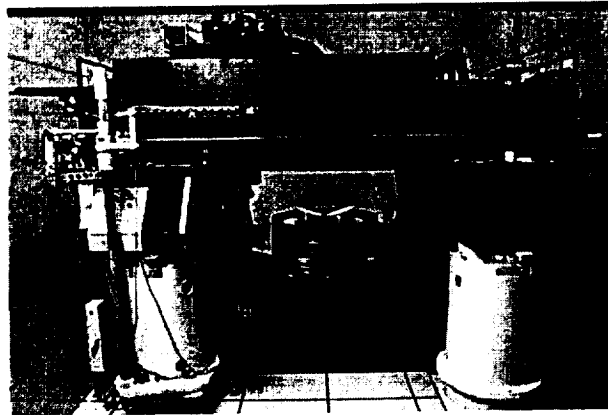


UAH

## Beam Expanding Telescope

CAO  
Center for Applied Optics

Primary Mirror on Large Optic Diamond Turning Machine (LODTM)  
at Lawrence Livermore National Laboratory



**SPARCLE**

COHERENT TECHNOLOGIES, INC.

UAH

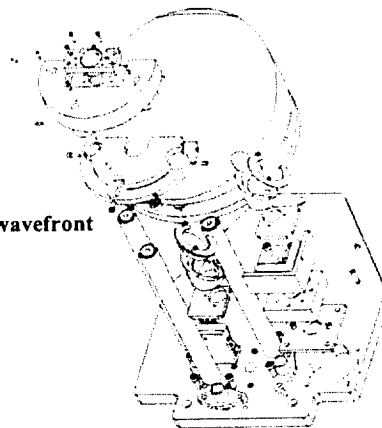
## Beam Expanding Telescope

CAO  
Center for Applied Optics

### Alignment Tolerances

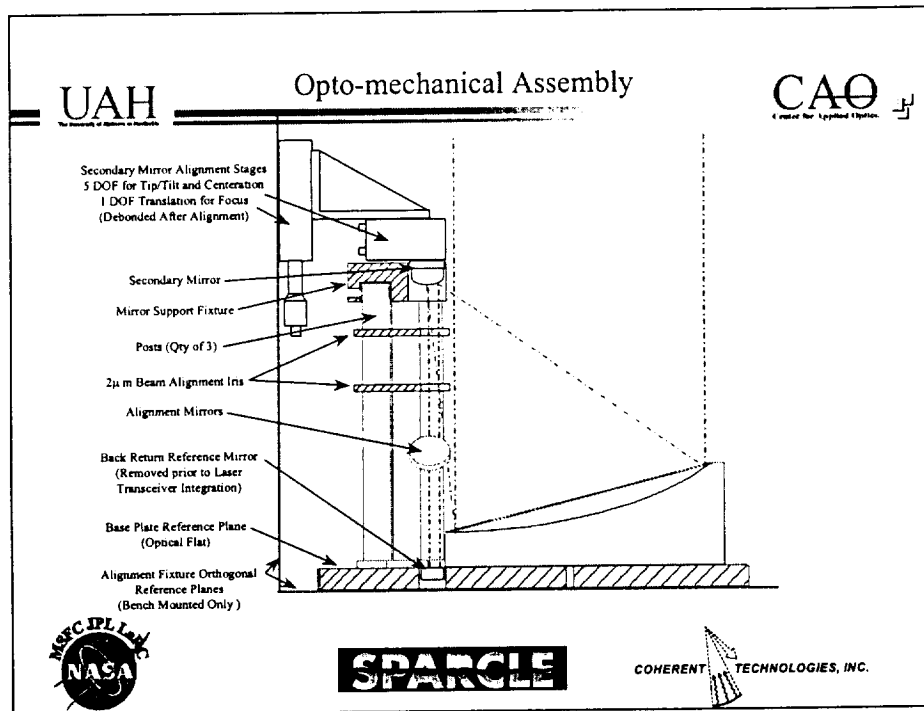
Some of alignment tolerances to achieve  $\lambda/20$  wavefront  
quality (Requirement  $\lambda/15$ )

mirrors spacing :	4.2 $\mu\text{m}$
x - de-center:	8.2 $\mu\text{m}$
y - de-center:	5.5 $\mu\text{m}$
x - tilt:	23 $\mu\text{rad}$
y - tilt:	35 $\mu\text{rad}$



**SPARCLE**

COHERENT TECHNOLOGIES, INC.



**UAH**

The University of Arizona Herndon

## Telescope Analyses

**CAO**

Center for Applied Optics

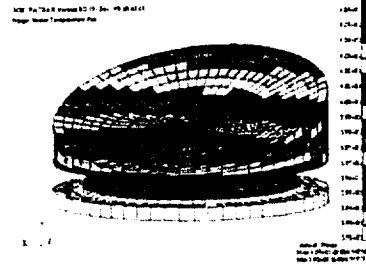
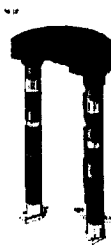
Performance Analysis	Design Case Strehl Ratio = 99 %
Fabrication Tolerance Analysis	Primary Conic Constant = $\pm 0.3 \mu\text{m}$ Secondary Conic Constant = $\pm 1.0 \mu\text{m}$
Alignment Tolerance Analysis	Mirrors Spacing = $4.2 \mu\text{m}$ De-center = $5.5 \mu\text{m}$ Primary Tilt = $22 \mu\text{rad}$
Thermal Analysis	Insensitive to 25 C bulk temperature variation Steady-state temperature gradient tolerance = 2 C
Structural and Dynamic Analyses	Withstands launch loads and Tolerates scanner-induced vibration during operation

*Telescope exceeds the wavefront quality requirement of  $\lambda/15$*

**SPARCLE**

**COHERENT TECHNOLOGIES, INC.**

## Thermal Analysis



# SPARCLE

**COHERENT TECHNOLOGIES, INC.**

Optical Wedge provides 30 degrees deflection angle for scanning the beam in a step-stare fashion

### Design Specifications

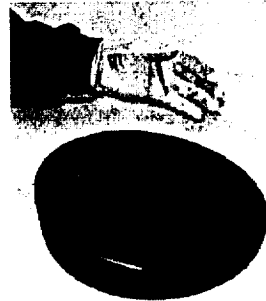
- |                                |  |
|--------------------------------|--|
| - Material                     | Silicon ( $n = 3.4508 @ 2.0518 \text{ :m}$ ) |
| - Wedge Angle                  | 11.7 deg. +/- 10 min.                        |
| - Thickness of center          | 38.495 mm                                    |
| - Polarization                 | Circular                                     |
| - Optical Transmission         | >0.9 at 2.051 mm at required incident angles |
| - Total Solar Reflection       | > 65%  |
| - Total IR Reflection          | > 48%  |
| - Transmissive Wavefront Error | 1/30 wave RMS at 2.051 $\mu\text{m}$         |
| - Clear aperture diameter      | 22.6 cm                                      |
| - Physical diameter            | 24.7 cm                                      |



# SPARCLE

COHERENT TECHNOLOGIES, INC.

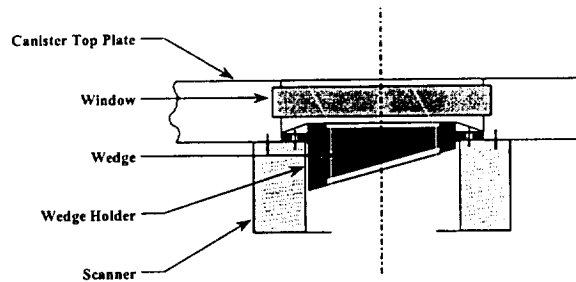
- Optical Wedge is rotated by a precision motor/encoder to provide a 30 degrees scanning pattern
- Flight unit design is almost identical to the prototype Silicon Wedge, that was acquired and characterized in FY 96
- Silicon Wedge design modifications for the flight unit are:
  - Physical diameter (Prototype wedge is 30 cm, SPARCLE requires 24.7 cm)
  - High solar and IR reflection coating for better thermal characteristics



- Optical Window provides the optical interface between pressurized optics canister and space
- Optical Window is made of a high quality Fused Silica with a multilayer coating for high transmission at 2 microns and high reflectivity over solar region of spectrum
- Dimensions: 12.75" Diameter, 2" thick
- Optical Window is sufficiently thick to avoid deflection due to half atm. of pressure difference between the canister and space
- Deflection of optical window can directly affect the optical wavefront quality and consequently the lidar performance



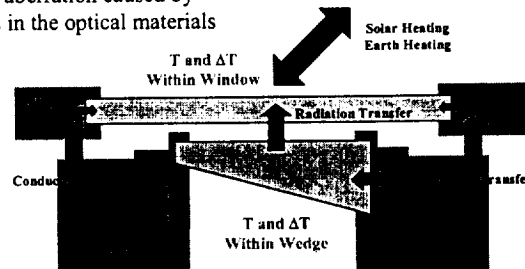
- Top surface of silicon wedge is 0.375 in. from bottom surface of window to minimize window size in top plate
- Window clear aperture: 11.5 in. diameter



SPARCLE



One of main issues concerning the optical wedge and window is the optical aberration caused by temperature gradients in the optical materials

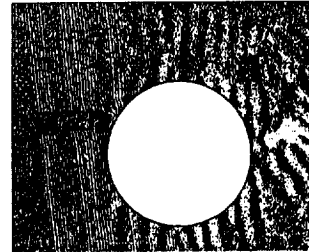
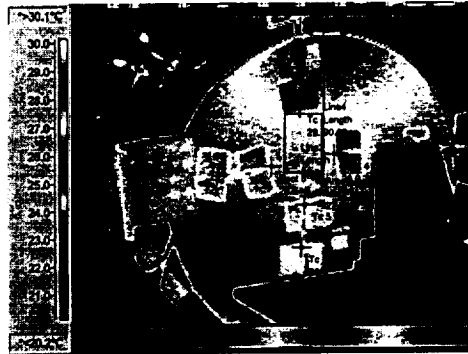


- Bulk temperature of wedge driven by conductive transfer of heat from scanner into wedge
- Gradients in wedge driven by temperature difference between wedge and window and the radiative coupling of wedge to window
- Bulk temperature of window driven by conductive coupling to top plate, solar heating, earth heating, and radiative coupling to wedge



SPARCLE





Interference pattern caused by a linear temperature gradient of about 1°C over 2.5"

Temperature profiles were determined by calibrating the IR measurements with the thermocouple data



**SPARCLE**



- The analysis of the laboratory data provided the wedge critical  $dn/dT$  parameter  
 $dn/dT = 163 \times 10^{-6}$  with standard deviation of  $6 \times 10^{-6}$
- Optical Modeling Result:
  - Aberration: 0.1 wave RMS for 0.1 degree C of temp. radial gradient
  - Pointing angle change: 40  $\mu$ rad/degree
- High performance coatings were employed to limit the temperature gradients within the wedge to less than 0.07 C

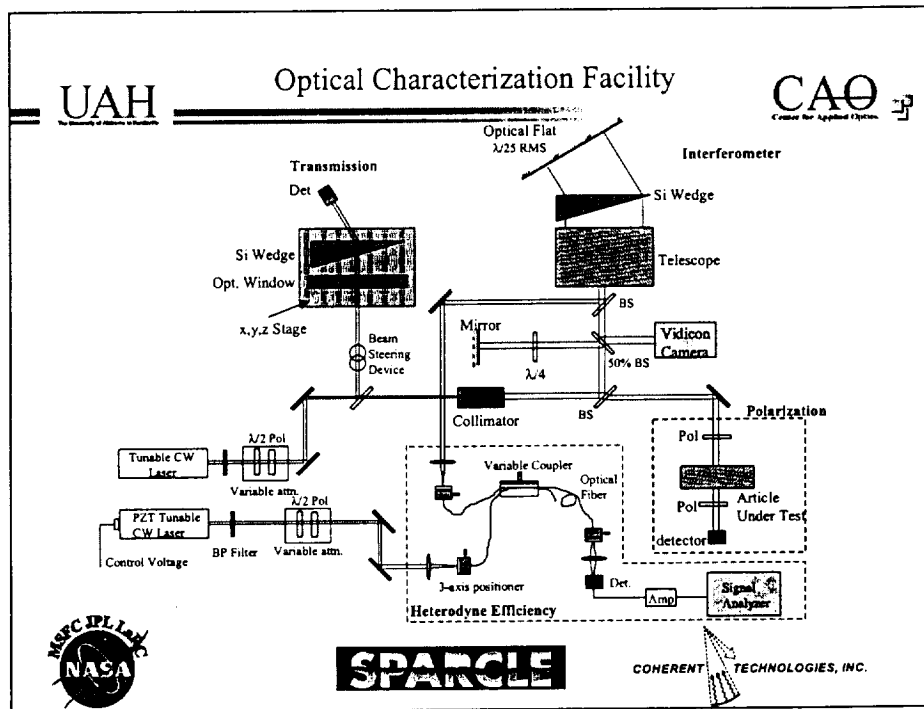
Surface	Reflection Coating
Window Outside	High Solar
Window Inside Surface	Relatively High IR
Wedge Top Surface	High Solar
Wedge Bottom Surface	High IR



**SPARCLE**







**UAH**

### Optical Characterization Facility

**CAO**  
Center for Applied Optics

An Optical Characterization Facility was developed at NASA/MSFC capable of testing lidar optical components and subsystems at the operating wavelength of 2-micron

- Interferometry (Wavefront Quality)
- Optical Throughput
- Polarization
- Beam Profilometry
- Dislocation planes

- This facility can also be used for measuring 2-micron detection devices and evaluating heterodyne receivers

NASA

**SPARCLE**

COHERENT TECHNOLOGIES, INC.

## OPTICAL SUBSYSTEM INTERFACES

### 1.0 SCOPE

This section covers all external optical and mechanical interfaces between the telescope and the Lidar transceiver subsystem, between the optical wedge and scanner subsystem, between the telescope to wedge subsystem, and between the window and top plate assembly. The Telescope and the Laser Transceiver shall mechanically interface to opposite sides of a support plate that is part of the Optics Canister internal structural skeletal system. The Wedge interfaces to the scanner through a wedge mounting assembly. The window interfaces into the top plate directly.

This document dictates all optical interconnections necessary to interface the Lidar transceiver to the telescope and the remaining optics in the optical subsystem. This document does not cover operational sequences or alignment/integration procedures.

### 1.1 Description of operation

A collimated laser beam is generated in the Laser Transceiver and transmitted through the Telescope/Laser Interface to the Telescope where it is expanded and directed along the system optical axis (the axis is at point  $(0, A_y)$  shown in Figure 1), through the wedge where it is diverted off axis, through the window and out of the canister and into the atmosphere. Returning laser energy is collected in reverse order by the telescope, collimated, and passed to the Transceiver through the Telescope/Laser Interface shown as a point with location  $(B_x, B_y)$  in Figure 1.

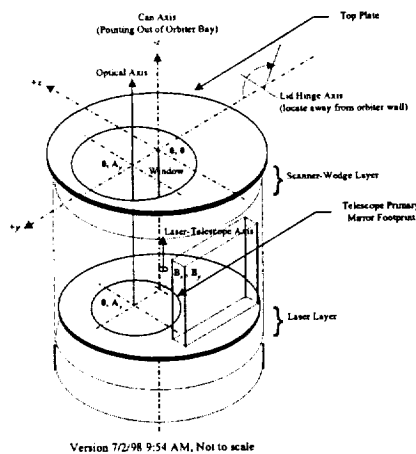


Figure 1. SPARCLE Coordinate System

A hole exists at the interface location to permit the passage of the laser beam in both directions. The hole is centered on the point  $(B_x, B_y)$ .

## 1.2 Definition of Interface Location

To attain the desired performance, alignment of the Telescope to the Laser Transceiver must be controlled, along with the optical quality of the beam at the Telescope/Laser Interface. The physical/mechanical interface between the laser transceiver and the telescope occurs at the top surface of the plate of the MSFC canister structural system. The optical interface is defined at this same plane; but, for convenience of measurement and verification of laser performance and convenience of measurement and verification of telescope optical performance, the optical characteristics may be measured at a different plane from the interface plane.

The telescope optical performance measurement may be made up to 20 cm below the interface plane as shown in Figure 1, prior to integration of either of the subsystems into the canister. The Lidar laser performance measurement may be made up to 20 cm below the interface plane as shown in Figure 1, prior to integration of either of the subsystems into the canister.

The optical axis of the system exiting the telescope is centered at location 0, Ax (0, 1.5235 in.) as shown and it is determined mechanically. The wedge and window diameters are oversized to permit ease of integration such that decenter or clipping of the beam will not be a problem. After completed assembly the optical system pointing direction shall be determined to increase pointing knowledge.

## 2.0 Lidar Transceiver to Telescope Interface

### 2.1 Optical Beam Characteristics

The output beam from the lidar transceiver into the optics subsystem/telescope is designed to have the following characteristics shown in Table 1.

**Table 1. Lidar Transceiver Output Beam Characteristics**

Beam Diameter	0.74 cm. +/-0.10 cm. at the $1/e^2$ intensity point
Half Angle Beam Divergence	Less than 350 $\mu$ rad
Beam Pointing Vector	Along -z - axis (optical axis) +/- 0.5° Located at (Bx, By) = 4.6, - 4.1 in.
Beam Pointing Vector Position Stability	Within 75 $\mu$ rad from 0-25° C.
Beam Pointing Angle Stability	Short Term: $\leq 25 \mu$ rad (1 sigma) pulse to pulse. Long Term: $\leq 50 \mu$ rad from 0-25 ° C ambient temperature.
Polarization	Circular to within 5% (intensity between two orthogonal polarizations to be less than 5%)
Beam Quality	$M^2$ value of less than 1.4

The input beam to the lidar transceiver from the optics subsystem has the following characteristics:

**Table 2. Telescope to Transceiver Beam Characteristics**

Beam Diameter	0.9 cm. +/-0.20 cm.
Beam Pointing Vector	Along -z - axis +/- 0.5° located at (Bx, By) 4.6, -4.1 in.
Polarization	Circular to within 5% (intensity between two orthogonal polarizations to be less than 5%)
Wavefront Quality	1/10 wave RMS at 2.0 microns wavelength

## 2.2 Electrical Interface

There are no electrical connections between the Telescope and the Transceiver.

## 2.3 Mechanical Interface

The centerline of the Telescope/Laser Interface Axis (Bx, By) shall be located at (4.600 in, -4.125 in) with a tolerance of  $\pm 0.001$  in at the start of the integration and alignment process. There shall be a hole in the support plate and the optics base plate at the same interface location. The hole shall be centered on this position to a tolerance of  $\pm 0.001$  in and have a dimension of 4.25 x 4.50 in. as shown in Figure 2.

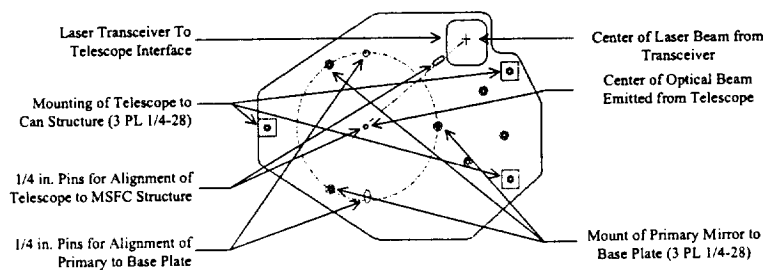


**Figure 2. Optics Base Plate**

The telescope interface to the support structure is entirely through the optics base plate shown in Figure 4. It rests on three pads that are in contact with the canister structure and is positioned by two 0.25 in. dowel pins and secured by three 0.25-28 UNF bolts, located as shown in the above figure.

At the time of integration, the telescope optical axis and the laser transceiver axis shall be roughly aligned to be parallel to the instrument optical axis (z-axis) as specified in the SRD. The two mirrors within the telescope shall be adjusted to achieve best possible alignment of the Telescope/Laser Interface axis after integration of the telescope and transceiver as shown in Figure 3. After alignment verification, the mirrors shall be fixed in place to prevent further adjustment or possible misalignment.

The mirrors shall provide sufficient translation and rotation to permit the direction of the laser beam from the transceiver onto the incident secondary mirror of the telescope.

### Alignment Mirrors

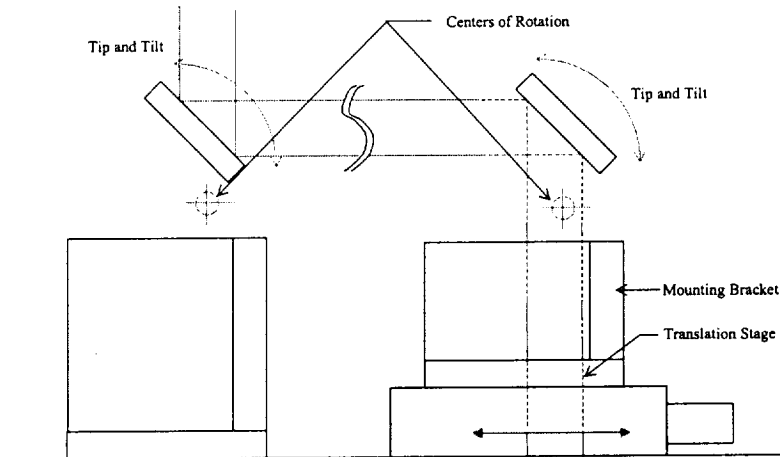


**Figure 3. Lidar Transceiver to Telescope Optical Alignment Mirrors**

After alignment, the Telescope/Laser Interface Axis shall meet or exceed short term and long term pointing stability criteria as specified in the SRD. The short term (3 msec duration) pointing stability of the laser beam axis at the Telescope/Laser Interface, defined as any additional motion or tilt occurring after final alignment and during operation, shall not exceed 25  $\mu$ rad. Any additional long term angular deviation shall not exceed 50  $\mu$ rad.

The xy-plane displacement stability of the Telescope/Laser Interface Axis, defined as the change in the relative location of the laser beam from the final aligned position, shall not exceed  $\pm 0.003$  in. ( $\pm 75 \mu$ m) during operation.

#### 2.4 Thermal Interfaces

There is no thermal interface between the transceiver and the telescope.

### 3.0 Optical Wedge to Scanner Interface

#### 3.1 Definition

The scanner unit is a component of the SPARCLE system. The scanner unit located within the Optics Canister consists of the motor/encoder (manufactured by BEI) the optical wedge (procured by NASA), and the wedge mounting fixture (procured by NASA). The purpose of the

scanner unit is to accurately measure and position the laser beam to fulfill mission requirements as specified in the SRD.

The purpose of the optical wedge is to divert the outgoing laser beam at an angle relative to the z-axis of the canister by a nominal  $30^\circ$  to create a conical sweeping of the beam.

### 3.2 *Electrical Interface*

The scanner unit in Optics Can shall have be interfaced to the scanner controller unit through a cable that supplies input power, incoming motor commands, outgoing data, and unit status. The cable shall have connectors and a pin configuration as specified in the Scanner Component Specification Document.

### 3.2 *Mechanical Interface*

The scanner shall be mounted to the top plate as detailed in the Scanner Component Specification Document and the Scanner ICD and shown in Figure 4 and Figure 57.

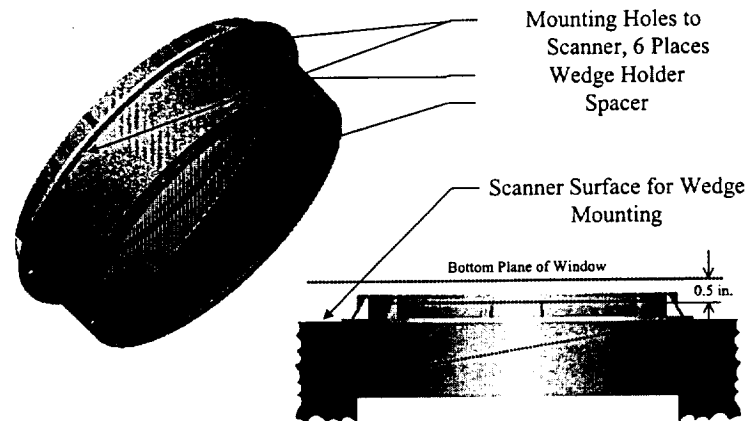


**Figure 4. Wedge Assembly Interface to Scanner Surface**

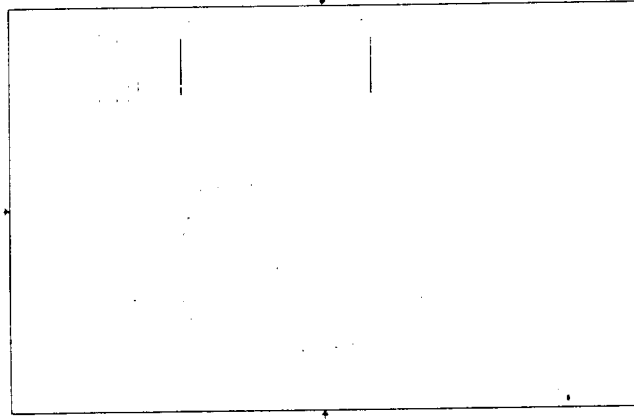


**Figure 5. Wedge Assembly**

The centerline of the scanner axis ( $0, A_y$ ) shall be located  $(0, 1.5235)$  with a tolerance of  $\pm 0.05$  in. at the start of the integration and alignment process. During alignment, shims shall be placed as appropriate to orient the scanner and wedge assembly axis to the optical axis of the experiment.

The wedge assembly consisting of the optical wedge, wedge bracket, and the fasteners shall be mounted to the scanner unit with six bolts as detailed in the Scanner Component Specification Document.

### **3.3 Optical Interface**

The top surface of the wedge, defined as the flat surface facing the window, and the bottom of the window, defined as the window surface inside can #1, shall be no more than 0.50 in. apart after integration and alignment.

## **4.0 Window to Top Plate Interface**

### **4.1 Definition**

Both the top plate and window are components of the SPARCLE Program. The top plate serves to hold the optical window as specified. The window (procured by NASA) shall mechanically interface to the top plate (fabricated by NASA) through a window mounting fixture or ring (Figure 6).

### **4.2 Electrical Interface**

There are no electrical connections between the window and the top plate.

### 4.3 Mechanical Interface

The window shall be offset from the can centerline and shall be centered on the optical axis, (0,  $A_y$ ) located at (0.0, 1.5235 in) with a tolerance of  $\pm 0.05$  in. The angular deviation of the window optical axis, defined as the difference between the normal to the top surface of the window located at its center from the instrument optical axis, shall not exceed TBD  $\mu$ rad at the time of assembly. Any additional angular deviation (either static, transient or dynamic) shall not exceed TBD  $\mu$ rad during the operation, transportation, or storage, of the experiment.

The xy-plane displacement of the window optical axis, defined as the in-plane difference between the location of the normal to the top surface of the window located at its center from the location of the instrument optical axis, shall not exceed 0.02 in. after assembly or during operation, transportation, or storage, of the experiment. The out of plane displacement of the window, defined as pure piston motion along the z-axis, shall not exceed 0.10 in. after assembly or during operation, transportation, or storage, of the experiment. The magnitude of the deformation of the window, defined as the difference between the center and the edge of the window, when integrated into the top plate and under operational conditions shall not exceed 0.00016 in. (4  $\mu$ m).

### 4.4 Optical Interface

The top plate shall accommodate a window of fused silica with a thickness of 2.0 in. The window once integrated into the top plate shall have a minimum clear aperture diameter of 11.5 in. with no obstructions within this clear aperture during operation. The top plate shall accommodate the 12.25 in. outside edge diameter of the window. The top plate and window mounting fixture shall include an elastic seal that will maintain the integrity of the environment within the can and prevent the window from fracturing when exposed to space under the defined operational temperatures and pressures. The window mounting fixture will withstand launch loads without fracturing the window. The window mounting fixture shall induce no more than TBD waves of stress induced optical birefringence within the window.

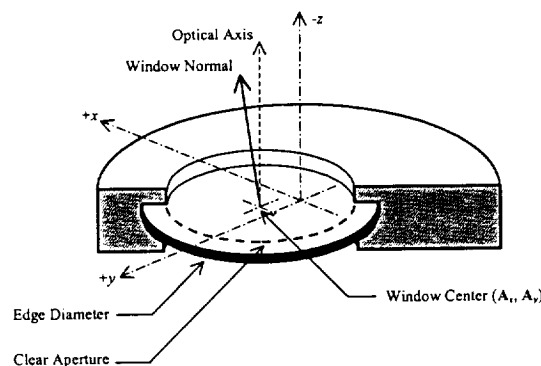


Figure 6. Window to Top Plate Interface

The window seat, defined as the surface of the top plate that is in contact with the window, shall be sufficiently clean of machining residue, burs, particulates, and sharp edges so as not to stress



or fracture the window when assembled. The seat shall incorporate a gasket material with suitable elasticity to create an environmental seal while still maintaining window positioning tolerances over the specified loads, pressures, and temperatures.

## Telescope Fabrication Process

### 1. PRIMARY MIRROR

#### Specification and Requirements:

Substrate Material	Aluminum alloy 6061-T6
Plated material	Electroless Nickel with 11% of Phosphor by weight
Mass	= 8.0 kg
Radius of curvature	= 468.750 mm (Concave)
Conic Constant	= -1.00000 (Paraboloid)
Physical Aperture	= 260 mm
Optical Aperture	= 240 mm
Off-axis value	= 150 mm (center of aperture to optical axis)
Surface Figure	= $\lambda/4$ peak - valley @633 nm wavelength
Surface Finish	= 30 A - 50 A RMS
Surface Quality	= 60-40 (scratch and dig)
Surface Coating	= Gold
Reflectivity	= 98.5% @ 2.0 $\mu\text{m}$

#### 1.1 Design of mirror blank

The light weighted mirror blank was designed based on the structural analyses. The machining drawings were finalized based on finite element analysis of diamond turning machine fixture. Two mirror blanks were machined at MSFC/EH or a selected machine shop. A 1" and a 12" Diameter witness samples of blank material from vendor were inspected and tested to ensure that it would produce the parts with sufficient optical quality. Since the primary mirror has the shape of off-axis parabola, two mirrors were needed for balancing during diamond turning of surfaces. One of the mirrors was used for as spare to the flight unit.

#### 1.2 Design of the fixtures of diamond turning machine

The fixtures serve as the interface of mirrors and diamond turning machine for completing the optical fabrication with single-point diamond turning machine. The detail design of the fixture was completed with the collaborate with the Lawrence Livermore National Laboratory (LLNL) engineers.

#### 1.3 Rough machining and heat treatment of mirrors

The mirror blanks and fixtures was rough machined at selected machine shops. The mirror blanks were heat treated and thermally cycled with liquid nitrogen and boiling water for stress relief and thermal stabilization at UAH/CAO.

#### **1.4 Diamond turning of aluminum primary mirror**

The Large-Optics Diamond-Turning Machine (LODTM) at LLNL was used for fabricating the parabolic primary mirrors. LODTM is a well-characterized machine capable of satisfying the figure accuracy requirement of the primary mirror.

#### **1.5 Optical Testing**

The 18" diameter ZYGO interferometer at MSFC/EB52 was utilized for testing the figure accuracy. The mounting structure and concave retro-reflector were designed and built testing of the mirrors. The surface finish was measured by WYKO TOPO -3D profiler.

#### **1.6 Electroless nickel plating**

The aluminum mirrors were plated with electroless nickel with 11% phosphor by weight at MSFC/EH Lab. A minimum of 0.005" of nickel plating thickness needed for final diamond turning and polishing. The heat treatment was required for good adhesion (baking for 4 hours at 275°F).

#### **1.7 Final diamond turning of nickel surface of the mirrors**

The nickel plated mirrors were diamond turned again to the required surface finish by LODTM at LLNL. The surface finish better than 150 Å RMS was achieved at this step. The surface figure accuracy of  $\lambda/4$  peak-valley at HeNe wavelength was achieved after this diamond turning.

#### **1.8 Testing and Post-polishing of diamond turned mirrors**

The diamond turned mirrors were polished on the polishing machine at SORL to get rid of the diamond turning grooves, and to achieve the surface finish of 30 Å - 50 Å. A ZYGO interferometer set-up was used to monitor the surface figure changes. The surface figure of  $\lambda/4$  p-v at HeNe for the finish mirror need to be achieved. This surface figure gives about  $\lambda/22$  of the RMS wavefront error of the primary mirror at 2.0  $\mu\text{m}$  wavelength.

#### **1.9 Gold plating of the post-polished mirrors**

The post-polished mirrors were sent to EPNER Technology, New York for gold plating to increase the reflectivity of the mirror. The reflectivity of better than 98.5% of the mirror surface were achieved at 2.0  $\mu\text{m}$  wavelength. A coupon of 1" diameter mirror was fabricated with each mirror for gold plating. The gold plated coupons were used for reflectivity and ellipsometry measurements.

## **2. SECONDARY MIRROR**

### **Specification and Requirements:**

Substrate Material	Aluminum alloy 6061-T6
Plated material	Electroless Nickel with 11% of Phosphor by weight
Mass	= 20g
Radius of Curvature	= 18.750mm (Convex)
Conic Constant	= -1.00000 mm (paraboloid)

Physical Aperture	= 32 mm
Optical aperture	= 22 mm (10 mm dia. at off-axis of 6 mm will be used for imaging. The whole symmetric mirror will be fabricated for easy diamond turning, polishing and alignment mounting)
Surface Figure	= $\lambda/4$ p-v @ 633 nm
Surface Finish	= 15 - 20A RMS
Surface Quality	= 60-40 (scratch and dig)
Surface coating	= Gold
Reflectivity	= 99% @ 2.0 $\mu$ m wavelength

### **2.1 Design of the blank of secondary mirror**

The secondary mirror blank was designed based on the telescope optical design and the diamond turning machine dynamics characteristics. The secondary mirror blank design also addresses the telescope integration and alignment issues. The rough machining drawings for producing the mirror blank were generated. Two secondary mirror blanks were fabricated at selected machine shops. The material of aluminum alloy used for this mirror was the same to the primary mirror.

### **2.2 Design of the fixture of diamond turning machine**

The design drawings for the diamond turning fixture was updated to be compatible with vacuum chuck of diamond turning machine. The fixture was machined with the blank of the mirror by machine shop based on the mechanical drawings.

### **2.3 Diamond turning**

After heat-treatment of stress relief and thermal stabilization, the aluminum mirror blank were fabricated on the Pneumo ultra2000 diamond turning machine at UAH/CAO based on optical design specification. The surface finish of better than 50A RMS can be expected at this step. The surface figure of better than  $\lambda/4$  at HeNe wavelength was achieved.

#### **2.4 Optical testing**

The surface finish was tested by WYKO TOPO-3D profilometer. The Taly-surf profiler was then used to directly test the figure error of the mirror.

#### **2.4 Electroless nickel plating**

The diamond turned aluminum secondary mirrors were electroless nickel plated at MSFC/EH Lab along with the primary mirrors. The thickness of the nickel plating is 0.005". Heat-treatment was needed after plating for a good adhesion (baking for 4 hours at 275°F).

#### **2.5 Final diamond turning**

The nickel plated mirrors were diamond turned again to the final surface finish requirements. The surface finish of better than 80A RMS was achieved using the UAH machine. The surface figure had to be controlled to better than  $\lambda/4$  at HeNe wavelength.

#### **2.6 Post-polishing of diamond turned mirror**

The final diamond turned mirrors were polished at SORL to surface roughness of better than 20 A RMS.

#### **2.7 Final optical testing of the mirror**

The final diamond turned mirror were tested and satisfied the specification.

#### **2.8 Gold plating of the mirrors**

The finished mirrors were sent to EPNER Technology for high reflectivity of gold plating.

### **3. OPTICS BASEPLATE**

The optics baseplate, that holds the primary mirror and the support posts for the secondary assembly, were also diamond turned. The baseplate was fabricated using the same Aluminum material as the mirrors.

#### **3.1 Design of optics baseplate blank**

The optics baseplate blank was designed based on the telescope optical design. Several features were incorporated into the optics baseplate design to facilitate the telescope integration and alignment procedures. The optics baseplate rough machining was performed at a selected machine shop.

#### **3.2 Design of the fixture of diamond turning machine**

The design drawings for the diamond turning fixture were generated to provide the interface between the baseplate blank and the LLNL LODTM. The fixture was machined at the same time as the primary mirror fixture.

#### **3.3 Diamond turning**

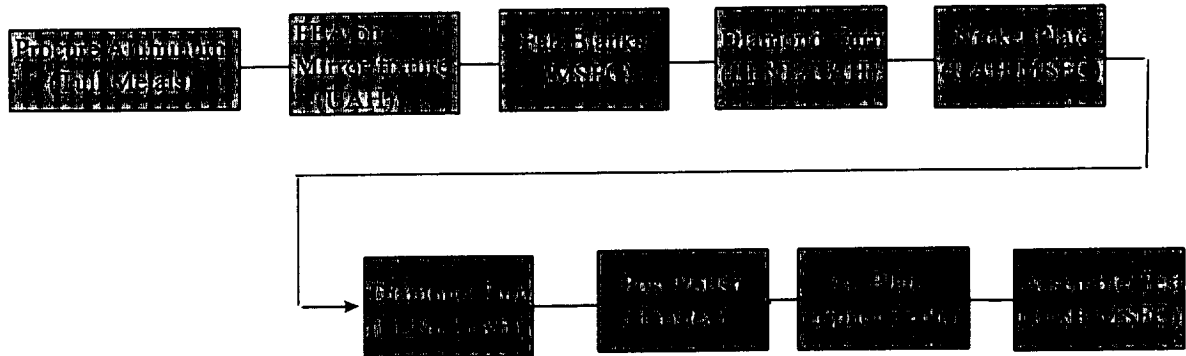
After heat-treatment of stress relief and thermal stabilization, the optics baseplate blank was fabricated at LLNL. The surface finish of better than 100 A RMS and surface figure of  $2\lambda$  at HeNe wavelength was expected after diamond turning.

### 3.4 Optical testing

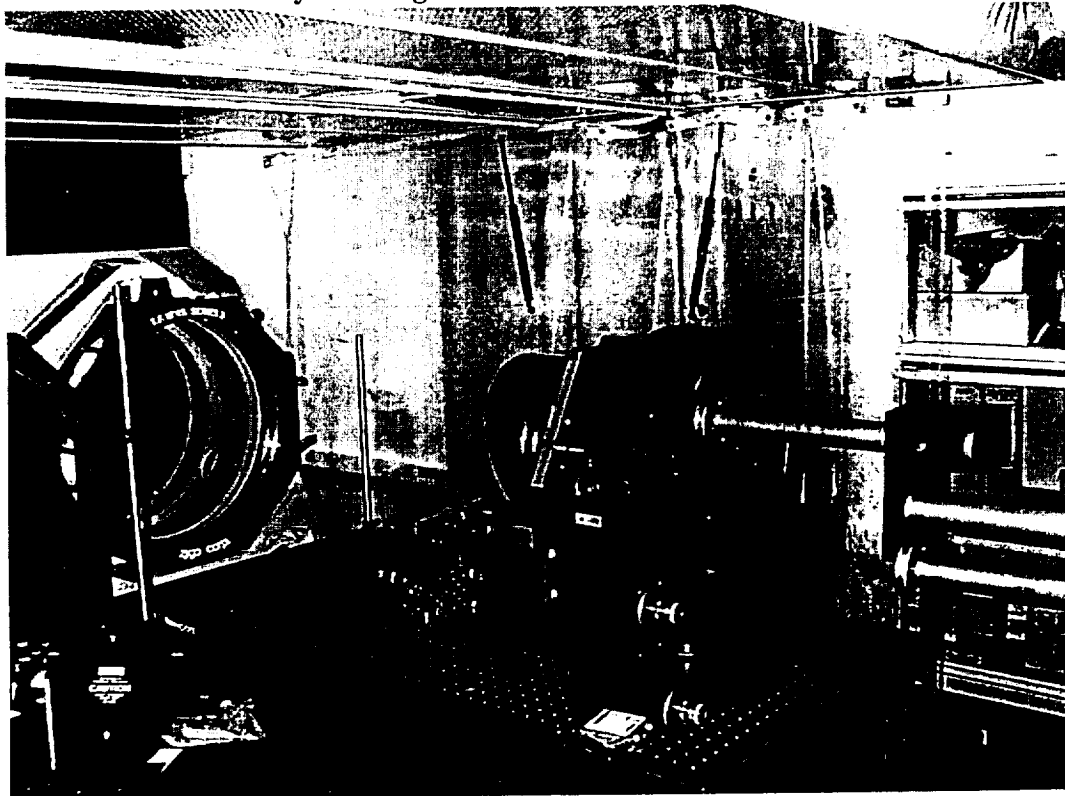
The surface finish was tested by WYKO TOPO-3D profilometer. The surface figure was tested by ZYGO interferometer.

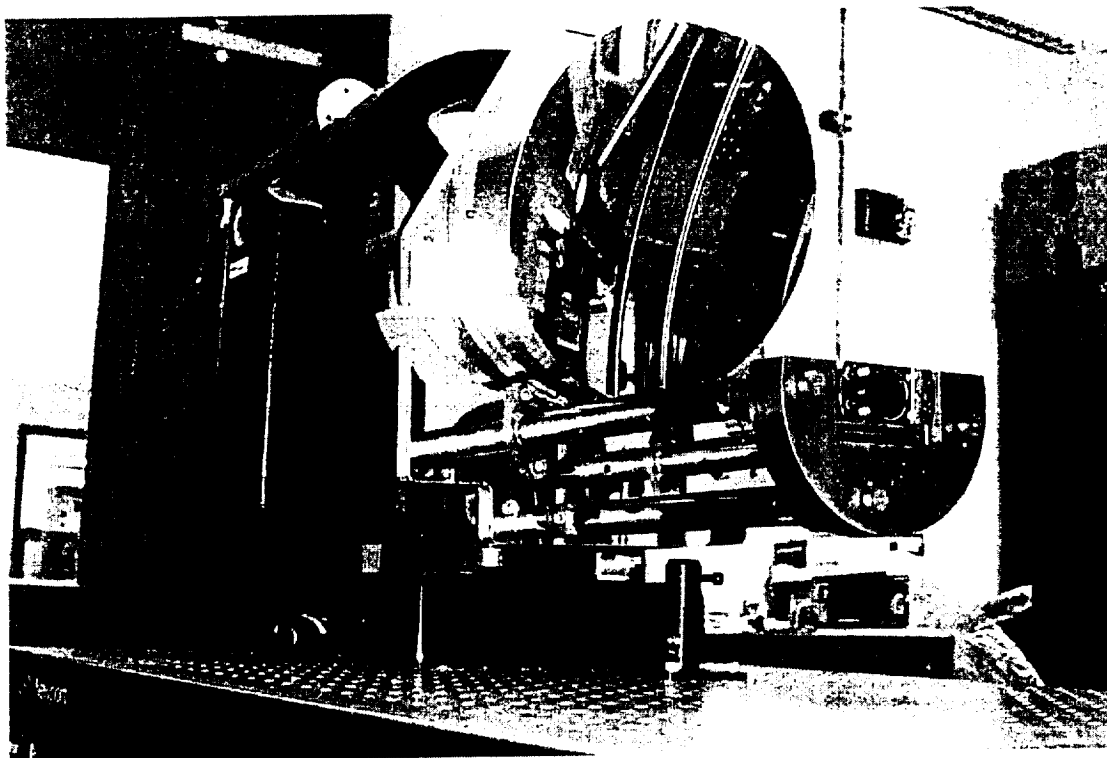
The diagram below summarizes the telescope primary and secondary mirrors fabrication process.

#### Primary/Secondary Mirrors Fabrication Plan



#### Assembly and Alignment of SPARCLE Telescope





## SPARCLE Telescope Performance

	Primary	Secondary	Beam Expander Pre ASSY	Post ASSY	Interface Mirrors
Wave RMS@2 $\mu$	1/67	1/125	1/42	1/18	1/50 (ea)
Wave P-V @2 $\mu$	1/11	1/27	1/6	1/3	1/5

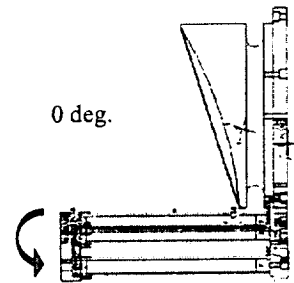
Performance improves in gravity-free space environment.

## Gravitational Sag Tests

Secondary supported      1/22 wave rms

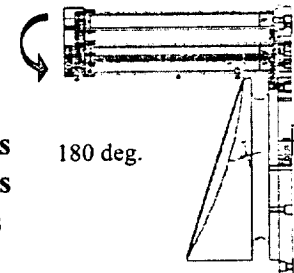
Rotate and measure Beam Expander wavefront

0 deg	1/18 wave rms
90 deg	1/31
180 deg	1/15
270 deg	1/30

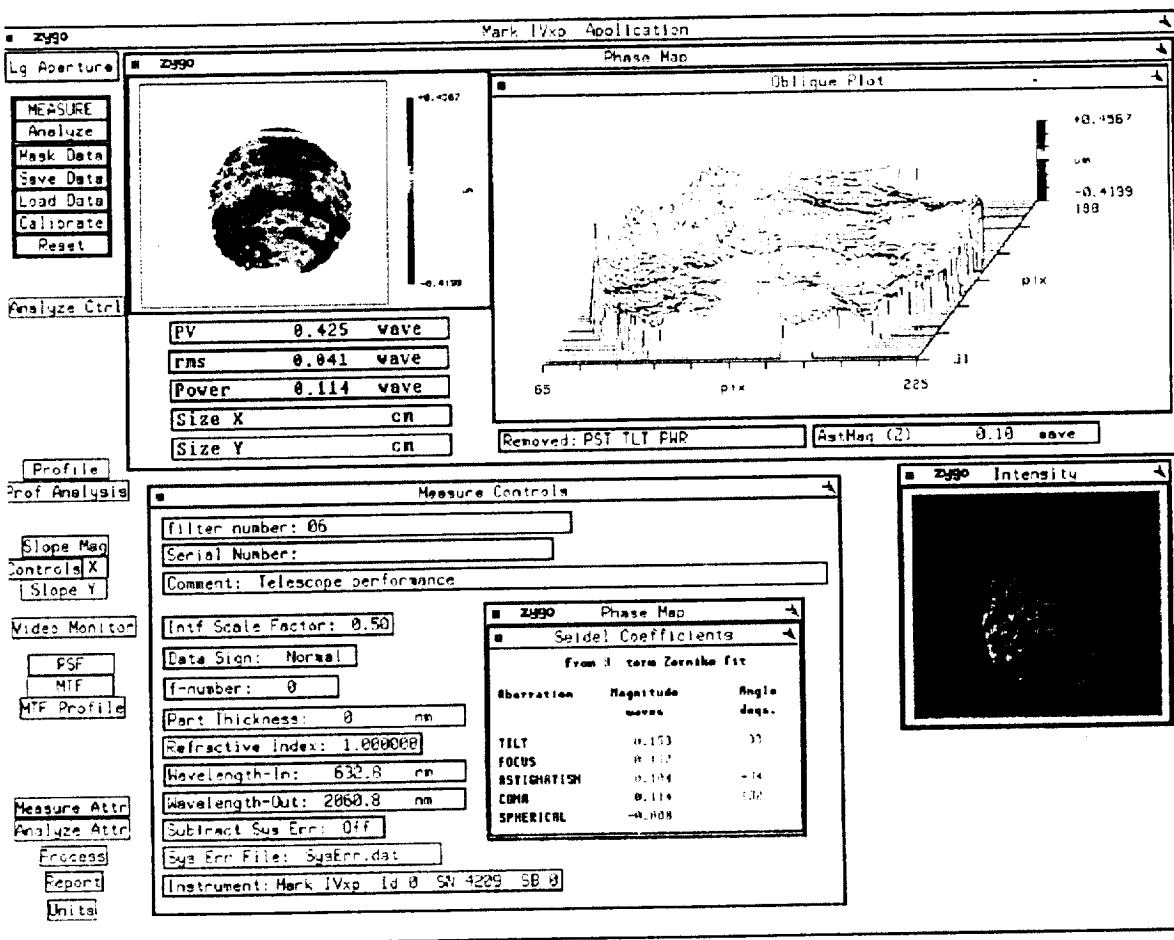


Estimated Telescope (w/ interface mirrors) performance in orbit:

- Performance in the lab      1/15 wave rms
- Subtract gravity effect      1/18 wave rms
- Add thermal variations and gradients 1/15 wave rms

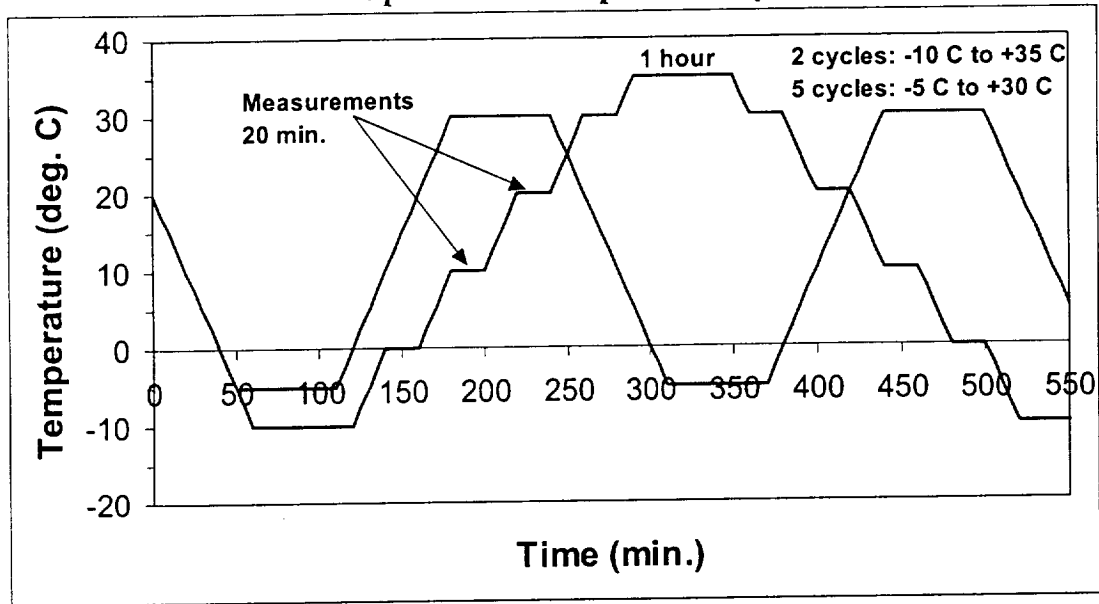


### Example of telescope Wavefront Data



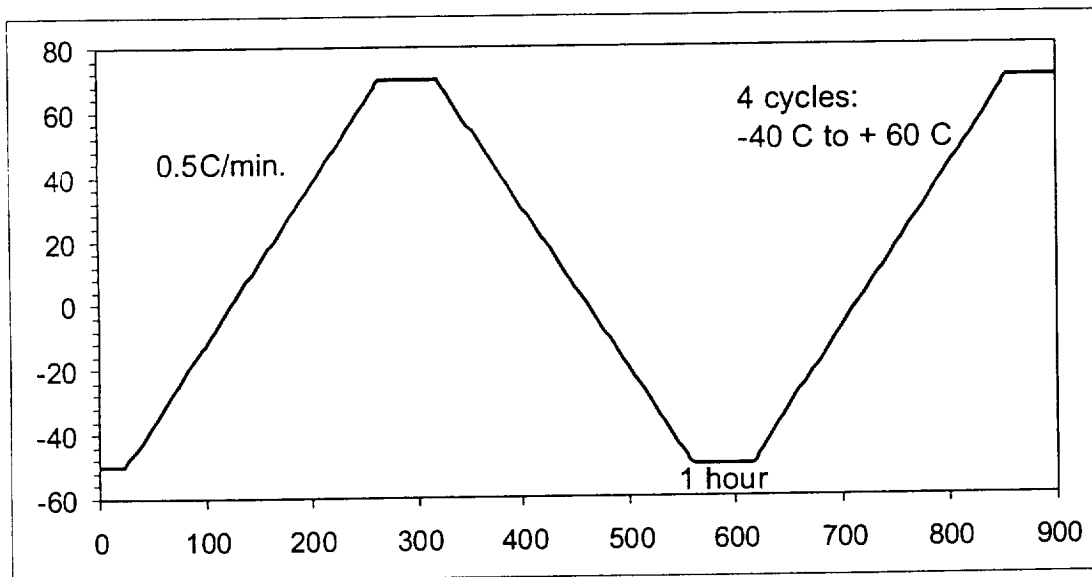


## Thermal Tests Operational Temperature Cycles



Performance is measured from -10°C to 35°C at 10°C intervals

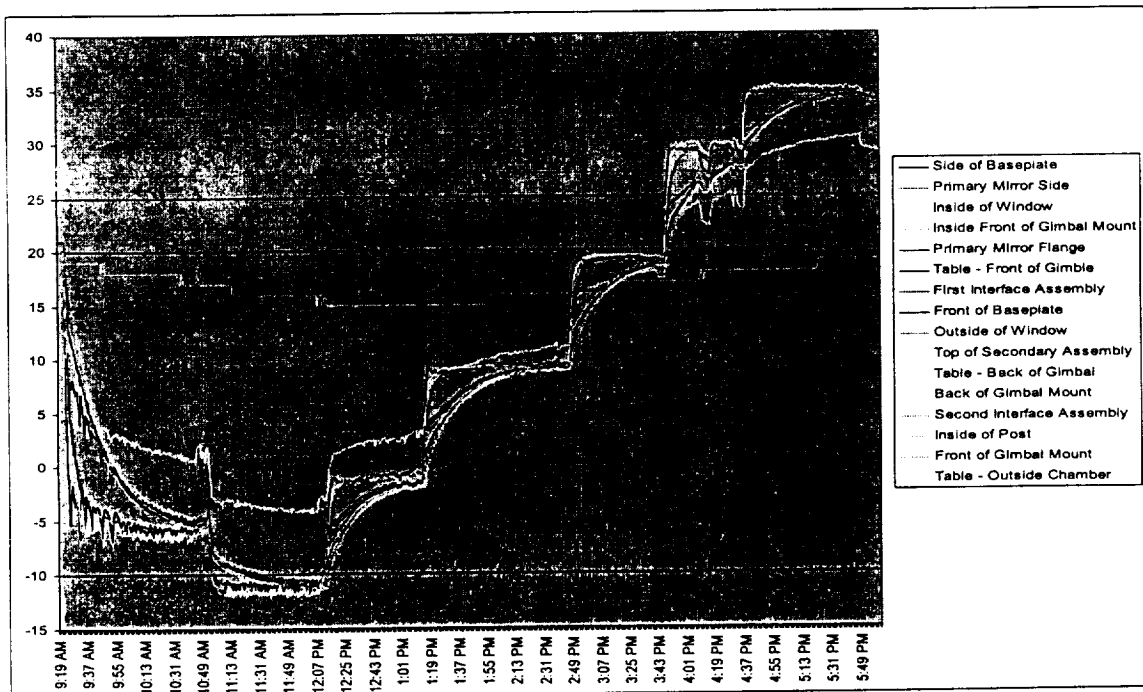
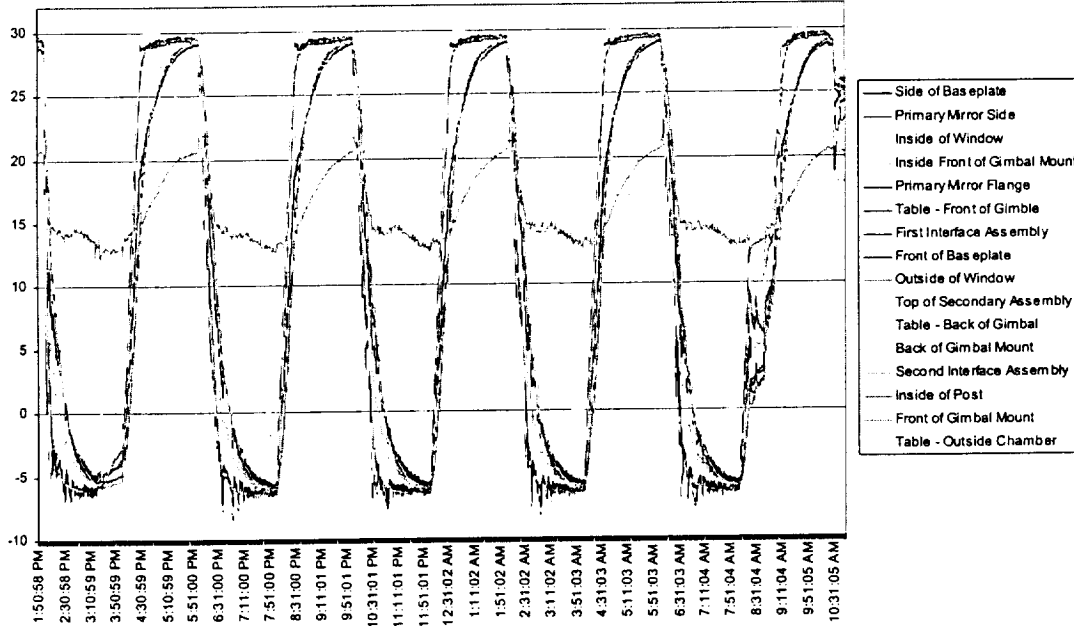
## Survivability Temperature Cycles



Performance is measured before and after 4 cycles

Temperature at several strategic locations of the telescope were measured and recoded during the thermal test.

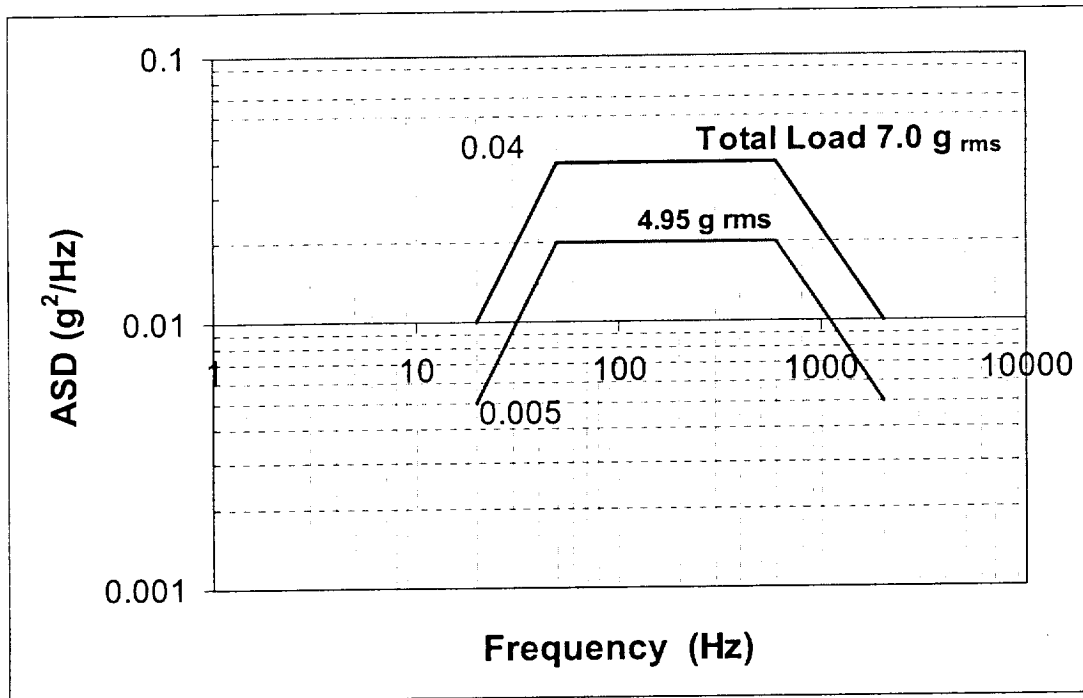
### Thermal Tests



### Vibration Tests

Telescope wavefront performance was measured before and after application of Shuttle qualification loads.

**Random Vibration Spectrum**



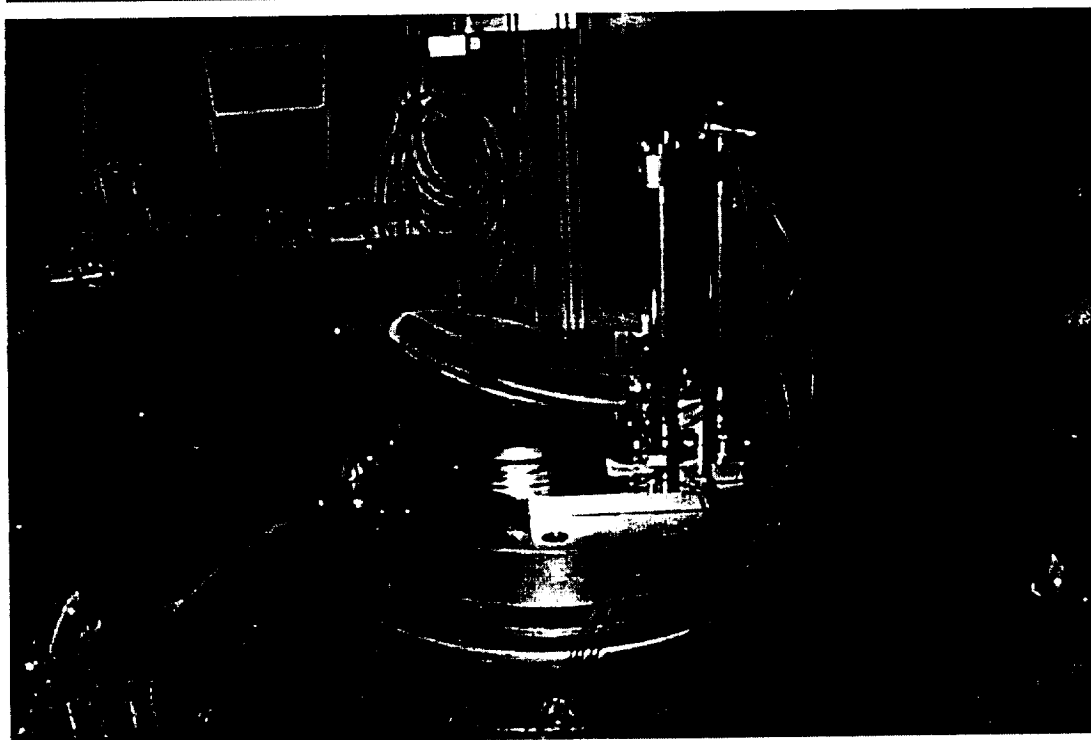
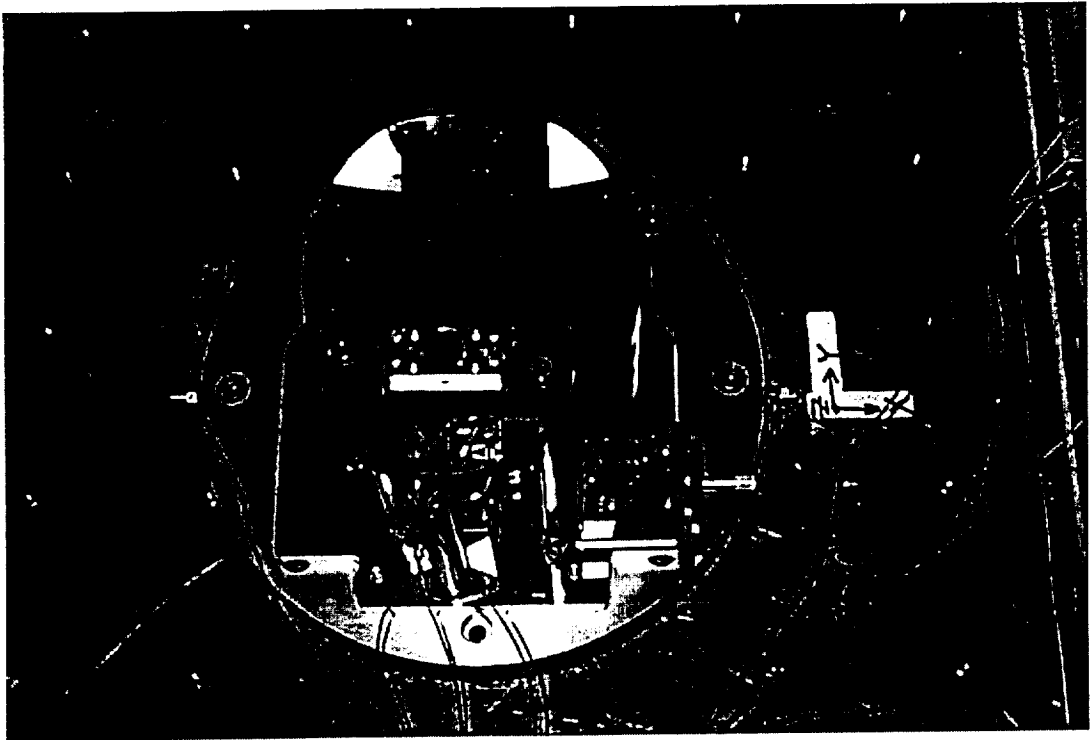
**Acceleration Spectral Density  
Qualification Levels**

Frequency (Hz)	ASD Level (g²/Hz)
20	0.01
20-50	+4.5 dB/oct
50-600	0.04
600-2000	-3.5 dB/oct
2000	0.01
Composite	7.0 g rms

Duration = One minute per axis

A sine sweep vibration test was conducted in each axis. The sine sweep was from 5 to 2000 Hz at one octave per minute, one sweep up, with an input amplitude of 0.25 g peak-to-peak.

### **Vibration Test on SPARCLE Telescope**



## Wide Bandwidth Heterodyne Photoreceiver

A space-based coherent lidar system requires a frequency-agile local oscillator laser to compensate for the large Doppler frequency shift caused by the spacecraft motion. Since the laser beam is conically scanned and the spacecraft velocity is not constant, the frequency of the local oscillator (LO) laser must be controllable over a several GHz tuning range. Therefore, it is necessary to monitor the local oscillator frequency in order to generate the necessary control signal for the LO laser feedback control network. For the SPARCLE instrument, the required tuning range of the LO laser is about  $\pm 4$  GHz which requires a heterodyne photoreceiver with a bandwidth of at least 4.5 GHz. In an earlier work, UAH/CAO had demonstrated that a 2 GHz 3-dB bandwidth heterodyne photoreceiver, operating at 2 microns wavelength, was feasible. The same receiver would have a useful bandwidth of over 4 GHz sufficient for monitoring the MO/LO frequency difference.

### MO/LO Wideband Detector Specifications

#### *Description*

High speed InGaAs detector, with bias circuit, packaged in a housing with fiber optic pigtail and SMA connector output port meeting the following specifications.

#### *Performance Specifications*

The wideband detector performance is shown in the figure below as a function of output signal frequency. The detector performance is defined as the signal power into a 50 ohms load. The detector performance is shown in the figure. The detector output frequency is equal to the frequency difference between the Master Oscillator (MO) laser frequency and Local Oscillator (LO) laser frequency. The detector performance assumes that MO and LO beams are mixed before being launched into the detector fiber pigtail. The two curves in this figure correspond to lower and upper bounds of the detector output signal power. The detector output signal power is given by:

$$P_{\text{signal}}(f) = 2 \rho^2 R_L (P_{\text{MO}} P_{\text{LO}}) H(f)$$

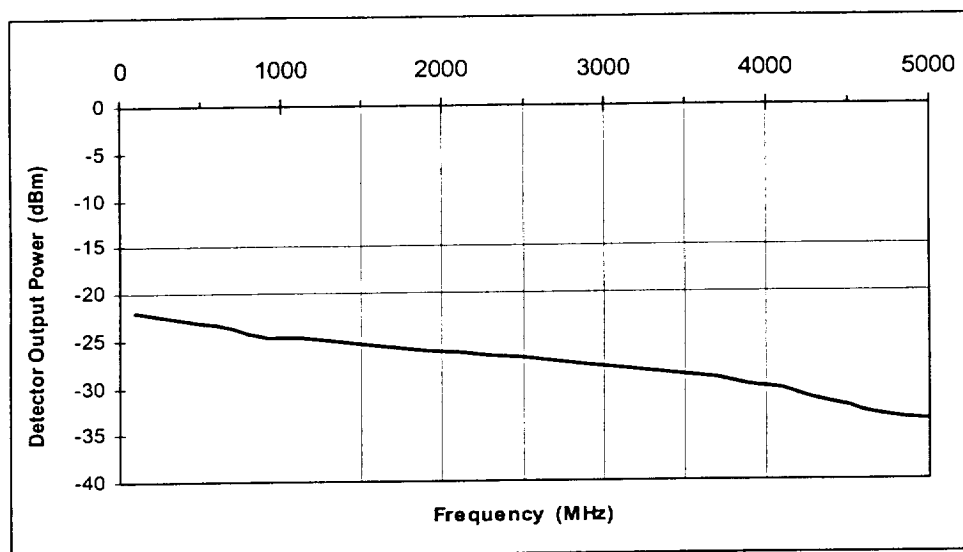
$$\text{dBm} = 10 \log (P_{\text{signal}} / 1\text{mW})$$

The followings are the parameters used for estimating the detector performance.

MO optical power = 0.75 mW

LO optical power = 0.75 mW

Detector load impedance = 50 ohms



### Electrical Interface

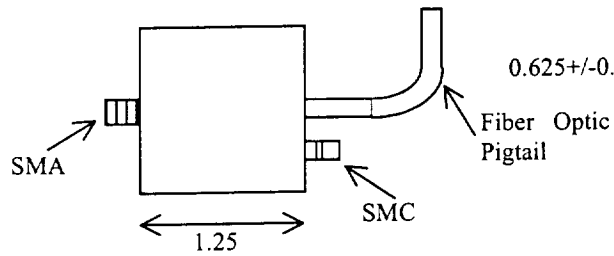
Bias Voltage (input) -5 volts  
 Output impedance (output) 50 ohms

### Physical Specifications

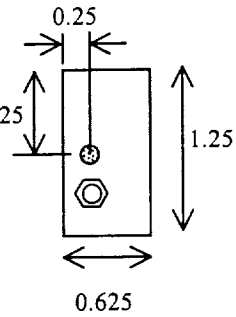
Fiber optic pigtail	50/125 microns core/clad multi-mode Fiber
Fiber optic length	30 centimeters
Fiber cable reference number	RIFOCS Part Number H05
Fiber optic connector	AVIM-PC connector
Fiber optic connector reference number	RIFOCS Part Number D-6206.6
Output signal connector	SMA female
	Manufacturer: MACOM-OMNI SPECTRA
	Part number: 2058-5029-00
Bias voltage connector	SMC
	Manufacturer: MACOM-OMNI SPECTRA
	Part number: 5058-0000-09
Package type	Square with 4 mounting screws
Package specifications	Dimensions and interfaces as per drawing below
Epoxies	TRA-BOND BB-2116 DuPont 5504N

# Package Specifications

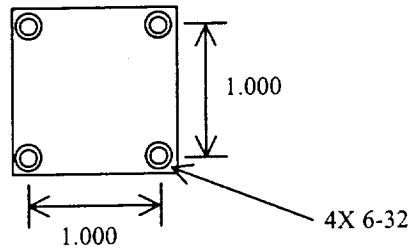
TOP VIEW



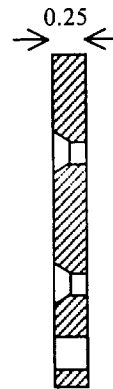
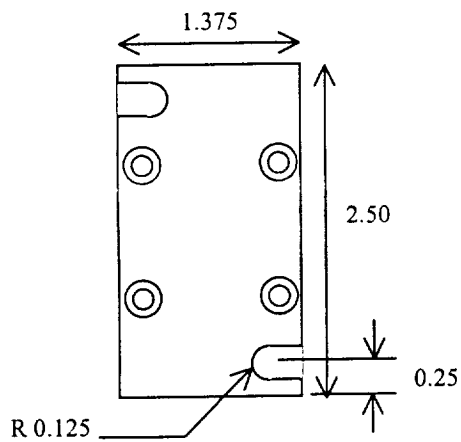
SIDE VIEW



BOTTOM VIEW

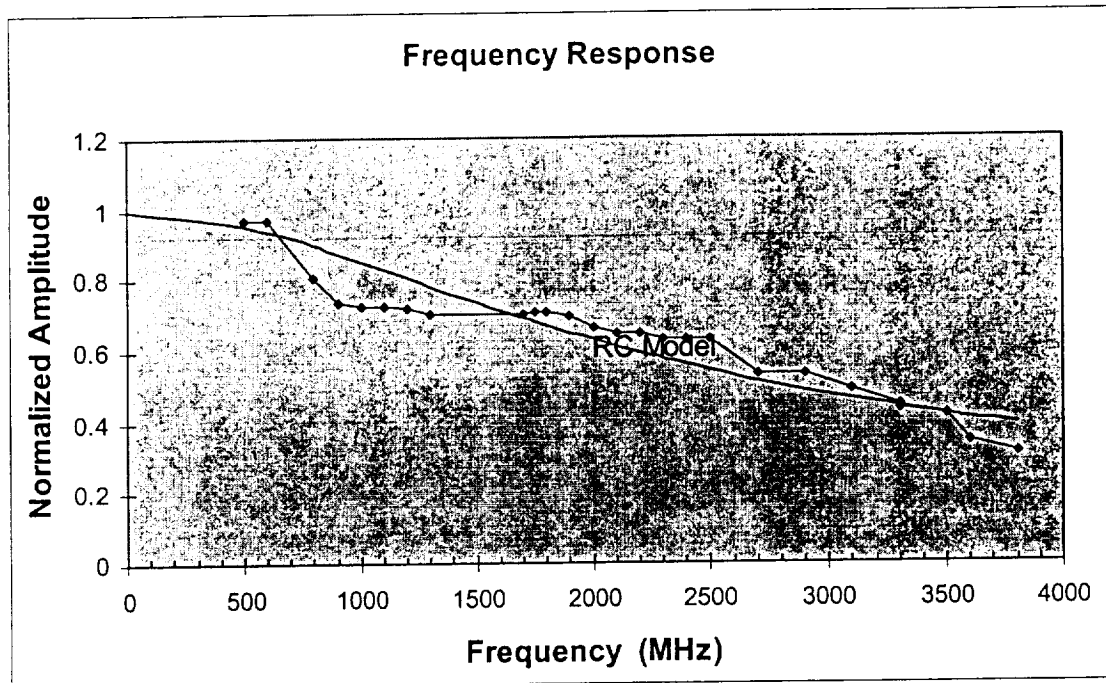


Tolerance: x.xx +/- 0.01  
x.xxx +/- 0.005



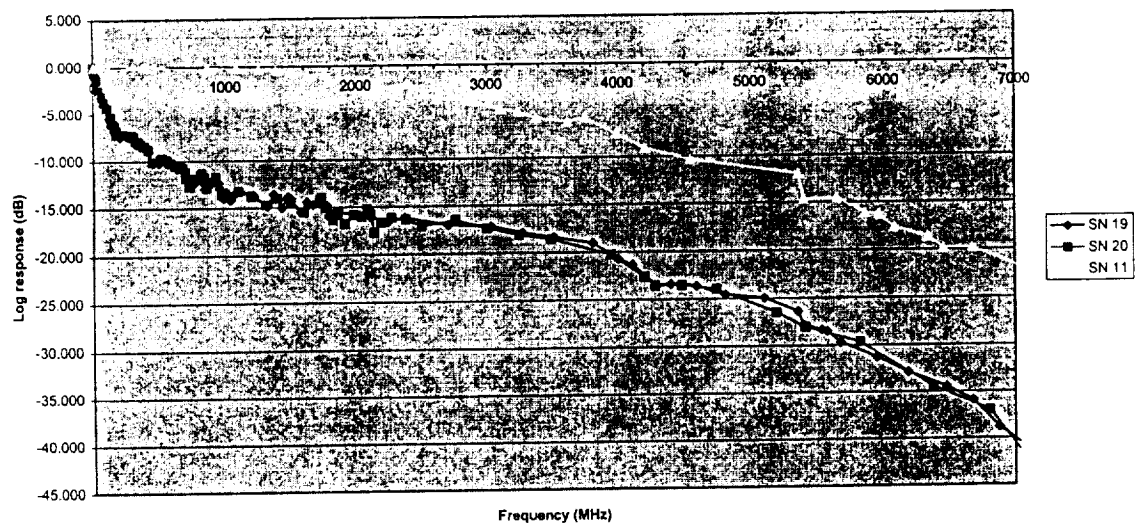
Tolerance: x.xx +/- 0.01  
x.xxx +/- 0.005

## Measured Frequency Response of the Wideband Detector



## Frequency Response Data for three different Wideband detectors

Opto-Electronics PD2 Detector Frequency Response at 2.05 micron wavelength  
Optical heterodyne signal power measurement



## Optical Integration Plan



## ALIGNMENT PROCEDURES TO BE PERFORMED ON THE ZYGO INTERFEROMETER

- OPTICS BASE PLATE TO ZYGO
  - ALIGN THE OPTICS BASE PLATE OPTICAL REFERENCE SURFACES TO THE ZYGO 1.84 MILIRAD
- PRIMARY MIRROR TO BACKING PLATE
  - ALIGN THE OPTICAL REFERENCE SURFACE ON THE PRIMARY MIRROR 1.84 MILIRAD TO THE ZYGO AND MOUNT PRIMARY TO OPTICS BASE PLATE
  - CONFIRM ABSENCE OF OPTICAL STRESS ON OPTICS BASE PLATE DUE TO THE MOUNTING
- POSTS TO OPTICS BASE PLATE
  - CONFIRM THE ABSENCE OF OPTICS BASE PLATE OPTICAL STRESS DUE TO MOUNTING RODS
  - APPLY SUPPORT STRUTS TO MITIGATE GRAVITATIONAL SAG
- SECONDARY TO SECONDARY MOUNTING PLATE
  - REFERENCES ALIGNED IN ZYGO 1.84 MILIRAD
  - ATTACH MOUNTING PLATE
  - CONFIRM ABSENCE OF OPTICAL STRESSES ON SECONDARY REFERENCE SURFACES DUE TO MOUNTING

UAH

## CONTINUED

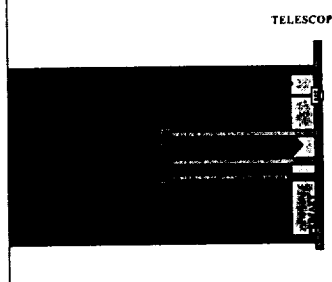
## ALIGNMENT PROCEDURES TO BE PERFORMED ON THE ZYGO INTERFEROMETER

- SECONDARY ASSEMBLY TO ALIGNMENT STAGES
  - SECONDARY COURSE POSITIONING USING ALIGNMENT FEDUCIAL MARKINGS ( $<0.5\text{mm}$ )
  - SECONDARY FINE POSITIONING USING ALIGNMENT STAGE ( $30\text{nm}$  RESOLUTION)
- SECONDARY/ ALIGNMENT ASSEMBLY TO POSTS
  - BASELINE MIRROR POSITIONING FEDUCIALS USED ( $<1.0\text{mm}$  in x,y,z)
  - THETA (x,y,z) MONITORED USING REFERENCE SURFACES ON SECONDARY MIRROR ( $1.84\text{ mrad}$ )
  - PICO MOTORS USED TO POSITION THE SECONDARY MIRROR TO SPECIFICATIONS ( $30\text{nm}$ )
- FINAL ALIGNMENT USING ZYGO INTERFEROMETER, PICO MOTORS, AND INTERFERENCE ANALYSIS ( $\lambda/15\text{ RMS}$ )
- TRANSFER ASSEMBLED TELESCOPE TO TWO MICRON WAVELENGTH TEST STATION

UAH

## INSTALL CTI INTERFACE ALIGNMENT IRISES ON POSTS

## SCHEMATIC OF ALIGNMENT MIRRORS



UAH

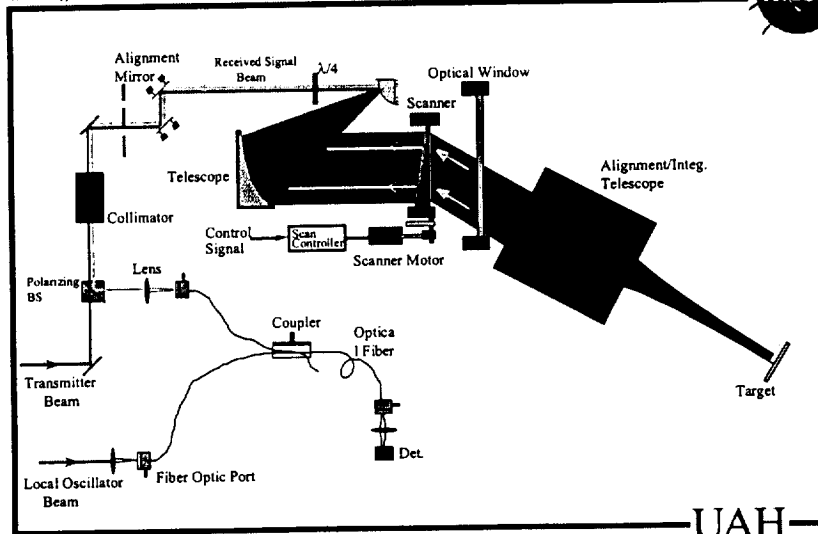
#### Optical Integration Plan Summary

- Mount the optics canister internal structure assembly onto the Ground Support Equipment (GSE) fixture
- Mount the telescope in the interface handling GSE
- Lower the telescope into position and align the fiducial indicators
- Mount the telescope to the structure intermediate plate
- Mount the assembled structure in the verticle interface ground support fixture
- Install the reference HeNe laser and align it to the reference mirror installed on the telescope optics baseplate
- Install the fiducial alignment indicators and align them to HeNe laser beam



Optical Integration Plan Summary (Cont.)

- Mount CTI Slave Oscillator Optical Bench to the structure intermediate plate
- Align the two micron laser to the alignment Feducials
- Mount the scanner motor/encoder to the top plate
- Mount integrated scanner motor/encoder and top plate to the structure
- Install silicon optical wedge in the scanner motor/encoder
- Align the scanner and optical wedge using the reference HeNe laser
- Install and align the window in the top plate using the reference HeNe laser



- Simulated far-field measurements require a 25 cm beam expanding telescope
  - R>500 m for a 10X telescope
  - R>125 m for a 20X telescope
- Shorter target range reduces atmospheric effects
- Atmospheric effects can be further minimized by using MSFC X-ray or Straylight facilities

# **APPENDIX**

## **PUBLICATIONS**

## Design and Operational Characteristics of the Shuttle Coherent Wind Lidar

Farzin Amzajerdian, Gary D. Spiers, Bruce R. Peters, Ye Li, Timothy S. Blackwell, Joseph M. Geary  
Center for Applied Optics  
The University of Alabama in Huntsville  
Huntsville, Alabama  
Phone: (205) 890-6030, Fax: (205) 890-6618, E-mail: farzin.a@msfc.nasa.gov

### INTRODUCTION

Ongoing NOAA interdisciplinary investigations rely on data from various satellite instruments, other sources, and a variety of models to construct an integrated view of atmospheric climate. Topics of interest include the role of circulation, clouds, radiation, water vapor, and precipitation in climate change and prediction, and the role of ocean-atmosphere interactions in the energy and water cycles. Without quality data anchoring improved models, it will be difficult to achieve a comprehensive understanding of these global processes. NOAA has identified the measurement of atmospheric wind velocities as one of the key unmet data sets for its next generation of sensing platforms.

The merits of coherent lidars for the measurement of atmospheric winds from space platforms have been widely recognized; however, it is only recently that several key technologies have advanced to a point where a compact, high fidelity system could be created. Advances have been made in the areas of the diode-pumped, eye-safe, solid state lasers and room temperature, wide bandwidth, semiconductor detectors operating in the near-infrared region. These new lasers can be integrated into efficient and compact optical systems creating new possibilities for the development of low-cost, reliable, and compact coherent lidar systems for wind measurements. Over the past five years, the University of Alabama in Huntsville (UAH) has been working toward further advancing the solid state coherent lidar technology for the measurement of atmospheric winds from space. This work has been conducted in support of a NASA technology development initiative led by the NASA Marshall Space Flight Center (MSFC) and supported by the NASA Langley Research Center (LaRC) and Jet Propulsion Laboratory (JPL). As part of this effort, UAH had established the design characteristics and defined the expected performance for three different proposed space-based instruments: a technology demonstrator, an operational prototype, and a 7-year lifetime operational instrument.

SPARCLE is an ambitious project that is intended to evaluate the suitability of coherent lidar for wind measurements, demonstrate the maturity of the technology for space application, and provide a useable data set for model development and validation. The SPARCLE instrument will be developed, deployed, and operated by a team led by NASA/MSFC, which will provide project management, instrument command and data management unit, support systems (power, thermal, etc.), integration and space qualification. NASA/LaRC, JPL, and Coherent Technologies, Inc. (CTI) are collectively responsible for providing the laser subsystem. UAH will provide the instrument optical subsystem, opto-mechanical design, mission simulation, integration support, and calibration. NASA Goddard Space Flight Center will provide Hitchhiker (HH) Canisters, and shuttle interfaces. This paper describes the SPARCLE instrument's major physical and environmental design constraints, optical and mechanical designs, and its operational characteristics.

### LIDAR SYSTEM

The SPARCLE instrument shown, schematically in figure (1), is a compact and relatively low power solid state coherent lidar designed to fit within the volume, mass, and power constraints of two pressurized space shuttle Hitchhiker canisters. The laser subsystem consists of three diode-pumped Ho,Tm:YLF lasers: a pulsed transmitter laser, a continuous wave (CW) master oscillator (MO) laser, and a CW local oscillator (LO) laser. The transmitter laser uses a part of the master oscillator laser output to generate stable, single frequency pulses which are then expanded by an off-axis, afocal telescope and refracted by 30 degrees off nadir by a silicon wedge. The wedge is rotated by a precision motor/encoder assembly in a step/stare fashion, to provide a conical pattern in the atmosphere.

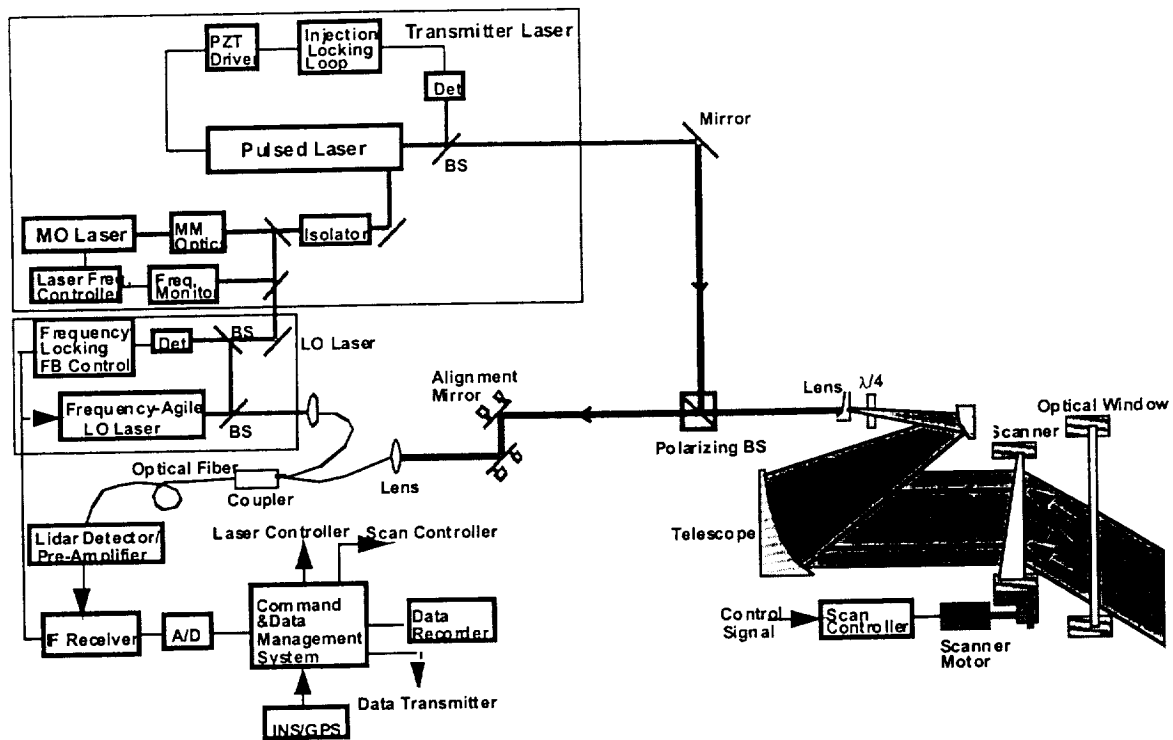


Figure 1. SPARCLE System Schematic.

A small portion of the master oscillator laser output beam is used for frequency locking of the local oscillator laser. The output of the LO laser is directed to the optical detector to be mixed with the signal beam. In order to compensate for the large Doppler shift due to the spacecraft velocity and the earth's rotational velocity, the frequency of either the LO or MO laser is varied as a function of the azimuth angle of the conical scan and the current orbit position. The returned photons from the atmosphere are collected by the telescope and fiber coupled with the local oscillator beam. The output of the fiber optic coupler is focused onto a high-quantum efficiency, wideband InGaAs detector. The general system parameters are listed in table 1.

Table 1. SPARCLE System Parameters

Transmitter Laser Energy Per Pulse	100 mJ
Pulse Repetition Rate	6 Hz
Transmitter Pulse Width	~ 200 nsec
Aperture Diameter	23.3 cm
Maximum Scanner Speed	45°/sec
Scan Full Angle	60°
Wavelength	2.06 $\mu$ m
Receiver Bandwidth	500 MHz
Trans./Rec. Boresight Alignment Budget	7.2 $\mu$ rad over pulse round trip time
Vertical Range Resolution	250 m
Optical Subsystem Efficiency	0.1
Receiver Subsystem Efficiency	0.25

### **INSTRUMENT DESCRIPTION**

As currently configured, the instrument will be housed in two pressurized Hitchhiker canisters. The laser and optical subsystems will be placed in one canister (optics canister), and all the support electronics, data and command system, and inertial navigation system will be packaged in the second canister (electronics canister). The canisters will be connected by several cables for data transmission between canisters and for providing the necessary conditioned electrical power to the optics canister system.

The integrated instrument optical design is shown in figure 2. The instrument opto-mechanical design allows for maintaining the required optical alignment while meeting the Hitchhiker physical constraints. The opto-mechanical design of the instrument is driven by the precision and accuracy required from the wind velocity measurements. Accurate transmitter laser beam pointing is also required to ensure that the tunable LO laser frequency adequately extracts the gross spacecraft and earth rotation velocities. Therefore, to meet the scientific requirements, a pointing error budget was defined and used to derive the optical system structural and thermal designs. The combination of tight alignment tolerances and the restricted volume, mass, and power constraints of the Hitchhiker canisters forces an integrated design approach. The design goals and currently configured design parameters for the optics canister are listed in table 2.

Table 2. Optics Canister Design Constraints

Parameter	Design Goal	Current Design
Volume	19.75" D X 28.25" H	19.75" D X 28.25" H
Mass	160 lbs.	240 lbs.
Power Consumption	Not defined	180 W
Operating Temperature Gradient	20°C	4 °C
Laser Cooling Fluid Temp. Range	2 °C	4 °C

### **CONCLUSION**

The current concept for the system configuration meets most of the stringent limitations imposed on volume, mass, and power without sacrificing instrument performance. However, actual system performance will be driven by the accumulated system level errors, especially those introduced during the integration of the various components and subsystems. To minimize the impact of these integration induced errors, additional modeling work is required. High fidelity system modeling will also be of benefit to completing the system optical and mechanical designs, and useful for evaluation of the system performance. More work is required to complete the instrument pointing knowledge sensor specifications and design its SW algorithms.

### **ACKNOWLEDGMENTS**

This work was supported by NASA Marshall Space Flight Center. The authors are grateful to Dr. Michael J. Kavaya, for providing technical guidance.



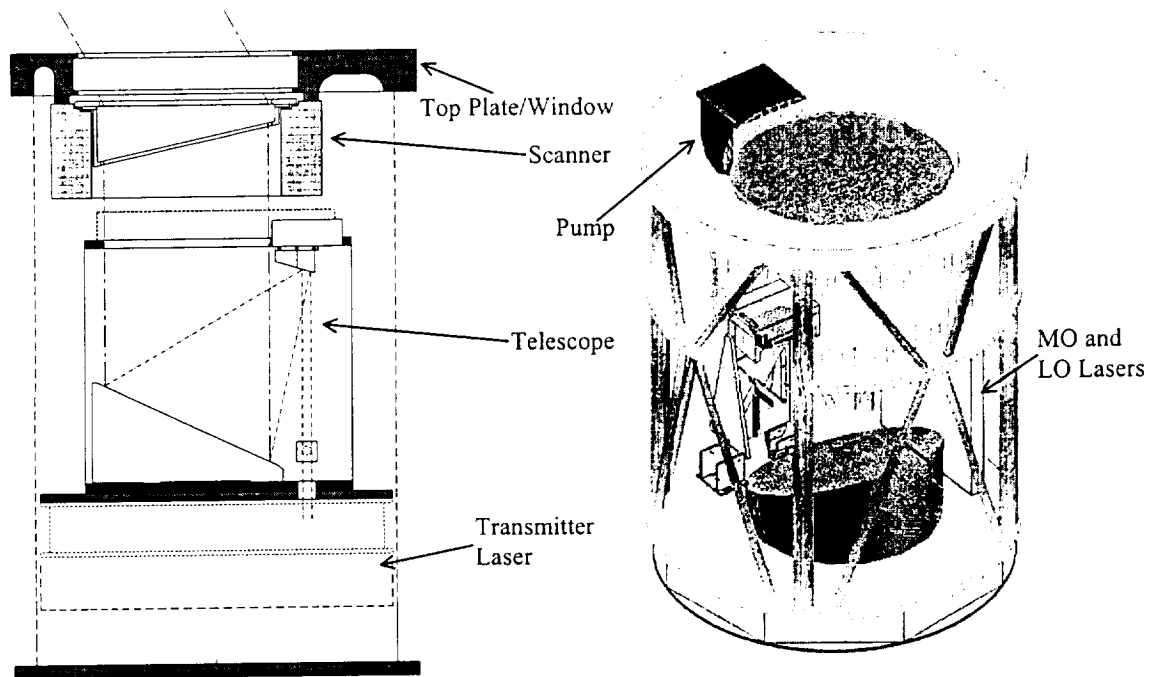


Figure 2. Optics Canister Configuration.

#### REFERENCES

1. M. J. Kavaya, G. D. Spiers, E. S. Lobl, J. Rothermel, and V. W. Keller, "Direct global measurements of tropospheric winds employing a simplified coherent laser radar using fully scalable technology and technique," Proc. SPIE Vol. 2214, Space Instrumentation and Dual-Use Technologies, 2214-31, Apr. 6, 1994.
2. W. E. Baker et al., "Lidar measured winds from space: An essential component for weather and climate prediction," Bulletin of American Meteorological Society, 76(6), 869-888, 1995.
3. A. Ahmad, C. Feng, F. Amzajerdian, and Y. Li "Design and fabrication of a compact LIDAR telescope," Proc. SPIE Vol. 2832, Denver, CO, August 4-9, 1996.
4. U. N. Singh et al., "Diode-pumped 2-mm solid state lidar transmitter for wind measurements," SPIE Vol. 3104, 173-178, June 16-18, 1997.

## Optical System for the Space Readiness Coherent Lidar Experiment

Farzin Amzajerdian, Bruce R. Peters, Ye Li, Timothy S. Blackwell, Joseph M. Geary, Diana Chambers

Center for Applied Optics  
The University of Alabama in Huntsville  
Huntsville, AL 35899

### Abstract

The SPACe Readiness Coherent Lidar Experiment (SPARCLE) is the first demonstration of a coherent Doppler wind lidar in space. Operating at 2-micron wavelength, SPARCLE system performance is dominated by the optical quality of the transmitter/receiver optical system. The stringent optical performance requirements coupled with the demanding physical and environmental constraints have created the need for novel optical and opto-mechanical designs as well as unique alignment and characterization techniques.

---

The SPACe Readiness Coherent Lidar Experiment (SPARCLE) is the first demonstration of a coherent Doppler wind lidar in space. Global measurement of atmospheric winds has been identified by NOAA, NASA, and the Department of Defense as one of the key unmet data sets for the next generation of sensing platforms. SPARCLE will be flown aboard a space shuttle in early or middle part of 2001 as a stepping stone towards the development and deployment of a long-life-time operational instrument in the later part of next decade. SPARCLE is an ambitious project that is intended to evaluate the suitability of coherent lidar for wind measurements, demonstrate the maturity of the technology for space application, and provide a useable data set for model development and validation. This paper describes the SPARCLE's optical system design, its anticipated performance, and its operational characteristics. The instrument's optical characterization methodology and the integration issues will be also discussed.

Coherent lidars can accurately measure the wind velocity by extracting the Doppler frequency shift in the back-scattered signal from the atmosphere through optical heterodyne (coherent) detection. Coherent detection is highly sensitive to aberrations in the signal phase front, and to relative alignment between the signal and the local oscillator beams. Consequently, the performance of coherent lidars is usually limited by the optical quality of the transmitter/receiver optical system. For SPARCLE having a relatively large aperture (25 cm) and a very long operating range (400 km), compared to the previously developed 2-micron coherent lidars, the optical performance requirements are even more stringent.

The functions of the optical system include expanding the laser beam, directing it to the atmosphere in a conical scan pattern, receiving the backscattered radiation, while maintaining a highly accurate pointing to ensure adequate extraction of the Doppler frequency shift due to the spacecraft and earth rotation velocities. Therefore, the overall system performance is very much dominated by the telescope, scanner, and the optical window used for environmentally isolating the lidar instrument. The stringent optical performance requirements combined with the imposed size and mass constraints create many challenges in the design, fabrication, assembly, and testing of the optical subsystems. The results of optical measurements on the prototype telescope and silicon optical wedge scanner element, that have already been fabricated, along with the results from the optical and mechanical analyses indicate that all

the optical requirements including the wavefront quality, polarization purity, optical throughput, and very low optical backscatter can be met over the specified physical and operational constraints.

#### REFERENCES

1. Ahmad, C. Feng, F. Amzajerdian, and Y. Li "Design and fabrication of a compact LIDAR telescope," Proc. SPIE Vol. 2832, Denver, CO , August 4-9, 1996.
2. Amzajerdian and M. J. Kavaya, "Development of solid state coherent lidars for global wind measurements" 9th Conference on Coherent Laser Radar, Linkoping, Sweden, June 23-27, 1997.
3. Li, T. S. Blackwell, J. M. Geary, F. Amzajerdian, G. D. Spiers, B. R. Peters, and D. M. Chambers, "Characterization of Optical subsystem for 2  $\mu$ m Coherent Lidars," International Symposium on Optical Science, Engineering, and Instrumentation, San Diego, CA, July 19-24, 1998.
4. Amzajerdian, G. D. Spiers, B. R. Peters, Y. Li, T. S. Blackwell, and J. M. Geary, " Design and Operational Characteristics of the Shuttle Coherent Wind Lidar," 19th International Laser Radar Conference, Annapolis, MD, July 6-10, 1998.

# Optomechanical design of a multi-axis stage for the SPARCLE telescope

Bruce Peters, Tim Blackwell, Ye Li, Joe Geary, Farzin Amzajerdian, Deborah Bailey

Center for Applied Optics, The University of Alabama in Huntsville, Huntsville, AL 35899\*

## ABSTRACT

A critical component in the 2- $\mu\text{m}$  coherent spaced-based lidar system (SPARCLE) is the compact, off-axis, 25-cm aperture telescope. The stressing optical performance demanded from this telescope coupled with the difficulty associated with aligning such a fast, off-axis system; has created the need for a multiple-axis alignment stage for the secondary mirror. Precision micrometer kinematic mounts were used in the laboratory to demonstrate the ability to successfully align the telescope. For the flight configuration, a more robust and considerably smaller stage (both in size and weight) had to be designed in order to fit within the space shuttle packaging constraints. The new stage operates with multiple degrees of freedom of motion to achieve micrometer precision alignment and then uses a mechanical multiple point support to lock-in the alignment and provide stability. The optomechanical design of the flight stage is described.

**Keywords:** lidar, telescope, optomechanical design

## 1. INTRODUCTION

Ongoing Earth Observing System (EOS) interdisciplinary investigations rely on data from various satellite instruments, data from other sources, and a variety of models to construct an integrated view of atmospheric climate over the oceans. Topics of interest include the role of circulation, clouds, radiation, water vapor, and precipitation in climate change, and the role of ocean-atmosphere interactions in the energy and water cycles. These investigations attempt to incorporate the interactions among clouds, water vapor, radiation fluxes, and various scales of motion from small-scale to planetary. These investigations often utilize existing data to continue the development and testing of improved models; but this is often not enough. To maintain these activities, additional data is needed. While new data can come from satellites, sensors, and ground stations, the quality of the data must fulfill very exacting science requirements to be of use. Without quality data anchoring improved models, it will be difficult to achieve a comprehensive understanding of global climate and predict future climate changes.

The surface climate of Earth is strongly influenced by the amount and distribution of water vapor, liquid water, and ice suspended in the atmosphere. Seven-tenths of the surface of Earth is covered with ocean, so that processes that occur over the oceans substantially determine the climate over land areas. The processes that control water in the atmosphere are very complex and extend across a wide range of spatial scales from the few centimeter scale of turbulence in the boundary layer to the tens of thousands that characterize the scale of global atmospheric circulation systems. Currently, no one sensor platform can adequately obtain all the data needed to address this broad range of scales so it becomes necessary to synthesize data from a variety of different sensor platforms at a number of different locations.

The prevalence of water instead of land covering the surface of the Earth further complicates the logistics associated with using ground-based systems to monitor global atmosphere. While airborne sensors can alleviate some of these problems by providing mobile platforms that can range over much of the earth, local weather, loitering time, and operations costs can limit their use. The access of space-based sensors to the global atmosphere is not as limiting since satellites can theoretically gain access to any portion of the atmosphere to provide long-term monitoring of atmospheric phenomena. A further advantage to satellite sensors is that the satellite provides a unique viewpoint since it is above the atmosphere looking down and can thereby provided easy access to the upper levels of the atmosphere. An integrated, multisensor-based, worldwide observation system is needed to obtain the desired data and advance the scientific investigations. The multitude of issues associated with a scientifically complex mission as this makes the identification, development, selection, and operation of different sensor platforms a critical task.

---

\* Further corresponding author information -

Dr. Bruce R. Peters: Email: [petersb@email.uah.edu](mailto:petersb@email.uah.edu); WWW: <http://www.uah.edu/cao/faculty/peters.html>; Tel: 256-890-6030 ext. 471; Fax: 256-890-6618.

Despite many of the challenges mentioned above, the measurement of global atmospheric wind velocities, from ground to upper atmosphere, remains one of the fundamental data sets necessary to advance the understanding and forecasting of weather.<sup>1</sup> As stated earlier, logistics and instrumentation limitations conspire to limit the ability to obtain data on a globally relevant scale with sufficient precision to support climate modeling. These limitations can be overcome by employing a space-based measurement platform, specifically coherent Doppler lidar. Coherent Doppler lidar for horizontal wind velocity measurements relies on the backscatter from aerosols in the atmosphere to derive a velocity map of the horizontal winds at a given height within the troposphere. The Space Readiness Coherent Lidar Experiment (SPARCLE) is a first step towards demonstrating the feasibility of measuring tropospheric wind velocities using the space shuttle in lieu of a satellite.<sup>2</sup> This is an ambitious project that intends to evaluate the appropriateness of coherent lidar for wind measurements, demonstrate the maturity of the technology for space application, and provide a useable global data set for model development and validation. SPARCLE has been selected for the New Millennium Program and will be managed by NASA Marshall Space Flight Center (MSFC) where the instrument engineering and integration will occur with additional support provided by NASA Langley Research Center (LaRC), NASA Jet Propulsion Laboratory (JPL), The University of Alabama in Huntsville (UAH), Coherent Technologies Inc. (CTI), and Simpson Weather Associates (SWA). SPARCLE will be packaged in two Hitchhiker (HH) canisters and flown aboard the space shuttle, scheduled for early 2001.

## 2. COHERENT DOPPLER WIND LIDAR

The use of coherent Doppler lidar for determining wind velocity has long been recognized as a viable approach.<sup>3,4</sup> The coherent Doppler lidar technique employs heterodyne detection to increase signal-to-noise (SNR) and thereby increase sensitivity by overcoming the noise problems inherent in incoherent lidar systems.<sup>5</sup> In operation, a short laser pulse is transmitted from the instrument into the atmosphere. The photons scattered off of the aerosol particles within the atmosphere are collected by the same telescope and focused onto a detector. The return signal is Doppler shifted due to the combination of the spacecraft and the velocity of the wind driven aerosols. The signal is mixed with the frequency stable reference beam on the detector and the velocity bias of the spacecraft is removed to determine the wind velocity. By scanning the laser beam about the nadir, different lines-of-sight (such as looking forward and backward relative to the ground path of the satellite) for the same volume of atmosphere will permit the calculation of the horizontal wind vectors.

A CO<sub>2</sub> laser Doppler wind lidar measurement capability was demonstrated as early as 1968 and lidar remains the only space-based instrument capable of measuring tropospheric wind velocities.<sup>6</sup> MSFC conducted a series of studies to develop instrument designs utilizing both CO<sub>2</sub> and solid state laser technology with an emphasis on spacecraft adaptation and reducing system cost.<sup>7,8</sup> While technologically feasible, the drawbacks to utilizing CO<sub>2</sub> lasers, such as greater mass, volume, power requirements and cost, limited the development of a space-based system. However, with the advent of solid state laser technology beginning in the 1980's, a space-based wind velocity instrument became attractive.<sup>9,10</sup> The coherent Doppler lidar wind profiling instrument first described in 1996<sup>11</sup> has further evolved into the instrument used in SPARCLE.

Table 1. SPARCLE System Parameters

Transmitter Laser Energy Per Pulse	100 mJ
Pulse Repetition Rate	6 Hz
Transmitter Pulse Width	~ 200 nsec
Aperture Diameter	23.3 cm
Maximum Scanner Speed	45°/sec
Scan Full Angle	60°
Wavelength	2.05 $\mu$ m
Receiver Bandwidth	500 MHz
Trans./Rec. Boresight Alignment Budget	7.2 $\mu$ rad over pulse round trip time
Vertical Range Resolution	250 m
Optical Subsystem Efficiency	0.1
Receiver Subsystem Efficiency	0.25

The SPARCLE configuration has selected a step/stare conical scan 30° off of nadir as a compromise between aligning to

the horizontal wind component as closely as possible versus the signal loss due to long slanted paths through the atmosphere. The desired accuracy of the wind velocity measurement for SPARCLE of 1 m/s, combined with the Space Shuttle accommodation constraints determines the system parameters that are described in Table 1. The desired wind velocity accuracy drives the telescope aperture size, the laser pulse energy, the system efficiency. Inherent in the lidar instrument is some lidar inefficiencies but there are also SNR effects that lower overall system performance. Reference 2 has a detailed discussion of the affect of errors and both SNR and non-SNR effects and this is beyond the scope of this paper. The result of this analysis is that the alignment and stability of the lidar instrument becomes challenging in order to achieve the desired measurement accuracy.

The SPARCLE instrument, shown schematically in Figure 1, is a compact and relatively low power, solid state coherent lidar. The instrument consists of a solid state laser transceiver, a beam expanding telescope and beam scanning optics, a support structure, a thermal subsystem, and a computer based data management and control subsystem. As currently configured, the whole system is packaged into two pressurized HH canisters with an internal volume of 5 ft<sup>3</sup> each: the "optics can" or canister #1 and the "electronics can" or canister #2 (Figure 2). The canisters have a 50 cm internal diameter and a nominal usable experiment length of 71 cm. If additional volume is needed within the canister, the HH Program office has canister extensions to increase the can length in regular increments. Located within the electronics can are the electronic control equipment, power supplies, data storage, and system computer. The optics can contains the actual instrument sensing hardware such as the laser transceiver, the telescope, beam scanning optics, and a heat exchanger system mounted within a structural frame (Figure 3). A number of cables provide connections between the two canisters over which control signals, health and status monitoring, experimental data, and power is transmitted.

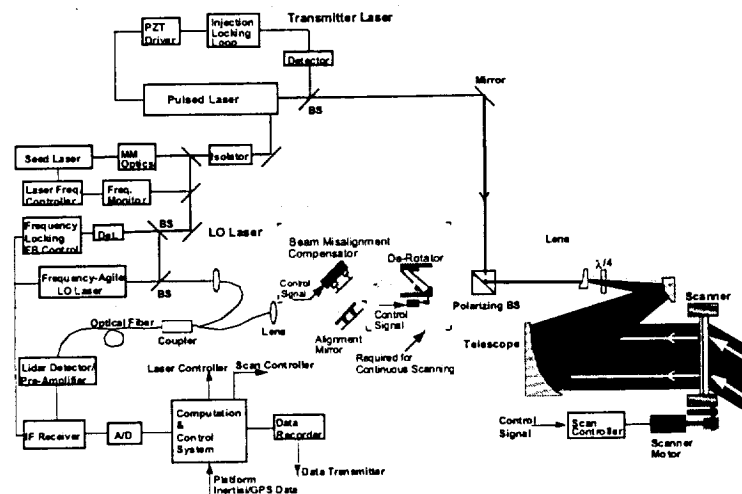


Figure 1. Schematic of compact low power, solid state coherent lidar.

The laser subsystem consists of three diode-pumped Ho,Tm:YLF lasers: a pulsed transmitter laser, a continuous wave (CW) master oscillator (MO) laser, and a CW local oscillator (LO) laser. The laser transmitter uses injection seeded, room temperature, diode pumped, pulsed, Tm,Ho:YLF laser technology demonstrated by LaRC. The transmitter laser uses a part of the MO laser output to generate stable, single frequency, narrow spectrum pulses. The laser technology has been transferred to CTI to be packaged into a more rugged and robust flight unit.<sup>12</sup> As currently configured, the unit will function at 2.05  $\mu\text{m}$  with 100 mJ of energy per pulse at 6 Hz pulse repetition rate.

The output laser beam is expanded by an off-axis, afocal telescope and refracted by 30° off nadir by a silicon wedge mounted in a rotating scanner. The wedge is rotated by a precision motor/encoder assembly in a step/stare fashion, to provide a conical pattern in the atmosphere. The output of the LO laser is directed to the optical detector to be mixed with the signal beam. In order to compensate for the large Doppler shift due to the spacecraft velocity and the earth's rotational velocity, the frequency of either the LO or MO laser is varied as a function of the azimuth angle of the conical scan and the current orbit position. The telescope collects the scattered photons from the atmosphere and fiber coupled with the local oscillator beam. The output of the fiber optic coupler is focused onto a high-quantum efficiency, wideband InGaAs detector.

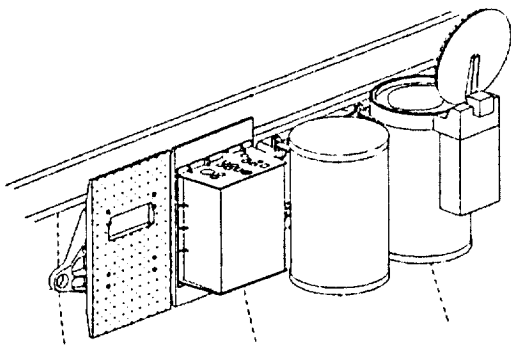


Figure 2. SPARCLE system in the Space Shuttle.

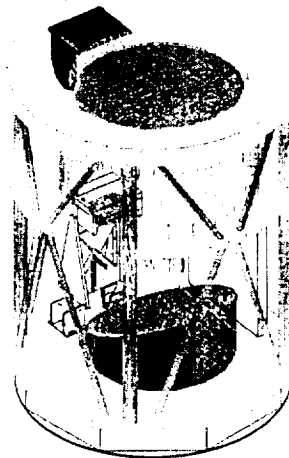


Figure 3. Conceptual SPARCLE optics canister

The instrument optical design allows for achieving the stringent wavefront qualities and optical performance within the tight physical constraints. The optomechanical design of the instrument is driven by the precision and accuracy required from the wind velocity measurements which demands achieving and maintaining the required optical alignment through out a range of operational scenarios and environments and within the HH physical constraints. The relative alignment of the received signal with respect to the local oscillator beam ( $7 \mu\text{rad}$  over a pulse roundtrip) is critical for maintaining a high detection efficiency. Furthermore, accurate transmitter laser beam pointing ( $90 \mu\text{rad}$ ) is also required to ensure that the tunable LO laser frequency adequately extracts the gross spacecraft and earth rotation velocities. The combination of tight alignment tolerances and the restricted volume, mass, and power constraints of the HH program forces an integrated design approach.

### 3. OPTOMECHANICAL DESIGN

The optomechanical design of the lidar system is concerned with the attributes associated with space-based sensors: low weight, compact, stable. The typical approach is to select materials for the optical system that have very high microyield strength (very stiff and usually brittle materials); but, these materials are also very expensive to fabricate. The system is going to need to operate over a temperature range that is not abnormally large (currently  $0-25^\circ\text{C}$  for SPARCLE) but the wavefront quality must be maintained throughout this range. Therefore, an athermal system is most desirable because the optics and the supporting structure are fabricated from the same material. The system is considered athermal if the optical properties of the mirrors (radius of curvatures, thickness, etc.) are perfectly balanced by the expansion/contraction of the structural supports such that the focus of the optical system does not change and the system maintains alignment.

One way to achieve athermal operation with a low weight and a reasonably costed fabrication approach is to use metal mirrors manufactured using single point diamond turning (SPDT) technology. The structural efficiency of Aluminum, the quotient of the material's elastic modulus (a measure of strength) and the material's density, is more than adequate at 102.1 compared to 73.5 for Invar, 96.6 for 304 Stainless Steel (SS), and 597 for Beryllium (Be). Furthermore, the optical surface of the mirror is typically overcoated with electroless nickel after diamond turning. This is done because the nickel is harder and accepts polishing. It is desirable to have the coefficient of thermal expansion (CTE) of the nickel coating ( $8.4 \text{ ppm}/^\circ\text{F}$ ) closely match the CTE of the bulk mirror material. The CTE of Aluminum is  $13.1 \text{ ppm}/^\circ\text{F}$  compared to  $0.7 \text{ ppm}/^\circ\text{F}$  for Invar,  $9.6 \text{ ppm}/^\circ\text{F}$  for 304 SS, and  $6.4 \text{ ppm}/^\circ\text{F}$  for Be. Because of its relative ease to machine, its availability, its good structural efficiency, and since it is a close CTE match to the nickel coating, the metal of choice was Aluminum 6061. This is the approach selected for the SPARCLE telescope.

In theory, the placement of the optics relative to each other could be built into the supporting structure. The typical machining tolerances available from low cost machine operations make this goal difficult to achieve with optical systems of this level of required precision. Therefore, alignment adjustments are often built into the system or translation/rotation stages are used to maneuver optical elements during system alignment. It is desirable to minimize the size and number of stages within flight systems because of their added weight and volume. Therefore, the optomechanical designer needs to carefully consider the

optimal location and complexity of alignment stages.

#### 4. TELESCOPE PERFORMANCE

The overall function of the optical system is to expand the laser beam, direct it towards the atmosphere at a  $30^\circ$  nadir angle, scan the beam in a conical fashion, collect the backscattered photons, and focus the energy onto the detector. The optomechanical design and analysis was a critical component in the development of the optical system. Because of the demanding system performance requirement, the choice of materials, the method of optics fabrication, the optics mounting approach, and the stability of the structural system all had to be considered in parallel with the optics design. The relative tight tolerances on position and alignment of the optics had to be maintained after experiencing launch loads aboard the Space Shuttle. In addition, the optomechanical system had to function passively – no on-orbit active correction or re-alignment would be possible in the SPARCLE system because of weight, volume, power, and cost constraints imposed by the selection of the HH canisters.

Table 2. SPARCLE Demonstration System Parameters as Designed

Input Beam Diameter	1 cm
Transmitted Beam Diameter	25 cm
Beam Quality	Diffraction Limited
Scanning Mode	Continuous and Step-Stare
Boresight Lag Angle Compensation	1 $\mu$ rad
Scan Full Angle	$60^\circ$
Field-of-View	$0.17^\circ$

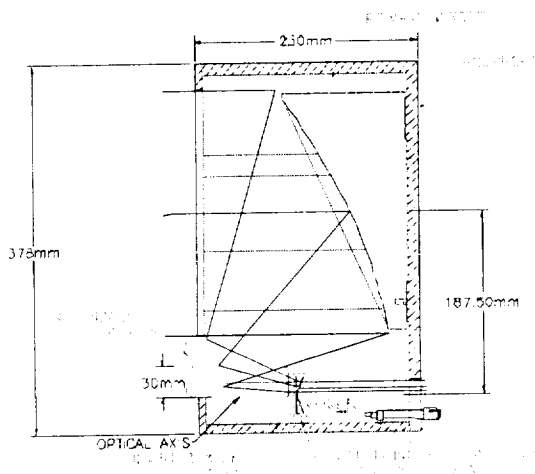


Figure 4. First generation telescope design.

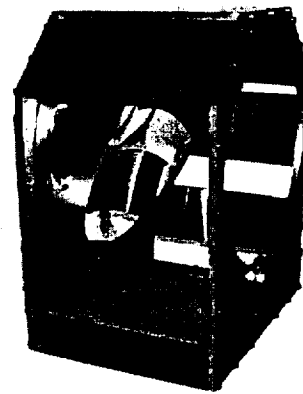


Figure 5. First generation telescope engineering model.

The first telescope design was based on an off-axis catadioptric configuration consisting of two mirrors and a collimating lens. The off-axis configuration was selected to eliminate the diffraction effects from an on-axis obscuration because that would degrade beam quality. This is important in a smaller aperture lidar system because coherent detection is highly sensitive to aberrations in the wavefront. The off axis configuration also minimized the backscatter of energy onto the detector. The system used a large diameter parabolic mirror and a hyperbolic secondary with an aspheric lens to expand a 1 cm diameter (measured at  $1/e^2$ ) Gaussian laser beam to a diameter of 25 cm (Table 2). This system fit within a 230 mm length (Figure 4). In anticipation of the SPARCLE mission, this telescope was designed, fabricated and tested as an engineering model.<sup>13,14</sup>

The telescope and support structure was fabricated from 6061-T6 Aluminum alloy to make the telescope athermal. The two mirrors were rough machined, thermally cycled to remove stress and to stabilize the blanks before diamond turning the optical surfaces. The aspheric surfaces were machined into the blanks using conventional SPDT technology in the Aluminum and then the



surfaces were electroless nickel plated and turned to the final surface figure. Post polishing was used to remove the diamond tooling marks and lower scattering by decreasing RMS surface roughness.

During the alignment of the system in the optics laboratory, it was found that a six degree-of-freedom (DOF) stage was needed on the secondary mirror and a single axis stage on the lens in order to achieve the required collimation and best wavefront quality possible. The complexity of the alignment requiring several multi-axis stages needed to be simplified.

### 5. SPARCLE TELESCOPE OPTOMECHANICAL DESIGN

In consideration of SPARCLE operational requirements, demanding different scanning patterns and accumulating several laser shots in each direction for improved sensitivity, a step-stare scanning method was selected over continuous scanning. Another reason for selecting the step-stare scanning method was to eliminate the need for optical derotator and misalignment angle compensator components, thus reducing the complexity and cost of the instrument's optical system. As a result, the telescope design became simpler. The step stare scanning lessened the constraint on the telescope by reducing its required field-of-view from 3 mrad to about 40  $\mu$ rad and eliminated the need for a back-relief space that would have been necessary for accommodating the derotator and misalignment angle compensator. The revised requirements are summarized in Table 3.

With the revised requirements, the telescope design was modified from a catadioptric design to a two element all reflective design. With the elimination of the lens, only the secondary mirror of the modified telescope needs to be adjusted to achieve optimal alignment. Currently, the system is envisioned to achieve alignment through the use of a 5-DOF stage instead of a 6-DOF stage on the secondary mirror, relying on complete radial symmetry of the secondary with respect to the optical axis to remove the need for one axis of motion. The complexity of alignment and the desired stability of the system once aligned meant that the stage could not be removed from the system prior to launch – the stage would have to fly.

Table 3. Second Generation SPARCLE Demonstration System Parameters as Designed

Input Beam Diameter	0.93 cm
Transmitted Beam Diameter	23.3 cm
Beam Quality	Diffraction Limited
Scanning Mode	Step-Stare every 22.5°
Boresight Lag Angle Compensation	None Required
Scan Full Angle	60°
Field-of-View	40 $\mu$ rad

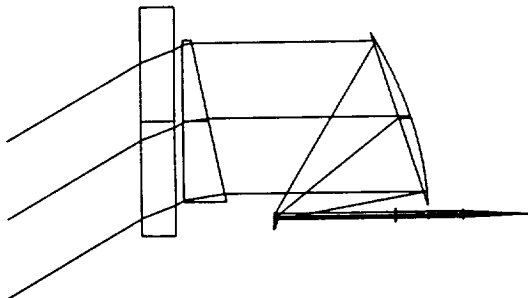


Figure 6. Improved telescope design.



Figure 7. Preliminary SPARCLE optics canister.

The complexity of the optomechanical design increased once the stage needed to fly because there were only two approaches to consider: have the stage be stiff enough to survive launch loads and maintain alignment or develop a means to anchor the stage after alignment which did not cause any stress induced creep over time. The first approach led to a robust design that was far too large and heavy to be accommodated within the experiment envelope. The second approach was lower weight but relied on a combination of mechanical and adhesive points to fix the stage in place after alignment. The latter approach was selected with the plan to align the optics on the laboratory bench and continue monitoring and adjusting the alignment while the adhesive cured. While this was labor intensive, it was lowest risk and acceptable since only one telescope system was going to be needed for SPARCLE. In addition, to maintain athermal design, the new stage should ideally be Aluminum to be compatible with the mirrors and telescope support structure. A solution in keeping with the philosophy of NASA to make use of high grade commercial components when possible has led to the consideration of a commercial 5-DOF stage. Commercial high precision linear actuators with electronic controls are more than capable of providing highly repeatable  $0.1\text{ }\mu\text{m}$  motion to achieve alignment. The low weight of the secondary (on the order of 2 lbs.) on the stage means that the actuators should have no difficulty in moving the mirror. One plan that is being considered is to monitor the telescope alignment (through interferometry) and secondary mirror orientation while applying slow-curing, low-shrinkage adhesive to selected areas of the stage to lock it in place. It is anticipated that the force of the actuators will be able to overcome the small distortions of the stage induced by the adhesive curing process and thereby realign the mirror. The adhesive contact at points will act much like an elastic flexure to provide tension to the stage. Once cured, the mirror should be fixed in position and the power and cables connected to the actuators will be removed. Because of the nature of the actuators, they will hold position with power down. If alignment is lost at a later date, the actuators can be used again to reacquire optimal alignment.

The modified design (Figure 6 and 7) increased the telescope length by nearly 5 cm, but it relaxed the fabrication tolerances and reduced system alignment complexity. Some other benefits were realized from this design approach. The removal of the lens negated any thermally induced index of refraction changes that would have adversely affected telescope focus. Also, the longer spacing between primary and secondary optics permitted a more gradual curvature on the primary and the use of a parabola in place of the hyperbola on the secondary. This eased the surface figure requirements only slightly; but, optically slower parabolic surfaces would be easier to fabricate and measure. The net effect is that the telescope has become easier to manufacture with the potential for better performance.

## 6. SUMMARY

An operating engineering model of the SPARCLE optical system has been designed, fabricated, and tested from which revised design specifications were derived. In addition, the SPARCLE operational scenario was revised which facilitated a redesign of the telescope. The net effect of both activities has produced a new telescope design. This design utilizes two mirrors without the need for a lens to expand and collimate the laser beam and only one 5-DOF alignment stage on the secondary mirror. Analysis is continuing to select the appropriate commercial alignment stage and the adhesive.

## 7. ACKNOWLEDGEMENTS

This work was supported by NASA Marshall Space Flight Center through a Cooperative Agreement with The University of Alabama in Huntsville at The Center for Applied Optics.

## 8. REFERENCES

1. R. Atlas, "Atmospheric observations and experiments to assess their usefulness in data assimilation," *J. Meteor. Soc. Japan*, Vol. 75, pp. 111-130 (1997).
2. M.J. Kavaya and G.D. Emmitt, "The space readiness coherent lidar experiment (SPARCLE) space shuttle mission," *Proc. of the SPIE Laser Radar Technology and Applications III Conference*, Vol. 3380 (1998).
3. R.T. Menzies and R.M. Hardesty, "Coherent doppler lidar for measurements of wind fields," *Proc. IEEE*, Vol. 77, pp. 449-462 (1989).
4. M. Huffaker and R.M. Hardesty, "Remote sensing of atmospheric wind velocities using solid state and  $\text{CO}_2$  coherent laser systems," *Proc. IEEE*, Vol. 84, No. 2, pp. 181-204 (1996).
5. M.J. Kavaya, S.W. Henderson and C.P. Hale, "Solid-state progress supports coherent laser-radar technology," *Laser Focus World*, August, pp. 83-93 (1989).
6. W.E. Baker, et.al., "Lidar-measured winds from space: a key component for weather and climate prediction," *Bulletin of*

- the American Meteorological Society, Vol. 76, No. 6, pp. 869-888 (1995).
7. R.G. Beranek, et.al., "Laser atmospheric wind sounder (LAWS)," Proc. of the SPIE Laser Applications in Meteorology and Earth and Atmospheric Remote Sensing, Vol. 1062, pp. 234-248 (1989).
8. M.J. Kavaya, et.al., Direct global measurements of tropospheric winds employing a simplified coherent laser radar using fully scaleable technology and technique," Proc. of the SPIE Space Instrumentation and Dual-Use Technologies Conference, Vol. 2214, pp. 237-249 (1994).
9. M.J. Kavaya, et.al., "Remote wind profiling with a solid-state Nd:YAG coherent lidar system," Optics Letters, Vol. 14, No. 15, pp. 776-778 (1989).
10. S.W. Henderson, et.al., "Eye-safe coherent laser radar system at 2.1-micron using Tm,Ho:YAG lasers," Optics Letters, Vol. 16, No. 10, pp. 773-7758 (1991).
11. M.J. Kavaya, "Novel technology for satellite based wind sensing," Proc. of the 1996 AIAA Space Programs and Technologies Conference, AIAA 96-4276 (1996).
12. U.N. Singh, et.al., "Injection seeded, room temperature, diode pumped, Ho,Tm:YLF laser with output energy of 600 mJ at 10 Hz," Proc. of the Advanced Solid State Lasers Conference, OSA AWC1, pp. 322-324 (1998).
13. A. Ahmad, F. Amzajerdian, et.al., "Design and fabrication of a compact lidar telescope," Proc. of the SPIE, Vol. 2832, pp. 34-42 (1996).
14. A. Ahmad, Y. Li, et.al., "Fabrication and testing of a low-cost compact lidar telescope," Proc. of the 9<sup>th</sup> Conference on Coherent Laser Radar, June 23-27, Linoping, Sweden (1997).

## Characterization of Optical subsystem for 2 $\mu$ m Coherent Lidars

Ye Li, Tim Blackwell, Joe Geary, Farzin Amzajerdian, Gary Spiers, Bruce Peters

Center for Applied Optics

University of Alabama in Huntsville, Huntsville, AL

and

Diana Chambers

Micro Craft Inc., Huntsville, AL

### ABSTRACT

This paper presents the test results on a compact, off-axis telescope which is the precursor projector/receiver for a NASA Shuttle-based coherent lidar system operating at a wavelength of 2 microns to measure atmospheric wind profiles. The afocal telescope has an entrance pupil diameter of 25 cm, and an angular magnification of 25x. To determine the transmitted and returned optical wavefront quality, the telescope was tested in a Twyman-Green configuration at the operational wavelength. Interferograms were obtained via an infrared camera, and analyzed using a digitizing tablet and WYKO WISP software. Interferograms were obtained with and without an 11.7 degree wedged silicon window located in the entrance pupil. This window, which rotates orthogonal to the telescope optical axis, serves as the lidar system scanner. The measured wavefront information from the interferometer was used in a GLAD heterodyne receiver model to predict the effect of the optical system on the lidar performance. The experimental setup and procedures will be described, and the measurement results of the coherent lidar optical subsystem will be presented in this paper.

### INTRODUCTION

The capabilities of coherent lidar systems for measurement of atmospheric winds have been demonstrated over the past 3 decades through successful ground-based and airborne campaigns<sup>1,2</sup>. However, it is only recently that several key technologies have advanced to a point where a compact, high fidelity system, suitable for deployment in space, could be developed. These technologies include high pulse energy, eye-safe, solid state transmitter lasers; Reliable continuous wave tunable lasers for use as master and local oscillator sources; Room temperature, wide bandwidth, semiconductor detectors operating in the near-infrared region; and light-weight, compact, athermal telescopes and scanners with high quality optical throughput. The lidar telescope and scanner along with their associated support structures account for most of the weight and size budget of any space-based coherent lidar instrument. Therefore, reducing their mass and size has a major impact on total mission cost. The imposed size and mass constraints, combined with stringent optical performance requirements create many challenges in the design, fabrication, assembly, and testing of such space based optical systems. Coherent detection is highly sensitive to aberrations in the signal phase front, and to relative alignment between the signal and the local oscillator beams. Consequently, performance is usually limited by the optical quality of the transmitter/receiver optical system. For relatively large apertures (25cm or greater), the lidar system performance is dominated by its telescope, scanner, or any other optical components that the signal radiation must transmit

through before entering the atmosphere. This includes any optical windows used for environmentally isolating the lidar instrument.

In anticipation of a space shuttle technology demonstration mission, we designed and fabricated a 25 cm prototype compact afocal telescope and specified a 30 cm polycrystalline silicon optical wedge scanner element that was then built by Diversified Optical Products. Both telescope and optical wedge were designed for operation at 2-micron wavelength in accordance with NASA's plan for the development and deployment of an eye-safe solid state coherent lidar to be placed in a hitchhiker payload canister inside the bay of the space shuttle.

The telescope design is based on an off-axis catadioptric configuration consisting of two mirrors and a collimating lens. This design eliminates any central obscuration generated by on axis systems. This telescope addresses all the major design issues associated with coherent lidars such as size, mass, wavefront quality, polarization purity, and very low optical backscatter. In this paper, we will discuss the design, fabrication technique, and performance of the telescope. Particular attention is paid to the interferometer configuration used for characterization of the telescope and wedge, and how the resulting measurements relate to coherent mixing efficiency and overall lidar performance.

### OPTICAL REQUIREMENTS AND DESCRIPTION

The functions of a coherent lidar optical system include expanding the laser beam, transmitting it to the atmosphere, receiving the backscattered radiation, and compensating for boresight errors caused by the scanner rotation and any spacecraft orbital motion. Design trade studies such as operational wavelength, atmospheric transmission, transmitted laser power, pointing accuracy and instrument sensitivity collectively determine the overall system requirements. Optical system requirements are additionally influenced by practical matters such as optical throughput, size and weight constraints, as well as ease of manufacture, alignment, and testing.

The requirements specific to this technology demonstration are:

- (1) input beam diameter of 1 cm
- (2) transmitted beam diameter of 25 cm
- (3) diffraction limited beam quality
- (4) accommodate both continuous and step-stare conical scanning
- (5) boresight lag angle compensation to within 1 micro-radian
- (6) 30 degree transmitter deflection angle

The telescope should also incorporate efficient polarization conversion from linear to circular and vice-versa for the transmitted and received beams. Optical transmission efficiency is a factor because the instrument must be as sensitive as possible to weak backscattering from atmospheric aerosols. The packaging constraints for this mission dictate that the system be more compact than standard configurations which leads to a faster optical system with more difficult fabrication requirements and tighter alignment tolerances. The optical design selected to meet these criteria was separated into two components, a telescope subsystem and a scanner subsystem. The telescope subsystem will perform the functions of beam expansion, polarization selection and

boresight correction while the scanner subsystem will deflect the beam through the required 30 degree angle and generate the conical scan pattern. Both were designed to be compact, as light as possible, and maintain optical throughput with high wavefront quality.

The beam expanding telescope design is an off-axis catadioptric system. An off-axis configuration was selected to eliminate any central obscuration which will degrade beam quality due to diffraction effects. This configuration also reduces direct backscattering into the lidar system receiver optical path. The telescope is a typical Cassegrain configuration with a parabolic primary mirror and a hyperbolic secondary mirror. The packaging constraints for this mission dictate that the system be considerably more compact than conventional configurations. To achieve such a compact package, a fast optical design was employed which led to more stringent fabrication and alignment tolerances. The telescope uses an aspheric negative tertiary lens to initiate expansion of the transmitted beam and to recollimate the received beam. The lens material was chosen because it transmits both the HeNe alignment beam wavelength and the 2.06 micron lidar system operational wavelength. An antireflection coated quarter-wave retardation plate was used in this design to distinguish polarization states between the transmitted and received beams. A lag angle compensation mechanism was designed to correct for boresight misalignment, due to scanner rotation during the round-trip time of a single pulse, to within 1 microradian. However, it was later decided to employ a step-stare scanning pattern, as opposed to a continuous scanning, for the technology demonstration instrument. The step-stare scanning eliminates the need for a dynamic lag angle compensator and allows for accumulating several laser shots at each pointing direction for improved sensitivity.

The optical layout of this compact telescope design is shown in Figure 1. The mirror axial spacing is 17.5 cm and the field-of-view is 0.17 degrees. No obscurations are present in the design and there is no vignetting. Further details of the optical design, wavefront error analysis and boresight sensitivity analysis for the telescope may be found in References <sup>3 4</sup>.

Design of the mounting and support structure for the telescope must also be considered. The primary requirements for this structure are that it be stable enough to maintain alignment during deployment and that it be compact enough to be accommodated within the hitchhiker can packaging constraints. The mechanical design for this prototype telescope consists of a box-type support structure where the mirrors and the quarter waveplate are mounted directly to the box. The recollimating lens is placed in a custom mount fixed to a translation stage, then attached to the box to facilitate alignment

Fabricating the mirrors and structure from the same material eliminates any misalignment due to differential thermal expansion. The scanner optical element is mounted separately. The most compact conical scanning technique currently in use for coherent lidar systems is a rotating optical wedge. The wedge material and specified wedge angle are chosen commensurate with the beam deflection requirements, then when the element is rotated about the telescope optical axis it will produce the required conical scan.

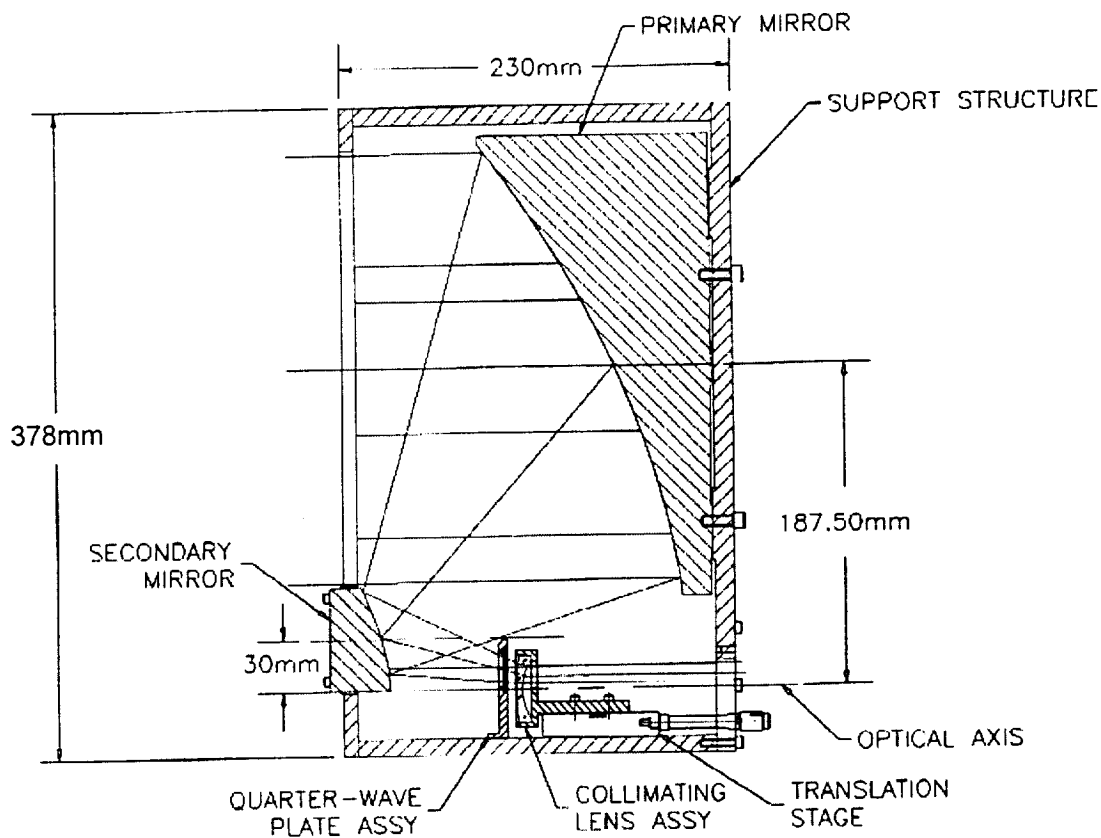


Figure 1. Telescope Optical Layout.

### IMPLEMENTATION OF PROTOTYPE OPTICAL SUBSYSTEM

This prototype optical subsystem was fabricated, assembled, and tested in order to evaluate its performance against the requirements set forth by this Shuttle mission. The telescope mirrors and support structure were all made from 6061-T6 aluminum alloy. The telescope primary and secondary mirrors were fabricated using precision diamond turning equipment. The primary mirror was machined on a 2-meter swing diameter Moore diamond turning machine and the secondary mirror was fabricated on a Pneumo 2000. The bare aluminum mirror blanks for both the primary and secondary were initially rough machined and then thermally cycled to enhance their long term stability. The front surface of each mirror was then diamond machined to obtain the desired aspherical surfaces. The mirrors were then plated with electroless nickel and diamond machined again to obtain the final optical figure. Post-polishing created the desired optical finish by reducing any surface roughness generated by the diamond tool. The post-polished mirrors were then gold plated to provide maximum reflectivity from the surfaces for maximum

transmission through the telescope. The gold plating also aids in maintaining polarization orientation upon reflection. Details of the opto-mechanical design and fabrication of the mirrors are described in Reference<sup>5</sup>. The assembled telescope is shown in Figure 2a.

The 30 cm diameter silicon optical wedge was fabricated and anti-reflective (AR) coated for the 2.06 micron operational wavelength. The wedge angle of this element is 11.7 degrees providing a 30 degree deflection angle. The wedge scanner is shown in Figure 2b.

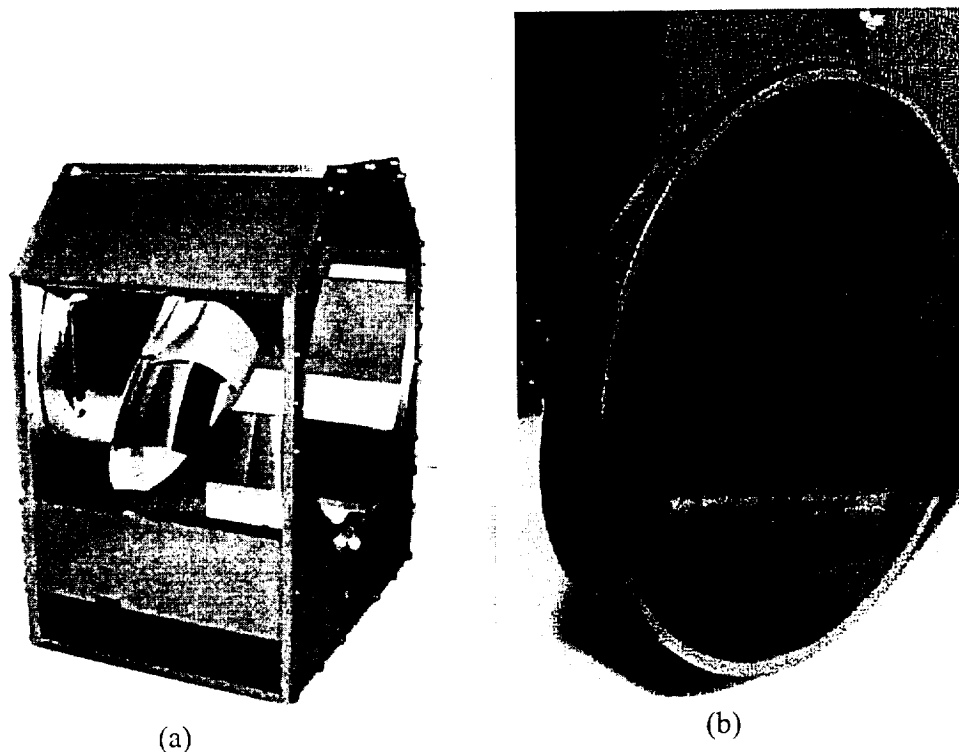


Figure 2. Telescope and Optical Wedge.

### CONFIGURATIONS FOR OPTICAL CHARACTERIZATION

The most critical performance characteristic for a coherent lidar optical subsystem is its optical wavefront quality which has a profound effect on system heterodyne efficiency. In order to quantify the wavefront quality at the instrument operational wavelength, a Twyman-Green interferometer was constructed using a 2.06 micron laser. Figure 3 illustrates the layout of the Twyman-Green interferometer. The beam source for the interferometer is a continuous wave Tm,Ho:YLF diode-pumped laser radiating 50 mW of power at 2.06 microns wavelength. The laser output is polarized and expanded by a factor of 2.2X yielding a 7.5 mm ( $1/e^2$ ) diameter collimated beam. This expanded beam passes through a 50-50 beamsplitter to create an object beam and a reference beam. The object beam passes through the components under test and is then reflected by a large optical flat. The optical flat has an RMS figure error of 0.014 waves at 0.6328 microns. After returning back through the telescope components, the object beam is re-combined with the reference beam by the beam splitter and directed to a camera that is sensitive in



the infrared spectrum. The reference arm of the interferometer contains a quarter-wave plate to ensure polarization matching with the returned object beam. The camera image containing the interference pattern is captured by an eight-bit frame grabber and stored on the computer for post-processing. The impact of the telescope and scanner performance on heterodyne efficiency is then predicted analytically by using the measured combined telescope and scanner element wavefront properties in a GLAD receiver model.

The effect of the optical subsystems on heterodyne efficiency can also be directly quantified by combining the object of the interferometer, as the received signal, with a second laser beam as the local oscillator. The signal and local oscillator beams are then combined by a beam splitter and directed toward a detector to generate a heterodyne signal. By comparing the magnitude of heterodyne signals with and without the telescope and scanner element, the effect of the optical subsystem on the overall lidar system efficiency can be determined. Construction of this test apparatus will be completed in the upcoming months.

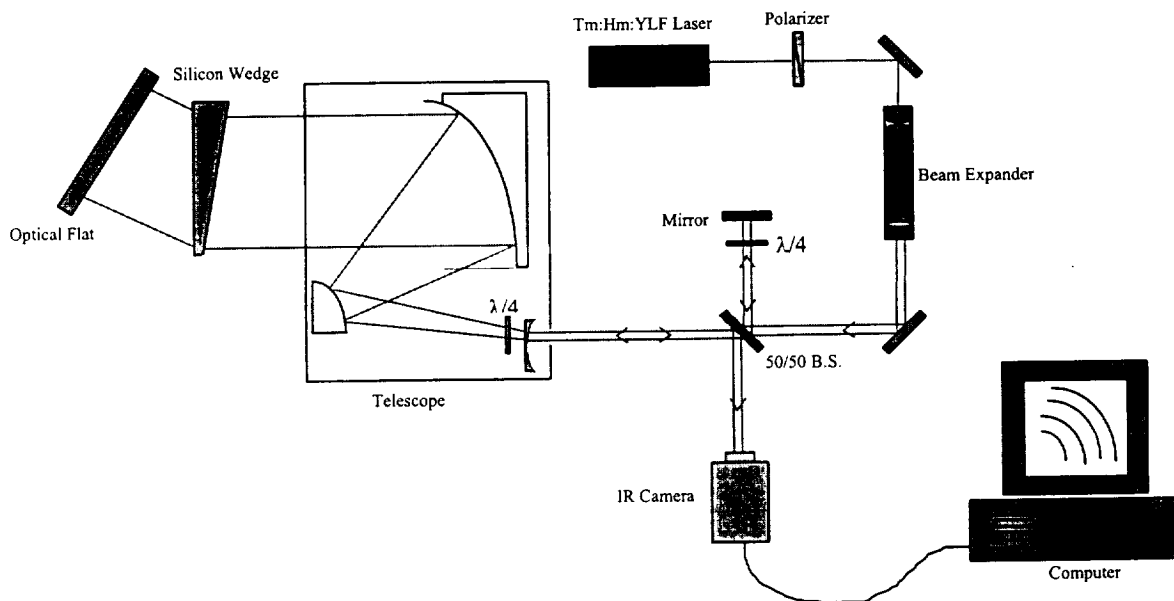


Figure 3. Twyman-Green interferometer setup.

## RESULTS

The Twyman-Green interferometer described above has been used to characterize the compact telescope independently and in combination with the optical wedge. The generated interference patterns were enhanced using an image processing software to reduce the background noise. The resulting patterns were then digitized to facilitate their interface with the WISP fringe analysis software. The WISP software provides wavefront analysis information, specifically the fourth order Seidel aberration coefficients and both the peak-to-valley and RMS wavefront error statistics.

One of the enhanced fringe patterns for the combined telescope and optical wedge is shown in Figure 4. The RMS wavefront error for the telescope alone was measured to be  $\lambda/11$ , and for the combined telescope and wedge was measured to be  $\lambda/9$ .

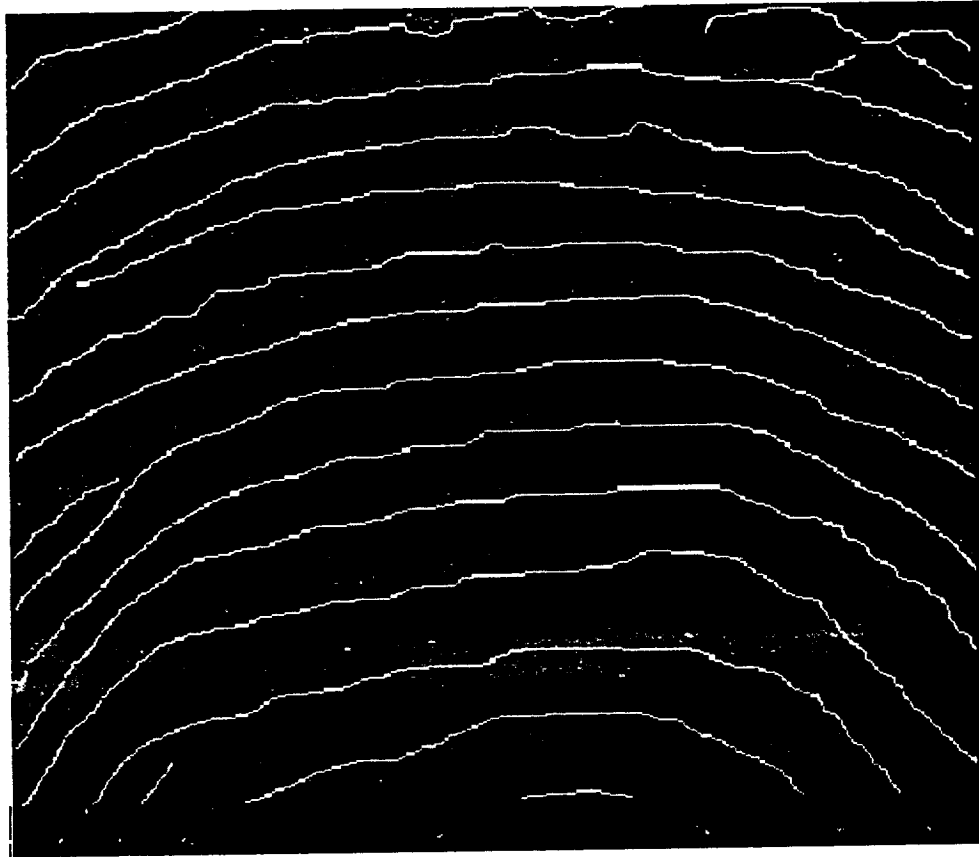


Figure 4. Interference pattern for combined telescope and optical wedge.

### SUMMARY

A prototype optical subsystem to meet the requirements of a space-borne coherent lidar technology demonstration mission planned by NASA has been designed, fabricated and assembled. The subsystem consists of a compact, off-axis, beam-expanding telescope and an optical wedge scanner. A Twyman-Green interferometer has been constructed in order to measure the optical subsystem performance at the operational wavelength of 2.06 microns and to determine its impact on overall lidar system sensitivity. Analytic efficiency predictions can be made by using the fringe patterns obtained during interferometric testing. Measurements of the telescope performance indicated a  $\lambda/11$  RMS wavefront when measured alone and  $\lambda/9$  RMS wavefront when measured in combination with the optical wedge. These wavefront figures, along with the measured optical transmission yield a reduction in heterodyne efficiency of approximately 50 percent. By incorporating a local-oscillator laser beam path with the interferometer, measurements of the effect of this optical subsystem on heterodyne efficiency can be directly quantified. Direct measurement of the heterodyne efficiency is planned to be performed in the near future.

This work was supported by NASA Marshall Space Flight Center.

#### REFERENCES

1. M. Huffaker and R. M. Hardesty, "Remote sensing of atmospheric wind velocities using solid state and CO<sub>2</sub> coherent laser systems," Proc. IEEE Vol. 84, No. 2, pp. 181-204, February 1996.
2. Targ, et. al., "Coherent lidar airborne wind sensor II: flight-test results at 2 and 10 micron," Appl. Opt. Vol. 35, No. 36, pp. 7117-7127, 20 December 1996.
3. Feng, A. Ahmad and F. Amzajerdian, "Design and analysis of a spaceborne lidar telescope," Proc. SPIE Vol. 2540, pp. 68-77, 1995.
4. A. Ahmad, F. Amzajerdian, C. Feng and Y. Li, "Design and fabrication of a compact lidar telescope", Proc. SPIE Vol. 2832, pp. 34-42, 1996.
5. Anees Ahmad, Ye Li, Farzin Amzajerdian, Darell Engelhaupt and Joseph Geary, "Fabrication and Testing of a low-cost Compact Lidar Telescope", 9:th Conference on Coherent Laser Radar, June 23-27, 1997, Linoping, Sweden

# Fabrication, metrology and modeling of the space-based lidar telescope for SPARCLE

B. R. Peters,\* P. J. Reardon, F. Amzajerian, T. S. Blackwell

Center for Applied Optics  
The University of Alabama in Huntsville  
Huntsville, Alabama 35899

## ABSTRACT

Over the past 7 years, NASA Marshall Space Flight Center (MSFC) through the Global Hydrology and Climate Center (GHCC) has been working; in collaboration with the University of Alabama in Huntsville (UAH) Center for Applied Optics (CAO), and others; towards demonstrating a solid state coherent Doppler lidar instrument for space-based global measurement of atmospheric winds. The Space Readiness Coherent Lidar Experiment (SPARCLE) was selected by NASA's New Millennium Program to demonstrate the feasibility and technology readiness of space-based coherent wind lidar. The CAO was responsible for the design, development, integration, and testing of the SPARCLE optical system. Operating at 2-micron wavelength, SPARCLE system performance is dominated by the optical quality of the transmitter/receiver optical system. The stringent optical performance requirements coupled with the demanding physical and environmental constraints of a space-based instrument necessitate extensive characterization of the telescope optical performance that is critical to predicting the lidar system efficiency and operation in space. Individual components have been measured prior to assembly and compared to the designed specifications. Based on the individual components, the telescope design was optimized to produce a suitable telescope. Once the telescope is completed, it will be tested and evaluated and the data shall be used to anchor computer based models of the optical system. Commercial optical modeling codes were used to evaluate the performance of the telescope under a variety of anticipated on-orbit environments and will eventually be compared to environmental tests conducted in the course of qualifying the telescope for flight. Detailed analysis using the "as built" data will help to reduce uncertainties within the lidar system model and will increase the accuracy of the lidar performance predictions.

**Keywords:** lidar, telescope, optical design, optical modeling, optical testing

## 3. INTRODUCTION

It is the stated goal of NASA's Earth Science Enterprise (ESE) to exploit the unique perspective of space-based remote optical instruments to observe and study large-scale environmental processes. The recent paradigm shift of ESE space flight programs has been away from missions that rely on large, expensive custom spacecraft with single instruments; and towards missions that are smaller, flexible, and more affordable yet while still accomplishing the science goals. In order to fit within the new requirements, the remote sensing instruments onboard must find innovative ways to reduce the size, weight, and power requirements of the sensor package along with realizing substantial reductions in cost.

As outlined in the NASA *Mission To Planet Earth: Capability/Technology Needs Assessment and Investment Plan*, several current optical instruments have a need for a meter-class telescope to support the study of land cover, atmospheric circulation, natural hazards, and lower tropospheric chemistry. Although the instruments proposed to study these science themes are different, they share a common unfulfilled technology need. Coherent Doppler lidar for vector wind measurement,<sup>1</sup> differential absorption lidar (DIAL) for atmospheric monitoring,<sup>2</sup> and Fourier transform infrared (FTIR) spectrometer to monitor concentration of gasses within the atmosphere<sup>3</sup> all incorporate a lightweight meter-class telescope within the instrument. The high quality telescope envisioned for each of these instruments has a 0.5-1.2 meter diameter primary mirror; with general performance parameters on the order of  $\lambda/10$  minimum wave front quality across the whole aperture; alignment stability over temperatures from  $-40^{\circ}$  to  $60^{\circ}\text{C}$ ; and overall optical system weights of  $15\text{ kg/m}^2$  of collection aperture.

---

\* Further corresponding author information –

Dr. Bruce R. Peters: Email: [petersb@email.uah.edu](mailto:petersb@email.uah.edu); WWW: <http://www.uah.edu/cao/>;  
Tel: 256-824-2526; Fax: 256-824-6618.

The instrument cost is usually directly related to instrument performance and the high quality, meter-class telescope can be a significant driver of total instrument costs. Lowering unit costs through production of many units (mass production) does not apply to space-based optical instruments because each instrument has specialized optical performance parameters that require different component designs and the quantities required are usually too low to benefit from economies of scale. There is also a direct cost associated with launching the significant mass/volume of a telescope. Telescope weight reduction is achievable but the current approaches tend to rely on exotic materials and specialized manufacturing techniques.<sup>4,5,6</sup> However, these materials typically have higher costs such as: more nonrecurring engineering, specialized tooling, and added handling costs (material quality, availability, waste disposal, etc.). Therefore, the cost of fabrication will rise along with an increase in technical risk that could negate the cost savings from the weight reduction. A remote sensing instrument with a meter-class telescope must be both lightweight, and economical to fabricate.

The Space Readiness Coherent Lidar Experiment (SPARCLE) was designed to be a first step towards demonstrating the feasibility of measuring troposphere wind velocities using the space shuttle in lieu of a satellite<sup>4</sup> and as a pathfinder for fabricating high optical quality telescopes, eventually meter class. The telescope was limited in size to a 25-cm aperture to permit easier packaging of the instrument into a Hitch Hiker canister. The SPARCLE instrument was designed to be an economical approach utilizing existing technologies and materials wherever possible. This resulted in many performance trade-offs to balance manufacturability against science mission requirements. In addition, the SPARCLE telescope was supposed to have regular metrology performed on parts and assemblies throughout the fabrication and alignment process in order to better characterize the final performance. This paper discusses the process of design, assembly and ongoing testing of the SPARCLE telescope. The project has since been cancelled but the telescope development, fabrication, alignment and testing for space qualification was continued.

## 2. DESIGN AND TOLERANCES

The SPARCLE telescope (Figures 1) consists of two off-axis parabolic mirrors in a Mersenne configuration. The off-axis configuration eliminates any central obscuration, eliminating undesirable diffraction effects and sources of direct back scattering into the lidar system receiver optical path. The size and mass constraints for any space-based coherent lidar dictate that the system be considerably more compact than conventional configurations. This telescope fits within an envelope of dimensions 38 x 32 x 33 cm and weighs slightly less than 20 kg. To achieve such a compact package, a fast optical design was employed which led to very tight fabrication and alignment tolerances.<sup>5</sup> The telescope is designed to have a full field of view of 80 microradians, an angular magnification of 25x, and a primary mirror aperture of 25-cm. The optical spacing between the primary and secondary mirror is 22.5-cm with the input and output beam offset by 15-cm.

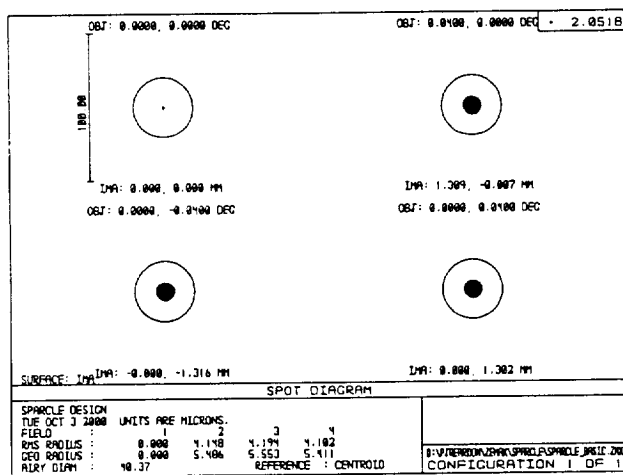


Figure 1a. SPARCLE telescope spot diagram.

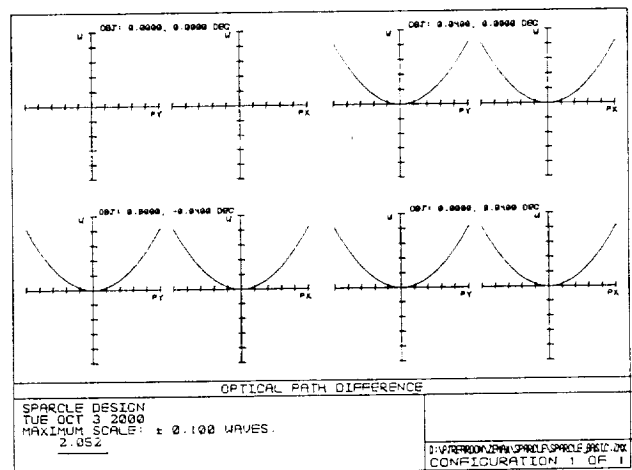
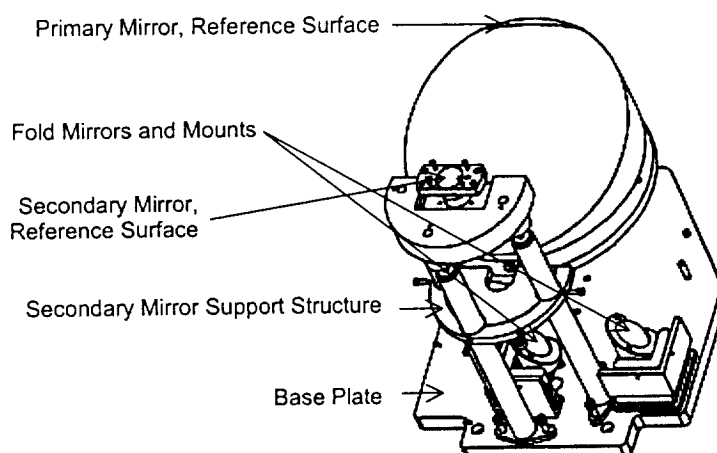


Figure 1b. SPARCLE telescope wavefront aberration.

To maintain the critical relative alignment between the primary and secondary mirrors over a relatively large operational temperature range and eliminate any misalignment due to differential thermal expansion, the telescope mirrors and its support structure are all made of the same type of aluminum material. Thus, this telescope system is athermal since the changes in the

optical properties of the mirrors (radius of curvature, thickness, etc.) with temperature are perfectly balanced by the expansion or contraction of the structural supports such that the system maintains its alignment.



**Figure 1c. SPARCLE optomechanical design.**

The telescope mirrors incorporate a number of alignment surfaces and precision pinholes for ease of alignment and integration with the lidar transceiver. The primary mirror has a 7.0-mm wide reference surface on the edge of its optical surface and three mounting pads, with optical-grade surfaces, on its back side. All four of the primary's reference surfaces are diamond turned to be parallel to each other and perpendicular to the virtual axis of the mirror's parabola. The combination of these reference surfaces and two precision pinholes establish the exact position and direction of the parabola's axis. The secondary mirror also has reference flat surfaces on the front and back. The primary mirror and the secondary support posts are mounted to an optical baseplate. The top surface of the optical baseplate is diamond turned to generate a large flat optical surface to serve as a datum plane and to further reduce any distortion that can result from attaching the primary mirror and the secondary mirror support posts to the baseplate. The backside of the optical baseplate also has three flat and parallel pads for mounting to the lidar transceiver without distorting the telescope alignment. Location and alignment of the transceiver beam to the telescope is achieved through two mirror tip-tilt-stages and a linear stage on one mirror that together deliver 5 degrees of freedom.

**Allowed Positional Errors**

Mirrors spacing	4.2 $\mu\text{m}$
De-center	5.5 $\mu\text{m}$
Tilt	23 $\mu\text{rad}$

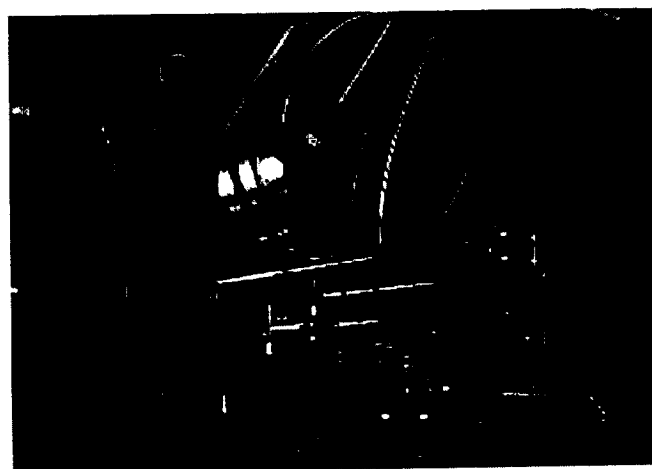
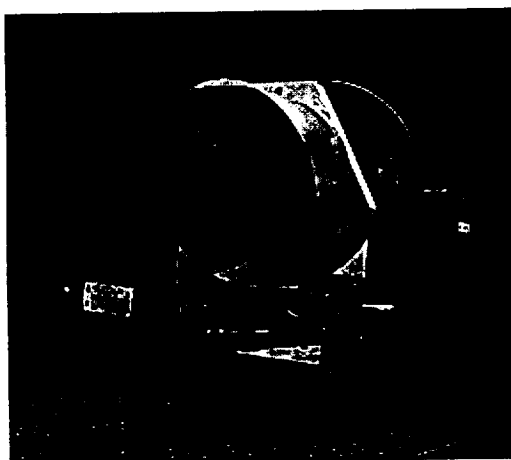


**Figure 2. Assembled engineering model of the SPARCLE telescope.**

The assembled engineering model of the SPARCLE telescope is shown in Figure 2. The telescope is shown mounted to a tip and tilt stage that is not part of the telescope and is only intended to facilitate optical testing.

### 3. FABRICATION AND COMPONENT PERFORMANCE

The required wavefront quality necessary for efficient coherent detection necessitated a high level of surface figure accuracy on the mirrors. Selection of aluminum for the mirror base material coupled with the aspheric surface geometry of the mirrors and the required surface figure accuracy dictated the use of high precision single point diamond turning fabrication techniques. However, the level of surface roughness that can be obtained from a diamond turned surface is too high for coherent lidar application that requires a very low scattering and back reflection by the optics. To achieve the required surface roughness, the mirrors were plated by a thin layer of nickel, before finish diamond machining, and then polished to reduce the diamond-turning grooves.

The following summarizes the fabrication process of mirrors that involved several organizations including NASA/Marshall Space Flight Center (MSFC), Lawrence Livermore National Laboratories (LLNL), and the University of Alabama in Huntsville/Center for Applied Optics(UAH/CAO). The mirrors were first rough machined to right dimensions and then stress-relieved along with all the diamond turning fixtures. The mirrors were then diamond turned to generate the optical surfaces to a figure accuracy of about one micron. Next, the mirrors were nickel-plated using an electroless plating technique. The nickel plating of the primary mirror was performed at the NASA/MSFC and the secondary mirror was plated at Speedring, Inc. At this stage the mirrors were prepared for the finish diamond turning. The finish diamond turning of the primary mirror was performed on the Large Optics Diamond Turning Machine (LODTM), at Lawrence Livermore National Laboratories, and the secondary mirror was diamond turned at the NASA/MSFC and the UAH/CAO facilities. The primary mirror was post-polished by Space Optics Research Labs (SORL) using a zone-polishing technique. The diamond turned secondary mirror, due to its small size and symmetric shape, turned out to have a sufficiently small surface roughness, requiring no post-polishing. The mirrors were then coated by a high purity alloy of gold, with a high reflectivity and durability, using a unique process developed by Epner Technologies Inc.<sup>6</sup> Gold-plating increased the surface reflectivity at 2-micron wavelength to more than 98% for a circular polarized beam. The final surface figure accuracy and roughness of the mirrors were measured to be 0.1 micron peak-to-valley and 20 angstroms RMS, respectively.

An additional facet of the system performance is the magnitude of polarizance induced by the telescope on the transmitted and collected light. The Epner Gold plating was ellipsometrically tested by J.A. Woollam<sup>7</sup> and found to contribute from 0.04 to 2.41 degrees of retardance and from essentially 0% to less than 0.4% diattenuation across the pupil. Thus, incident circularly polarized light exits the telescope as essentially unaffected circularly polarized light, as computed in Synopsys.<sup>8</sup>

The mirrors were thermally treated several times over the course of fabrication process to enhance their long-term stability and ensure the desired performance in the thermal environment of space. The internal stresses in the mirror material were released following the rough machining by performing a boiling water-liquid nitrogen treatment. In addition, the mirrors were stabilized by thermally cycling them several times before and after nickel-plating. The last phase of thermal treatment was performed over the specified telescope survivability temperature of -40C to 60C to minimize the risk of any misalignment due to temperature variations on orbit.

### 4. SYSTEM PERFORMANCE

The performance of the telescope will be measured at both 633 nm and 2060 nm wavelengths. The all-reflective design of the telescope allows the use of a commercial interferometer for measuring its wavefront quality. The wavefront quality measurements provide the Zernike coefficients, which define all the contributing low spatial-order aberrations introduced by imperfect fabrication and alignment. The Zernike coefficients from these measurements have been fed into a variety of computer models for further analyses of the telescope's anticipated behavior in the space environment. The computer models utilized include ASAP (Advanced System Analysis Program) optical analysis code<sup>9</sup> to simulate the thermal and vibrational environments of the space for quantifying the impact of the temperature gradients and vibrations present within the instrument canister (Figure 3).

A series of interferometric measurements of the assembled telescope were taken (Figure 4). Since the telescope is oriented in a horizontal position, measurements were taken with the secondary assembly oriented at the top, right, bottom and left side to allow for the subtraction of gravity induced distortions and bending. Based on this series of measurements, the telescope is

expected to perform to about 1/20 wave RMS at 2-micron in laboratory environment and about 1/15 wave at worse-case thermal scenarios in space.

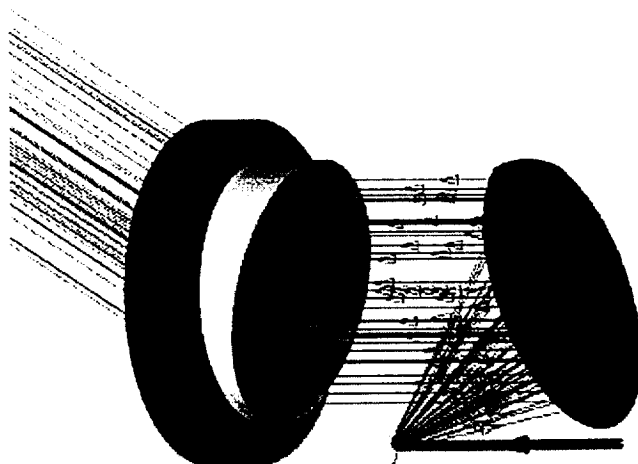


Figure 3. ASAP model of SPARCLE telescope.

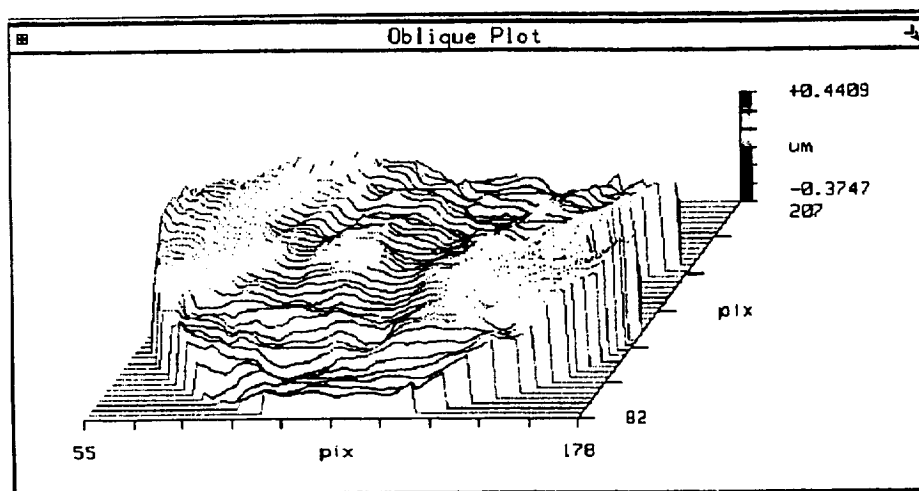


Figure 4. Interferometric measurements.

## 5. ENVIRONMENTAL TESTING

To meet space-qualified requirements, the SPARCLE telescope must undergo both thermal and vibration testing. Both tests are performed at NASA/MSFC with wavefront quality as the final merit function. In this section, we briefly discuss the setups (Figure 5) and current results for the testing of the first engineering model telescope. The testing is ongoing and the results presented here are preliminary in nature.

The telescope thermal tests were performed over its specified operational and survivability temperature ranges of 0 to 25 deg. C and -40 to 60 deg. C, respectively. For the operational thermal test, the telescope was cycled five times over the operational temperature range plus 5 degrees margin at both extremes, and twice from -10 deg. C to +35 deg. C. The telescope performance was continuously monitored by a phase-shift interferometer and its wavefront quality was recorded at 10 degrees intervals. The telescope maintained its alignment well over the whole measurement range. The wavefront quality changes



from -10 deg. C to +35 deg C were less than 0.02 rms wave at 2.05 microns. The telescope was then cycled four times over its survivability temperature range and its wavefront quality was measured displaying no change in its performance.

The telescope is currently being tested for survivability through launch loads. A sine sweep at 1/4g from 5 to 2000 Hz has already been applied in each of the telescope axes to determine its natural frequency. The natural frequency of the telescope was measured to be about 240 Hz along its optical axis (Z-axis) and 140 Hz in X and Y axes that are well beyond the 100 Hz design goal. The telescope is currently being prepared for a random vibration test at space shuttle qualification levels. The telescope will be vibrated along each of its orthogonal axes with a random spectrum having a composite load of 7.0g rms from 20 to 2000 Hz.

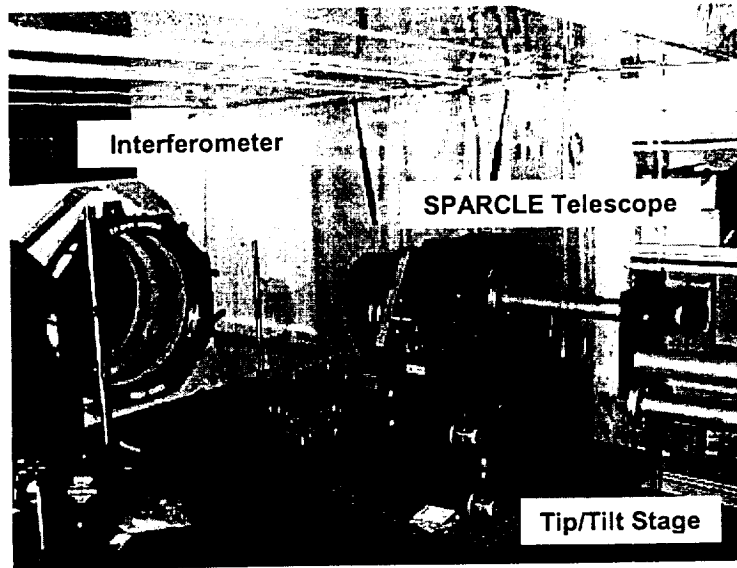


Figure 5. SPARCLE telescope under test.

## 6. CONCLUSION

The manufacturing of the SPARCLE telescope required careful consideration of all the competing performance, physical, and environmental requirements. Its design, fabrication, integration, and testing are particularly challenging for a coherent lidar instrument because of its sensitivity to wavefront quality. The development of SPARCLE telescope provided a valuable opportunity in understanding, baselining, and addressing the issues associated with a space-based lidar telescope and establishing a process for its space-qualification. The engineering model SPARCLE telescope has good wavefront quality and is capable of operating over a relatively large temperature range while tolerating the presence of considerable temperature gradients across its support structure and primary mirror. A number of optical and mechanical models have been developed for specifying the SPARCLE telescope fabrication and alignment tolerances, validating its design in withstanding the vibrational launch loads and operating over the anticipated temperature range. These analytical tools will be further adjusted for analyzing the results of the performance and environmental tests and predicating the telescope performance in orbit.

## 7. ACKNOWLEDGEMENT

This work was supported by NASA Marshall Space Flight Center Global Hydrology and Climate Center through a Cooperative Agreement with The University of Alabama in Huntsville at The Center for Applied Optics.

## 8. REFERENCES

1. M. J. Kavaya, G. D. Spiers, E. S. Lobl, J. Rothermel, and V. W. Keller, "Direct global measurements of tropospheric winds employing a simplified coherent laser radar using fully scalable technology and technique," *Proc. SPIE Vol. 2214, Space Instrumentation and Dual-Use Technologies*, 2214-31, Apr. 6, 1994.
2. H. Edner, K. Fredriksson, A. Sunesson, S. Svanberg, L. Uneus, and W. Wendt, "Mobile remote sensing system for atmospheric monitoring," *Appl. Opt.* 26, 4330-4338 (1987).

3. C. Camy-Peyret, "Ballon-borne infrared Fourier transform spectroscopy for measurement of atmospheric trace species," *Spectr. Acta* **51A**, 1143-1152 (1985).
4. M.J. Kavaya and G.D. Emmitt, "The space readiness coherent lidar experiment (SPARCLE) space shuttle mission," Proc. of the SPIE Laser Radar Technology and Applications III Conference, Vol. 3380 (1998).
5. Y. Li, F. Amzajerdian, B. R. Peters, T. S. Blackwell, and P. Reardon, Optical Design and Analyses of SPARCLE Telescope, 10th Coherent Laser Radar Conference, June 28-July 2, 1999, Mount Hood, OR, USA.
6. Herbert Kaplan (Contributing Editor), "Gold Rules the World of Infrared," *Photonics Spectra*, November 1997.
7. J.A. Woollam Co., Inc., Lincoln, NE
8. Synopsys, Optical Systems Design, Inc., East Boothbay, ME
9. ASAP, Breault Research Organization, Inc., Tucson, Arizona.

1. <sup>1</sup> M. J. Kavaya, G. D. Spiers, E. S. Lobl, J. Rothermel, and V. W. Keller, "Direct global measurements of tropospheric winds employing a simplified coherent laser radar using fully scalable technology and technique," Proc. SPIE Vol. 2214, Space Instrumentation and Dual-Use Technologies, 2214-31, Apr. 6, 1994.
2. <sup>2</sup> H. Edner, K. Fredriksson, A. Sunesson, S. Svanberg, L. Uneus, and W. Wendt, "Mobile remote sensing system for atmospheric monitoring," *Appl. Opt.* **26**, 4330-4338 (1987).
3. <sup>3</sup> C. Camy-Peyret, "Ballon-borne infrared Fourier transform spectroscopy for measurement of atmospheric trace species," *Spectr. Acta* **51A**, 1143-1152 (1985).
4. M.J. Kavaya and G.D. Emmitt, "The space readiness coherent lidar experiment (SPARCLE) space shuttle mission," Proc. of the SPIE Laser Radar Technology and Applications III Conference, Vol. 3380 (1998).
- 5 Y. Li, F. Amzajerjian, B. R. Peters, T. S. Blackwell, and P. Reardon, Optical Design and Analyses of SPARCLE Telescope, 10th Coherent Laser Radar Conference, June 28-July2, 1999, Mount Hood, OR, USA.
- 6 Herbert Kaplan (Contributing Editor), "Gold Rules the World of Infrared," *Photonics Spectra*, November 1997.

by Herbert Kaplan  
Contributing Editor

<sup>7</sup> J.A. Woollam Co., Inc., Lincoln, NE

<sup>8</sup> Synopsys, Optical Systems Design, Inc., East Boothbay, ME

<sup>9</sup> ASAP, Breault Research Organization, Inc., Tucson, Arizona.

## Thermal Considerations for the SPARCLE Optical System

Patrick J. Reardon, Bruce R. Peters, Farzin Amzajerjian\*  
University of Alabama in Huntsville  
Center for Applied Optics, OB 400  
Huntsville, AL 35899

### ABSTRACT

The SPAcE ReAdiness Coherent Lidar Experiment (SPARCLE) is the first demonstration of a coherent Doppler wind lidar in space. Coherent lidars can accurately measure the wind velocity by extracting the Doppler frequency shift in the back-scattered signal from the atmosphere through optical heterodyne (coherent) detection. Coherent detection is therefore highly sensitive to aberrations in the signal phase front, and to relative alignment between the signal and the local oscillator beams.

The telescope and scanning optics consist of an off-axis Mersenne telescope followed by a rotating wedge of silicon and a window of fused silica. The wedge is in very close proximity to the experiment window, and is essentially in contact with the scanner motor / encoder system. The can environment temperature is nominally 20°C, the window ranges from -20°C-0°C, and the scanner motor / encoder system alone could generate temperatures as high as 35°C. This thermal environment, coupled with the relatively large sensitivity of silicon's refractive index to temperature, has required careful thermal design and compensation techniques. This paper discusses the optical issues of these thermal effects and a variety of methods used to ameliorate them.

### 1. INTRODUCTION

The SPACe Readiness Coherent Lidar Experiment (SPARCLE) is the first demonstration of a coherent Doppler wind lidar in space<sup>1-3</sup>. SPARCLE will be flown aboard a space shuttle in middle part of 2001 as a stepping stone towards the development and deployment of a long-life-time operational instrument in the later part of next decade. SPARCLE is an ambitious project that is intended to evaluate the suitability of coherent lidar for wind measurements, demonstrate the maturity of the technology for space application, and provide a useable data set for model development and validation.

The SPARCLE optics consist primarily of an off-axis Mersenne telescope which expands the input laser by 25X to approximately 10" diameter followed by a rotating silicon wedge which produces the desired 30° half-angle conical scan, Figure 1. Also included in the beam path is a pair of beam steering mirrors for alignment and a fused silica window which provides the interface between the experiment environment and the vacuum of space.

Coherent detection is highly sensitive to aberrations in the signal phase front, and to relative alignment between the signal and the local oscillator beams. Consequently, the performance of coherent lidars is usually limited by the optical quality of the transmitter/receiver optical system. For SPARCLE, having a relatively large aperture (25 cm) and a very long operating range (400 km), compared to the previously developed 2-micron coherent lidars, the optical performance requirements are even more stringent. In addition with stringent performance requirements, the physical and environment constraints associated with this instrument further complicate the optical and opto-mechanical designs and challenge the limit of optical fabrication technologies.

In this paper, the thermal sensitivity of the SPARCLE optics is discussed. First, the results of a NASTRAN analysis evaluating the thermal displacements of the mirror and mount systems are briefly discussed; it was found that the all aluminum mirror and mount scheme yielded an essentially athermal system from 0-25°C. This is followed by a more detailed analysis of the thermally induced aberrations due to temperature variations in the silicon wedge. The analysis, which was verified experimentally, showed that isothermal changes in the wedge yields pointing changes of ~46 $\mu$ rad/°C, and that a 0.1°C radial

---

\* Correspondence: Email: [reardonp@email.uah.edu](mailto:reardonp@email.uah.edu), [petersb@email.uah.edu](mailto:petersb@email.uah.edu), [farzin.amzajerjian@msfc.nasa.gov](mailto:farzin.amzajerjian@msfc.nasa.gov), Phone:(256)890-6030; FAX: (256)890-6618

thermal gradient yields  $\sim 0.1$  waves of aberration RMS. Detailed thermal modeling of the entire canister/scanner/optics assembly has shown that, given proper coatings on the silicon wedge and fused silica window, the anticipated thermal gradients fall within optical performance tolerances.

## 2.0 THERMAL ENVIRONMENT OF SPARCLE

The experiment was designed to operate in an environment from  $0$ - $25^{\circ}\text{C}$  with a survival temperature of  $-40$  to  $60^{\circ}\text{C}$ . The laser lidar transceiver, telescope, and wedge will be housed in a Hitch Hiker Canister with a  $0.5$  atm of dry nitrogen. The experimental apparatus is not permitted to be attached to the inside of the canister; instead, the whole apparatus is mounted to the top plate which then supports the components and seals the canister. The top plate contains a  $32.385$  cm diameter  $5.0$  cm thick fused silica window to permit the lidar to exit and enter the instrument.

The heat sources within the optics canister are the transmitter, master oscillator, and local oscillator lasers, a scanner motor with encoder that rotates the wedge, and additional heaters regulated by an onboard life support system designed to maintain a minimal acceptable temperature within the can. The canister is planned to be located on a cross bay bridge within the shuttle bay with the shuttle bay pointing towards the earth throughout experiment operation. The canister would be exposed to reflected sunlight off of the earth and some small direct sun twice an orbit which would add to the heat load on the canister.

The laser system was equipped with an independent coolant thermal control system so most of its heat was drawn out of the canister. This was required because the lasers demanded high thermal stability in order to operate effectively and in fact, the control of the laser temperature became the driving parameter with regards towards experiment operational time. The inability of the independent laser coolant control system to maintain the laser coolant temperature to within  $\pm 2^{\circ}\text{C}$  for more than 2 hours was causing the experiment to have to cease operation after that time and to wait and cool down. It was believed that the cyclical operation would prevent any substantial increase in the ambient temperature of the canister.

The solar heating of the canister was minimized through reflective coatings on the exposed surfaces of the canister. The window on the top plate was also to be specially coated to reject solar energy and prevent it from entering the canister and heating the optics. With these measures in place and based on previous space shuttle data, the expected ambient interior environment within the canister was anticipated to be near or below  $0^{\circ}\text{C}$  and fairly uniform in temperature. The top plate however, was expected to be warmer and calculated to be as high as  $40^{\circ}\text{C}$  because the energy from the scanner motor turning the wedge was conducted into the plate. Therefore, the wedge which was conductively coupled to the scanner was also likely to heat up and conservative, worst-case calculations showed temperatures could reach  $60^{\circ}\text{C}$ . While the heat would eventually begin to be conducted down from the top plate through the structure and into the telescope, the large thermal mass and the limited conductive paths would serve to delay the heat flow until well after the experiment had finished operation.

Due to the sensitivity of the experiment to wavefront aberrations, the performance of the telescope under thermal variations became a major design driver. Because of power and space limitations, the telescope was not permitted to have any active realignment capability on orbit. This meant that the optics would have to passively operate over the specified temperature range and maintain adequate wavefront quality and pointing alignment. The only way to achieve this was to use an athermal design approach that would create uniform expansion or contraction with temperature changes. The use of aluminum for the mirrors and the telescope support structure would permit a change in the bulk temperature (all parts of the telescope would heat or cool uniformly) to be compensated for by a change in the radius of curvature of the mirrors (and hence the focal length) and a corresponding change in the mirror spacing. In this way, the telescope would theoretically always be in focus and maintain adequate wavefront quality. However, for the athermal system to work, the temperature gradients within the telescope needed to be minimized or the telescope would not experience a bulk temperature change. From finite element analysis to get displacements that were then evaluated with optical ray trace code, it was shown that a tolerable steady state temperature gradient within the telescope should be no more than  $2^{\circ}\text{C}$  to maintain diffraction limited performance, Figure 2. The optical performance of the perfectly aligned telescope and the performance from the thermally displaced telescope are compared in Figure 3, from which it is obvious that wavefront quality has not appreciably suffered. Furthermore, any temperature gradients that were created would not exist for long because the highly conductive aluminum and multiple conductive paths within the telescope would disperse the heat rapidly throughout the telescope within minutes.

As stated earlier, the wedge is mounted to the scanner motor assembly and will therefore be thermally coupled to the scanner through conduction. Heat loss from the wedge is limited to radiation and it is also minimal at best. While there is a cold window in very close proximity above the wedge, the radiative coupling of the wedge to the window is poor and there are no other significant paths for heat loss. Therefore, the bulk temperature of the wedge will be strongly influenced by the temperature of the scanner and will rise or fall accordingly while any temperature gradients within the wedge will be driven by the efficiency of the radiation coupling between the wedge and the window. As will be shown in a subsequent section, the potential for thermal gradients is of greatest concern to the wavefront quality of the beam transmitted through the wedge. Because of this heightened sensitivity to thermal gradients, it was determined that the wedge needs to perform as isothermally as possible.

## 2. WEDGE THERMAL RESPONSE

As previously discussed, the scanning of the lidar beam in SPARCLE is accomplished by rotating the wedge of silicon about the optical axis. Since the refractive index of silicon is fairly high,  $\sim 3.4$  at a wavelength of  $2\mu\text{m}$ , the wedge angle required to achieve the desired 30 degrees beam deflection is only 11.7 degrees. Thus, across its 10 inch diameter, the thickness of the wedge varies from 0.5-2.5 inches.

As a transmissive optical material, Silicon responds to temperature changes in two ways: bulk material dimensional changes driven by the coefficient of thermal expansion (CTE) and a change in the optical index of refraction as a function of temperature ( $dn/dT$ ). In the following sections, the thermal changes imparted to the wedge are separated into isothermal effects and thermal gradient effects. Each of these is further broken down into CTE and  $dn/dT$  effects, and their impact on SPARCLE performance is determined.

### 2.1 Wedge Response to CTE with Isothermal Variations:

The coefficient of thermal expansion (CTE) of silicon is given as  $2.7\text{--}3.1 \times 10^{-6}/^\circ\text{C}$  in a variety of references. This variation in CTE values is related to the specific material makeup and crystal structure and is typically measured and available from the material vendor. The positive CTE of silicon causes it to expand dimensionally when heated and to shrink when cooled. Mechanically, the differential thermal expansion of the metal wedge mount compared to the silicon wedge is incorporated into the gap between the edge of the wedge and the wedge mount. The maximum increase in the gap between the wedge and the aluminum wedge holder (nominally 0.007 in. at ambient conditions) as calculated over the operating temperature range of  $0\text{--}25^\circ\text{C}$  increases by 0.000043 in. This small variation is easily absorbed in the elastomeric gasket and should not affect the alignment of the wedge.

The optical effect of the CTE on the wedge under an isothermal temperature change can be described in the following manner. As the temperature of the wedge increases, the wedge expands uniformly and the wedge geometry and wedge angle will remain the same. Thus, the geometrical conditions of the wedge will remain the same, Figure 4 and the beam will not undergo a deflection change because of the isothermal CTE of the wedge.

### 2.2 Wedge Response to $dn/dT$ with Isothermal Variations:

The other way silicon responds to temperature change is in its optical index of refraction. The index of refraction change with respect to temperature, called here  $dn/dT$ , means that the optical path length through a given thickness of material will change as temperature changes. For the silicon wedge, this is equivalent to changing the wedge angle with changes in temperature. Since the wedge is designed and measured at one temperature, the optical index, and consequently the beam deflection due to the wedge, will be different if the temperature changes. For the SPARCLE wedge, the wedge was to be manufactured and measured at an ambient condition around  $20^\circ\text{C}$  but it may be operating at an elevated temperature on orbit. Although the wedge is assumed to be isothermal and therefore it will have similar geometry at both  $20^\circ\text{C}$  and the final operating temperature, the temperature increase will change the index of refraction for the

material. The effect will be to change the deflected angle of the beam, thereby affecting the pointing knowledge of the system, Figure 5.

Assuming that the  $dn/dT$  of the silicon is  $196 \times 10^{-6}/^{\circ}\text{C}$  (the most conservative value found in a search of several different references)<sup>4,5</sup> and assuming that the wedge undergoes a thermal soak (no gradients), then the deflection angle of the beam from the wedge will vary by  $\sim 46 \mu\text{rad}/^{\circ}\text{C}$ . As mentioned in the previous section, there is no contribution of CTE to this deflection angle variation because the wedge is assumed to be isothermal and ideally mounted.

### 2.3 Wedge Thermal Response to Temperature Gradients

While the bulk temperature  $dn/dT$  of the silicon wedge remains a minor challenge, a further complication is created when the effect of temperature gradients is incorporated into the optical performance of the wedge. Prior to this point, the wedge was assumed to be isothermal and the results of the material CTE and  $dn/dT$  on optical performance were described separately. If a gradient is present, the wedge will expand differentially, changing the wedge geometry, plus the index of refraction will no longer be uniform. The top and bottom surfaces of the wedge will develop curvature (concave on both surfaces if the center temperature of the wedge is lower) which will add aberration into the wavefront propagating through the wedge. The  $dn/dT$  effects will be exacerbated because the apparent wedge angle change will vary across the wedge; this can not be compensated with the calculated pointing correction approaches. To make matters worse, these aberrations will add to produce a larger aberration.

The wedge was thermally modeled at UAH for these preliminary environmental conditions; the circumference of the wedge was held at  $35^{\circ}\text{C}$ , the canister environment was held at  $20^{\circ}\text{C}$ , and the window was held at  $0^{\circ}\text{C}$ . The results of this analysis showed a thermal profile within the wedge as plotted in Figure 6; a gradient of  $\sim 1.2^{\circ}\text{C}$  could be present which yields approximately 6.9 waves peak-to-valley of aberration. The colder window located very close above, along with the very warm circumference of the wedge where it mounts to the scanner sets up a significant temperature gradient in the wedge. By arbitrarily setting the wedge edge temperature to  $27.5^{\circ}\text{C}$  the analysis showed that the gradient within the wedge was reduced to  $\sim 0.95^{\circ}\text{C}$  and the optical aberrations also decrease, scaling directly with the gradient reduction. In general, a  $0.1^{\circ}\text{C}$  temperature gradient from the thermal center to the edge of the wedge will produce  $\sim 0.6$  waves P-V of aberration.

Halving the temperature difference between the edge and the can environment does not halve the aberration. In fact, the aberration is more directly linked to the difference between the window and the edge temperature:  $6.9 \text{ waves} / 35.0^{\circ}\text{C} = 5.4 \text{ waves} / 27.5^{\circ}\text{C}$  and the actual gradient for the  $27.5^{\circ}\text{C}$  edge temperature produced 5.7 waves of aberration. Thus, based on this thermal model, the radiative thermal coupling between the wedge and the window is the primary driver for the creation of temperature gradients in the wedge.

The thermal analysis was calculated for a single slice through the wedge, hereafter called the meridional plane, and not for the full aperture. In order to determine the true impact on SPARCLE's performance, the full wave function is necessary. This calculation was far too cumbersome to extend using the analysis codes developed to this point, therefore, the full wavefront was estimated in two ways. The first method applies the standard optical aberration expansion terms<sup>6</sup> with consideration to the symmetry conditions of the wedge, the gradient, and the aberration functions. Using this method, we find that the aberration components that mostly comprise this radial thermal gradient induced aberration include tilt, defocus, 4<sup>th</sup> and 6<sup>th</sup> order coma, and 4<sup>th</sup> order spherical aberration, Figure 7. For a  $0.1^{\circ}\text{C}$  gradient, this aberration can be broken out as follows:

Aberration Type	Tilt	Defocus	4 <sup>th</sup> Order Coma	4 <sup>th</sup> Order Spherical	6 <sup>th</sup> Order Coma
Magnitude (waves) per $0.1^{\circ}\text{C}$	0.19	0.03	0.31	0.35	0.13

Table 1

It has been shown<sup>7</sup> that the contributions of the aberrations can be directly related to a reduction in heterodyne efficiency. The tilt induced by the radial gradient will not reduce the performance of the SPARCLE telescope; it will merely change the pointing direction by  $\sim 1.6 \mu\text{rad}/0.1^\circ\text{C}$  which is negligible. The defocus term is also negligible since it is so small, but both the 4<sup>th</sup> order coma and spherical aberration terms individually contribute about 1dB of heterodyne efficiency loss. As a very conservative estimate, these two contributions are added. Thus, each  $0.1^\circ\text{C}$  radial gradient will reduce the heterodyne efficiency by over 2dB, i.e.  $\sim 35\%$  of the signal is lost.

Although the method of aberration decomposition yields relatively simple coefficients to help understand how this particular aberration form will impact the SPARCLE performance, the resulting wavefront aberration does not truly conform to the constraints of the analysis. This analysis has assumed that the temperature at the edge of the wedge is a single value, i.e.,  $35^\circ\text{C}$ . This should result in a wavefront aberration around the edge of the wedge that varies directly with the thickness of the wedge at that point. However, the aberration decomposition method yields an oscillating value around the edge of the wedge. Therefore, an alternate method for generating the full wavefront aberration was implemented. In this method, a fitting function with a primarily quadratic and fourth order term was fit to the temperature gradient calculated along a single slice through the center of the wedge in the plane orthogonal to the meridional plane, hereafter known as the sagittal plane. This function was then fit across the entire aperture such that the calculated meridional temperatures are used and the correct edge temperature was used. Thus, the intervening values along the chord perpendicular to the meridional plane following the fitting function. Analyzing this wavefront also shows 0.1 waves RMS of aberration per  $0.1^\circ\text{C}$ , Figure 8. As there is essentially the identical RMS wavefront error between the two methods, and since the wavefront along the meridional plane is identical, we are quite confident that either result can be reliably used.

We note here that the nonuniform material expansion due to the CTE combined with the thermal gradient only accounts for about 4% of the total aberration; the large  $dn/dT$  of silicon is the primary source of this aberration.

It should also be noted that the optical analysis of thermal gradients described in this paper appears to ignore longitudinal gradients calculated in the wedge and considers only transverse gradients. In fact, an extension of the optical analysis was developed which subdivided the entire wedge into a stack of 5 identical wedges, each with a wedge angle 1/5th the total wedge angle, and applied the temperature gradient calculated for each individual layer. It was found that pure longitudinal gradients could be equivalently modeled by isothermally setting the wedge temperature to the average temperature of the longitudinal layers. Thus, longitudinal gradients contribute to pointing knowledge uncertainty.

To summarize, the thermal effects on the silicon wedge are tabulated in the following table.

Wedge Response	CTE	$dn/dT$	Significance
Isothermal	No Effect	$\sim 46 \mu\text{rad}/^\circ\text{C}$	Pointing instability, but pointing <i>knowledge</i> could be recovered with instrument modifications
Radial Gradients	$\sim 0.25$ waves aberration (P-V)/ $^\circ\text{C}$	$\sim 6.0$ waves aberration (P-V)/ $^\circ\text{C}$	Aberrations reduce heterodyne efficiency by $\sim 2\text{dB}/0.1^\circ\text{C}$ (35% signal reduction per $0.1^\circ\text{C}$ ).

Table 2

### 3. DETAILED MODELING

At this point, the preliminary analysis showed that a thermal gradient in the wedge may exist and that the gradient may be large enough to seriously impact the performance of the SPARCLE system. Thus, an effort was undertaken to refine the thermal model to determine more accurately the anticipated thermal



behavior of the experiment, verify our assumptions and material property constants, and investigate ways to ameliorate the thermal gradients.

### 3.1 Detailed Modeling: Optical Model

At this point, the modeling for the structure of the full wavefront aberration was considered sufficiently accurate, but experimental verification was desired. In addition, the magnitude of the aberration from the thermally altered wedge and its effect on SPARCLE performance needed refinement. Thus, an experiment was set up to both verify a value of the  $dn/dT$  of silicon and to confirm the model which tied thermal variations in silicon to optical path changes.

The experiment consisted of a 2mm laser source expanded up to a 50mm diameter collimated beam for use in a Twyman-Green interferometer, Figure 9. A prototype silicon wedge with roughly the same geometry as the SPARCLE wedge was placed in the object path of the interferometer with the beam passing through the thickest portion of the wedge. A mirror was then positioned to fluff on the fringes as much as possible. At this point, temperature sensors were placed on the wedge around the region through which the beam passed and an IR camera was set up to view the wedge. A heater, positioned at the thick edge of the wedge, was then turned on, and thermocouple data, IR camera images, and interference fringes were simultaneously taken as thermal gradients grew across the wedge, Figures 10-11.

Four data sets with essentially linear gradients of  $0.8^\circ\text{C}$ ,  $0.9^\circ\text{C}$ ,  $0.8^\circ\text{C}$ , and  $1.0^\circ\text{C}$  across the field of view of the interferometer were analyzed. The gradients and base temperatures were determined using the thermocouple and IR camera data. The fringe data was evaluated using the software package WISP<sup>8</sup>. The results were then used to calculate a  $dn/dT$  value for silicon. The result was a  $dn/dT$  value of  $163 \times 10^{-6}/^\circ\text{C}$  with a standard deviation of  $6 \times 10^{-6}/^\circ\text{C}$ . Thus, the experiment validates the modeling well within the tolerances of the experiment. In addition, the experiment yields a  $dn/dT$  value which is well within the values given in texts reviewed. Note, however, that it is 17% lower than the value of  $196 \times 10^{-6}/^\circ\text{C}$  used in the previous thermal modeling of the wedge.

Since there was now confidence in the  $dn/dT$  value and the model which connects temperature gradients in the wedge to wavefront aberration, a further refinement of the impact of this aberration on the performance of SPARCLE was undertaken. Using the full wavefront aberration form derived from the standard optical aberrations and symmetry arguments, this wavefront was decomposed into another standard representation of wavefront aberrations, Zernike polynomials<sup>9</sup>. The Zernike terms could then be implemented into the software package GLAD<sup>10</sup>. GLAD calculates the complete far-field propagation of the beam. This package can then be used to perform analysis based on the use of the back propagated local oscillator model (BPLO)<sup>11,12</sup> for evaluating coherent lidar performance. From this analysis, it is shown that a  $0.1^\circ\text{C}$  gradient will decrease the SPARCLE performance by 1.8dB; this value was determined to be within the requirements for the SPARCLE mission.

### 3.2 Detailed Modeling: Thermal Model

As the preliminary modeling had shown, the primary driver for the thermal gradient in the wedge was a result of the thermal coupling between the cold window and the hot wedge. Decreasing the temperature between these elements would reduce the gradient. Decreasing the radiative thermal coupling between the wedge and the window would also reduce the gradient. In addition to exploring ways of reducing the conduction from the scanner to the wedge by altering the wedge mount materials, we put our effort into investigating ways to radiatively decouple the wedge and window and to provide the resulting parameters for the detailed analysis.

Uncoated silicon reflects ~30% of the incident thermal radiation due to Fresnel losses. However, it transmits thermal radiation well except for the waveband from  $9\text{-}20\mu\text{m}$  where it strongly absorbs. Given the thermal energy of a 300K blackbody, this spectrum accounts for ~65% of the energy. Thus, the thermal emissivity of uncoated silicon is approximately 0.3. Fused silica, on the other hand, is an absorber of IR radiation except for low reflection losses, thus its emissivity is quite high, ~0.8. Note that a perfect blackbody has an emissivity of 1. To eliminate the radiative thermal coupling between the wedge and the window, reducing these emissivities is necessary. Thus, a special coating design is required which transmits the  $2.0\mu\text{m}$  SPARCLE operating wavelength very well, but reflects the thermal energy and therefore decouples the wedge and window.

An additional complication in the coating design is that the optical window must also reject solar radiation, both from the direct illumination the experiment undergoes twice per orbit and from the albedo. To make the coating designer's job even more difficult, the coating materials must be space qualified.

An initial survey of coating vendors provided data for coatings which reject 65% of the solar radiation at each surface of the fused silica window and 60% of the thermal radiation at each surface of the silicon wedge. These particular coating designs did not appreciably alter the IR emissivity. Thus, the physical parameters used in the thermal analysis are tabulated in Table 2.

Parameter	Values
<b>Fused Silica Window</b>	
Solar Absorption	0.0
Solar Transmission	0.2
Solar Reflection	0.8
IR Transmission	0
Total Hemispherical IR Emissivity (Top)	0.82
Total Hemispherical IR Emissivity (Bot)	0.82
<b>Silicon Wedge (Facing Window)</b>	
Solar Absorption	0.38
Solar Transmission	0.02
Solar Reflection	0.6
Total Hemispherical IR Emissivity	0.3
<b>Silicon Wedge (Bottom Facing Telescope)</b>	
Total Hemispherical IR Emissivity	0.3
<b>Silicon Wedge</b>	
Thermal Conductivity vs Temp (0-25C)	191W/(m-K) @ 250K, 140W/(m-K) @ 300K
Specific Heat vs Temp (0-25C)	0.18cal/(g C) = 0.75J/(g K)
Density	2.33g/cm <sup>3</sup> = 145.46lbs/ft <sup>3</sup>

Table 3

In addition to these new parameters, the thermal conditions of the canister had become better defined. The thermal analysis was performed using the thermal codes RadCAD<sup>13</sup> and SINDA<sup>14</sup>. The results of the thermal analysis showed that a gradient of ~0.06°C will result in the wedge. This value meets the specifications for the required performance of the SPARCLE mission. Thus, the SPARCLE telescope and scanner system should successfully function on its mission.

#### 4. CONCLUSION

SPARCLE is a demanding and aggressive scientific mission. As such, the demands on the individual components and their interdependence is high. The optical system, consisting of the 25x beam expanding telescope, the rotating Silicon wedge, and the canister window must perform to challenging levels. As designed, these components greatly exceed all of the scientific requirements for the mission. When integrated into the complete experiment, including the many heat sources, extensive modeling and experimental measurements have indicated that the system will still perform as required.

## ACKNOWLEDGMENTS

The authors would like to thank Tim Blackwell and Ye Li, of UAH/CAO for performing the wedge testing, and Gary Spiers also of UAH/CAO for the GLAD analysis. In addition, we would like to thank, John Sharp of NASA/MSFC for performing the detailed thermal analysis.

## REFERENCES

1. M.J. Kavaya, G.D. Emmitt, "The Space Readiness Coherent Lidar Experiment (SPARCLE) Space Shuttle Mission," Proc. SPIE Vol. 3380, p. 2-11, Conference on Laser Radar Technology and Applications III, 12th Annual International Symposium on Aerospace/Defense Sensing, Simulation, and Controls, AeroSense, Orlando, FL (1998).
2. A. Ahmad, F. Amzajerdian, C. Feng, Y. Li, "Design and fabrication of a compact lidar telescope," Proc. SPIE Vol. 2832, pp. 34-42, 1996.
3. Y. Li, T.S. Blackwell, J.M. Geary, F. Amzajerdian, G.D. Spiers, B.R. Peters, D.M. Chambers, "Characterization of an optical subsystem for 2-um coherent lidars," Proc. SPIE Vol. 3479, p. 122-129, 1998.
4. W.J. Tropf, M.E. Thomas, T.J. Harris, "Properties of Crystals and Glasses", *OSA Handbook of Optics; Devices, Measurements, and Properties*, M. Bass, Ed., McGraw-Hill, pp. 33.53, 33.58, 33.59, 1995.
5. M.J. Dodge, "Refractive Index," *Handbook of Laser Science and Technology*, Vol. IV, CRC Press, Inc., p. 38, 1986.
6. M. Born, E. Wolf, *Principles of Optics*, Pergamon Press, pp.211-218, 1964.
7. D.M. Chambers, "Modeling heterodyne efficiency for coherent laser radar in the presence of aberrations," *Optics Express*, Vol.1, No. 3, Page 60, 1997.
8. WISP, WYCO Corporation, Tucson, AZ.
9. Ref. 5, pp. 464-468.
10. GLAD, Applied Optics Research, Escondido, CA.
11. B. J. Rye, "Primary aberration contribution to incoherent backscatter heterodyne lidar returns," *Appl. Opt.* 21(5), 839-844 (1982).
12. B. J. Rye, R. G. Frehlich, "Optimal truncation and optical efficiency of an apertured coherent lidar focused on an incoherent backscatter target," *Appl. Opt.* 31(15), 2891-2899 (1992)
13. RadCAD, Cullimore and Ring Technologies, Inc., Littleton, CO.
14. SINDA, Network Analysis, Inc., Tempe, AZ.

## Optical Design and Analyses of SPARCLE Telescope

Ye Li, Farzin Amzajerdian, Bruce Peters, Tim Blackwell, Pat Reardon

Center for Applied Optics  
University of Alabama in Huntsville  
Huntsville, AL 35899

Phone: (205) 890-6030, Fax: (205) 890-6618, E-mail: liy@email.uah.edu

### Abstract

SPARCLE demands a high level of performance from its telescope system under stringent physical and environmental constraints. To meet the SPARCLE demanding requirements, the telescope system design utilizes state-of-the-art optical fabrication and coating technologies. This paper describes the telescope design, provides its fabrication and alignment tolerances, and discusses its sensitivity and performance analyses.

### 1. Introduction

SPARCLE is the SSpace Readiness Coherent Lidar Experiment. The project, supported by NASA, is a technology demonstration on the space shuttle for space-based Doppler coherent lidar atmospheric wind velocity measurement [1]. The optical telescope system includes a 25cm off-axis beam expanding telescope, a 25-cm silicon wedge scanner, and a 32-cm Fused Silica optical window. The 2.0 micron wavelength laser source is expanded with this optical system at a power of 25x and transmitted to the atmosphere at a conical scanning angle of 30 degrees. The optical system also serves as receiver for the back scattered radiation signal from the atmosphere.

Coherent laser radar records information about the phase of the back-scattered radiation with respect to a local reference or local oscillator. The phase of the light contains information about the Doppler shifted mean frequency, frequency spectrum, and polarization of the photons. The wind velocity information, which is the main interest of SPARCLE, is encoded in the mean frequency. The signal-to-noise ratio of coherent lidar system is very sensitive to the optical performance of the transmitting and receiving beams [Diana]. The major design issues for coherent detection lidar are the wavefront quality, polarization purity, and a minimum backscattering from the optical surfaces. Eliminating optical degradations from thermal effects on the mechanical structure and the optical components is also critical for the space-based coherent lidar system. In order to obtain a diffraction limited optical system, the optical fabrication technologies and tolerances, optical testing capabilities, and alignment sensitivities have to all be considered in the design phase to make sure that the optical system can be physically produced.

The SPARCLE telescope system was designed based on the gained experience from the prototyped telescope[2], and the state-of-the arts optical fabrication technologies. This technologies include utilizing the Large Optics Diamond Turning Machine(LODTM) at Lawrence Livermore National Lab for the primary mirror fabrication, Laser gold plating of optical mirrors at Epner Technology, and multi-layer anti-reflection coating at the operating wavelength of 2.0 microns and a high reflection coating to cut off the solar and IR thermal radiation for the optical window and silicon wedge at Diversified Optical Products Inc..

### 1. Optical Design

#### 1.1 Beam Expanding Telescope

The volume of the optical canister on the space shuttle and the step-stare scanning technique used by SPARCLE constrained us to choose a two paraboloid afocal Mersenne configuration as the beam expanding telescope. The off-axis beam expander was selected to eliminate the central obscuration and

back scattering of an on-axis system which would degrade the heterodyne mixing efficiency and signal to noise ratio. The all reflective optical components can be built with the same aluminum alloy as the mechanical structures eliminate differential thermal expansion due to different materials.

The diffraction limited beam expander was designed and modeled by using ZEMAX optical software and verified by using SYNOPSIS optical software with a full field of view of 80 micro-radians, angular magnification of 25x, and a primary mirror aperture of 25 cm. The optical spacing between the primary and secondary mirror is 22.5 cm with a primary mirror operating at F#0.9 and a de-center of 15 cm. The optical 3D layout is shown in Figure 1. In addition, a small optical flat with a width of 7 mm was designed on the outer radial edge of the primary mirror as a reference for optical fabrication, testing and system integration. The secondary mirror has a physical aperture of 3 cm with a symmetric shape to ease the optical fabrication and optical alignment stage. A portion 6 mm off-axis is used for delivering the laser beam. The backside of the secondary mirror was designed to have an optical flat surface of 2.5cm diameter on the central area for telescope alignment and integration using a ZYGO interferometer.

## 1.2 Optical Wedge and Optical Window

The wedge scanner in SPARCLE telescope system is required for deflecting the expanded and collimated laser beam to a conical angle of 30 degrees. Several materials have been investigated based on their indexes of refraction, optical properties, and thermal properties. Single crystal silicon at optical window grade was the best choice of material for the wedge scanner. The wedge angle of 11.7 degrees for silicon with an index of refraction of 3.45 at a wavelength of 2.0 microns was calculated for the scanning angle of 30 degrees. The physical diameter of 24.8cm of the wedge was decided based on the bolt circle for mounting of the wedge holder to the scanner. The optical clear aperture is 22.6cm in diameter, which is the entrance pupil for the receiving optical system. The surface figure for both wedge surfaces need to be better than 1/6 waves peak to valley at 0.633 micron wavelength, which will provide a 1/30 wave RMS transmitted wavefront accuracy. The wedge will produce a transmission of better than 93% for the operating wavelength with a circular polarization maintained at better than a 97% ratio of minor and major axes of the polarization states.

Fused silica material has been selected as the optical window material for the Hitchhiker canister because of its high index homogeneity, high transmission in IR, low thermal expansion and thermal optical coefficient, and excellent mechanical properties. The optical window for SPARCLE serves as the interface between the pressurized optical canister and the outside vacuum. The half atmosphere pressure of dry nitrogen inside the canister could deform the flat window consequently degrade the optical wavefront quality. The window thickness of 5 cm was decided by simulating the window deformation curve with high order even aspheric surfaces in the ZEMAX model and analyzing the optical performance with the criterion of diffraction limited performance. The surface figure for both surfaces of the window will be fabricated in 1/6 wave peak to valley at 0.633 microns. Then the transmissive wavefront will be better than 1/30 wave RMS at 2.0 microns. The total transmission will be better than 95% with application of an anti-reflection coating at 2.0 microns.

## 3. Optical Analyses

### 3.1 Optical performance

A Zemax optical design model was set up to send a bundle of geometrical rays from infinity through the pressurized fused silicon window, silicon wedge, and the confocal parabola telescope from infinity at a deflection angle of 30 degrees with a full field of view of 80 micro-radians. The spot size was obtained by using an ideal lens to focus the collimated output rays down to a point. The focussed spot was contained within the diffraction limited Airy disc with the Strehl ratio of 93% and the RMS wavefront error of 1/25 at the operating wavelength. The optical performance is also shown in the Figure 1.

### 3.2 Tolerance and Sensitivity

Tolerance and sensitivity analysis is very important to build a working optical system. Parametric sensitivity and tolerance of the telescope has been analyzed to determine its optical performance for the fabrication and assembly.

#### 3.2.1 Fabrication and Assembly Tolerances

The analyses assume a fixed focal point in space. However, the accepted focal point is surround by a volumetric tolerance.

Conic constant of primary mirror:	+/- 0.0003
Conic constant of secondary mirror:	+/- 0.001
Radius curvature of primary mirror:	+/- 10.0 $\mu\text{m}$
Radius curvature of secondary mirror:	+/- 5.0 $\mu\text{m}$
Total irregularity of each mirror:	0.5 fringes
y - tilt of primary mirror:	0.01° ( 170 $\mu\text{rad}$ )
x - tilt of primary mirror:	0.01 °
x and y de-center of primary mirror:	10 $\mu\text{m}$

### 3.2.2 Secondary mirror alignment ranges and sensitivities

Secondary mirror is used as a compensator with 5 DOF. The criteria of optical performance was set to be 1/20 RMS wavefront error.

z - translation:	10 $\mu\text{m}$ with resolution of 1.0 $\mu\text{m}$
x - de-center:	40 $\mu\text{m}$ with resolution of 1.0 $\mu\text{m}$
y - de-center:	65 $\mu\text{m}$ with resolution of 1.0 $\mu\text{m}$
x - tilt:	0.05 ° with resolution of 0.001 °
y - tilt:	0.05 ° with resolution of 0.001 °
z - tilt:	not needed due to the symmetry of the secondary mirror

### 3.2.3 Instability tolerances

Assuming the fixed focal point, to meet 8/20 RMS wavefront quality (Required wavefront quality is 8/15), the aligned telescope is required to be stable.

Mirrors spacing :	4.2 $\mu\text{m}$
x - de-center:	8.2 $\mu\text{m}$
y - de-center:	5.5 $\mu\text{m}$
x - tilt:	0.0013° (22 $\mu\text{rad}$ )
y - tilt:	0.002° (35 $\mu\text{rad}$ )
Radius curvature of pri. mir.:	8.5 $\mu\text{m}$
Conic constant of pri. mir.:	1.2 $\mu\text{m}$
Radius curvature of sec. mir.:	8.5 $\mu\text{m}$
Conic constant of pri. mir.:	3.0 $\mu\text{m}$

## 3.3 Thermal Analyses

The thermal effect has to be considered for any optical system used in space or any severe environment. Two thermal issues could affect the optical performance to the system. One is the thermal soak since the working temperature range for the telescope is from 0 to 25 °C, but the telescope was designed at 20 °C. Another one is the thermal gradient between or inside the optical components. These two cases have been analyzed in the optical design model for the beam expanding telescope. The thermal analysis of the window and wedge can be referenced to [3]

### 3.3.1 Telescope operated at equilibrium temperature from 0 to 25 °C

Since mirrors and structure made of the same material of aluminum alloy 6061-T6 with TCE (Thermal Coefficient of Expansion) of  $23.5 \times 10^{-6}$ , the radius of curvature and spacing of the mirrors changed simultaneously with the temperature change.

#### Analyzed results:

- (1) If temperature reduced to 0.0°C from the designed temperature of 20 °C,  
Primary mirror radius of curvature changes by -0.22 mm

Secondary mirror radius of curvature changes by -0.009 mm  
 Spacing between primary and secondary changes by -0.106 mm

(2) The optical performance had no effect from the different temperatures. So the beam expanding telescope is insensitive to thermal soaks. Due to the non-symmetry of the off-axis configuration, there maybe some minor effect from thermal expansion on a system level. The detailed thermal analysis can be done with the real geometry setup, or thermal testing maybe required to verify the optical performance.

### 3.3.2 Telescope thermal gradient analyses

The expansion of the structure between the primary and secondary mirrors was computed by assuming that the thermal gradient had a linear distribution over the length of structure and the temperature was constant in each small segment. The computed optical spacing from a thermal gradient and the different temperatures at the primary and secondary mirrors was entered into the optical design model for performance analysis.

Results for thermal gradient of 2 °C:

RMS wavefront error = 0.09 waves @ 2.0  $\mu\text{m}$  (when primary = 20°C, secondary = 20 +/- 2 °C)

RMS wavefront error = 0.07 waves @ 2.0  $\mu\text{m}$  (when secondary = 20°C, primary = 20 +/- 2 °C)

Less than 1.5 °C of thermal gradient in the telescope structure was computed at Severup and MSFC/NASA. Thus, not only will the optical performance be unaffected during operation due to a thermal gradient in the telescope itself, but since the mirrors and structures are all made from aluminum, a thermal gradient is not likely to persist.

## 4. Optical Fabrication and Testing

The primary and secondary mirrors of the telescope system are made from aluminum alloy, which is the same as the mounting structure. The parabolic optical surface of the off-axis primary mirror was fabricated with the DTM3 diamond turning machine at LLNL. A 0.005" thick of electroless nickel was then plated on the aluminum mirrors at MSFC/NASA. The final diamond turning of the nickel plated mirror was completed on LODTM at LLNL for a surface accuracy of 1/4 waves peak to valley at HeNe wavelength and a surface finish of about 150 angstroms RMS. The diamond turned mirrors will be post-polished to a surface finish of 50 angstrom RMS, maintaining the surface figure at 1/4 waves of HeNe at SORL, thus reducing the scattering at the operating wavelength. The polished mirrors will then be plated with high purity of gold to increase the reflectivity to 98.5% at 2.0 microns wavelength. The same procedure was used to fabricate the secondary mirrors, excepted that the diamond turning and post-polishing will be completed at CAO/UAH. The secondary mirror was fabricated in a center symmetry shape for diamond turning and optical aligning convenience. Both Taly-surf profiler and interferometric analysis can be used for the surface figure testing. The surface finish will be polished to 30 angstroms RMS and will be tested with WYKO profiler.

High purity Fused Silica from Corning and single crystal silicon from Silicon Crystals Inc. will be used to fabricate the optical window and optical wedge scanner at DIOP. The optical surfaces will be polished to a figure accuracy of 1/6 peak to valley at HeNe. The optical surface figure and transmission wavefront at 2.0 microns will be tested with 18" ZYGO interferometer and lidar characterization facility at MSFC/NASA. Due to potential thermal gradient effects to the window and wedge, a special coating will be applied to increase the reflection of the solar and mid-IR radiation to and between the optical components. The coating is also required to have a 95% transmission at operating wavelength and maintain the circular polarization. The coating and polarization can also be tested at the lidar characterization facility.

## Conclusion

The optical and mechanical design and analysis of the SPARCLE telescope system was completed based on the requirements of the system performance. The optical manufacturing and mechanical machining are

in process. The diamond turned primary mirrors meet the specification of  $\frac{1}{4}$  waves peak to valley at HeNe wavelength. The procedures of system assembly and integration are also planned. The whole lidar system which includes the simulation of volume backscattering of aerosol, telescope optics and mechanical structure, receiving system and local oscillator will be modeled in ASAP (Advanced System Analysis Program) optical analysis software. The final signal-to-noise ratio can also be analyzed in the model.

#### References:

1. M. J. Kavaya, G.D. Emmitt, "The Space Readiness Coherent Lidar Experiment (SPARCLE) Space Shuttle Mission," Proc. SPIE Vol. 3380, Conference on Laser Radar Technology and application III, 12<sup>th</sup> Annual International Symposium on Aerospace/Defense Sensing, Simulation, and Controls, AeroSense, Orlando, FL, 1998.
2. A. Ahmad, C. Feng, F. Amzajerian, Y. Li "Design and Fabrication of a Compact LIDAR Telescope", Proc. SPIE Vol. 2832, Denver, CO August 4-9, 1996.
3. P.J. Reardon, B.R. Peters, F. Amzajerian, "Thermal Considerations for the SPARCLE Optical System," SPIE Proc. 3707, Orlando, FL., April 6-9, 1999

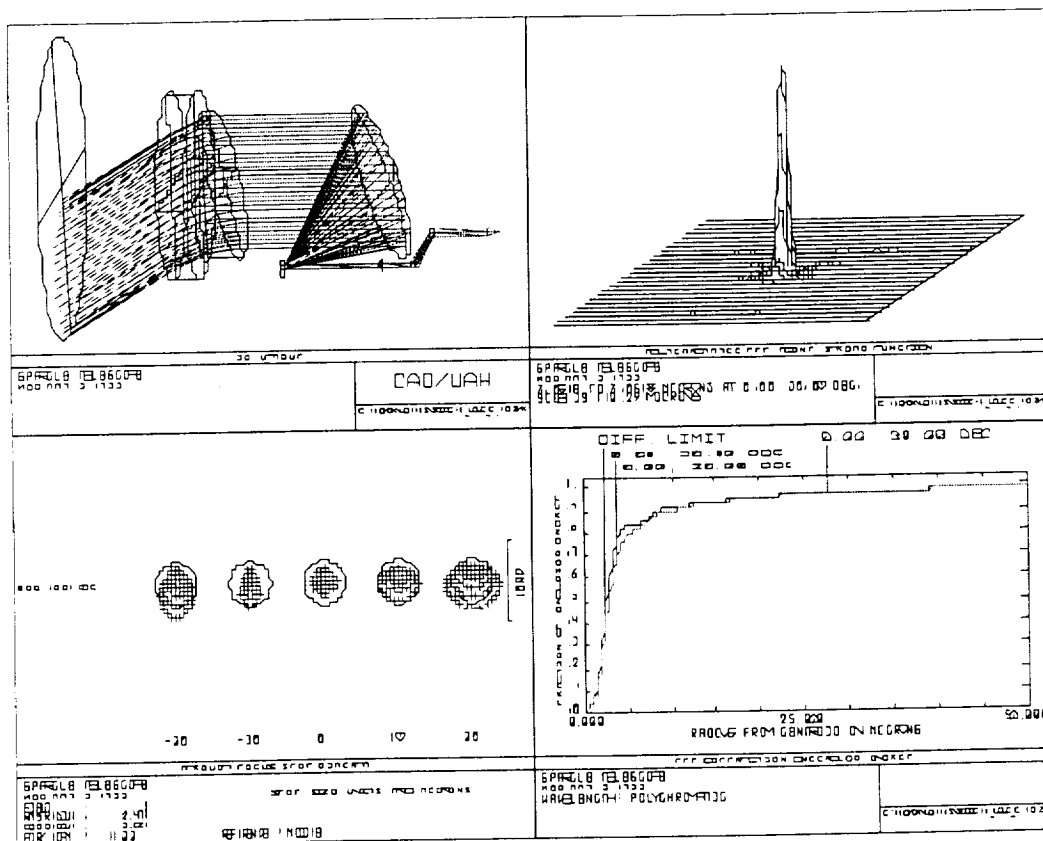


Figure 1



## SPARCLE Optical System Design and Operational Characteristics

Farzin Amzajerdian, Bruce R. Peters, Ye Li, Timothy S. Blackwell, and Patrick Reardon  
Center for Applied Optics  
The University of Alabama in Huntsville  
Huntsville, AL 35899

Phone: (205) 890-6030, Fax: (205) 890-6618, E-mail: farzin.a@msfc.nasa.gov

### Abstract

Operating at 2-micron wavelength, SPARCLE system performance is dominated by the optical quality of the transmitter/receiver optical system. The stringent optical performance requirements coupled with the demanding physical and environmental constraints have created the need for novel optical and opto-mechanical designs. This paper describes SPARCLE's optical system design features, fabrication and alignment techniques, and its anticipated operational characteristics.

## SPARCLE Optical System Design and Operational Characteristics

Farzin Amzajerdian, Bruce R. Peters, Ye Li, Timothy S. Blackwell, and Patrick Reardon  
Center for Applied Optics  
The University of Alabama in Huntsville  
Huntsville, AL 35899

Phone: (205) 890-6030, Fax: (205) 890-6618, E-mail: farzin.a@msfc.nasa.gov

### INTRODUCTION

The SPACe Readiness Coherent Lidar Experiment (SPARCLE) is the first demonstration of a coherent Doppler wind lidar in space. SPARCLE will be flown aboard a space shuttle in the middle part of 2001 as a stepping stone towards the development and deployment of a long-life-time operational instrument in the later part of next decade. SPARCLE is an ambitious project that is intended to evaluate the suitability of coherent lidar for wind measurements, demonstrate the maturity of the technology for space application, and provide a useable data set for model development and validation. This paper describes the SPARCLE's optical system design, fabrication methods, assembly and alignment techniques, and its anticipated operational characteristics.

Coherent detection is highly sensitive to aberrations in the signal phase front, and to relative alignment between the signal and the local oscillator beams. Consequently, the performance of coherent lidars is usually limited by the optical quality of the transmitter/receiver optical system. For SPARCLE having a relatively large aperture (25 cm) and a very long operating range (400 km), compared to the previously developed 2-micron coherent lidars, the optical performance requirements are even more stringent. In addition with stringent performance requirements, the physical and environment constraints associated with this instrument further challenge the limit of optical fabrication technologies.

### DESCRIPTION OF OPTICAL SYSTEM

The functions of the optical system include expanding the laser beam, directing it to the atmosphere in a conical scan pattern, receiving the backscattered radiation, while maintaining a highly accurate pointing to ensure adequate extraction of the Doppler frequency shift due to the spacecraft and earth rotation velocities. The optical system consists of a beam expanding telescope, an optical wedge scanner, and an optical window used for environmentally isolating the lidar instrument. Figure 1 provides an optical schematic showing various optical components. As shown in this figure, two mirror assemblies are used for providing the proper alignment between the lidar transceiver and the telescope. The telescope expands the transmitter beam by 25X and directs it to an optical wedge that deflects the beam by 30 degrees. The wedge is rotated by a precision motor/encoder assembly in a step-stare fashion, to provide a conical pattern in the atmosphere. Compared with continuous scanning, step-stare scanning provides a greater operational flexibility, by allowing different scan patterns and laser shot accumulation. Step-stare scanning also eliminates the need for a dynamic lag angle compensator for correcting the signal misalignment due to the continuous motion of the scanner, thus reducing the complexity and cost of the instrument's optical system. The scanner wedge is then followed by a high optical quality window that provides the lidar optical interface with space. The optical window is made of fused silica with a rugged anti-reflection coating for efficiently transmitting 2-micron wavelength radiation. Both the transmitted beam and the backscattered laser radiation from the atmosphere follow the same path to the lidar transceiver.

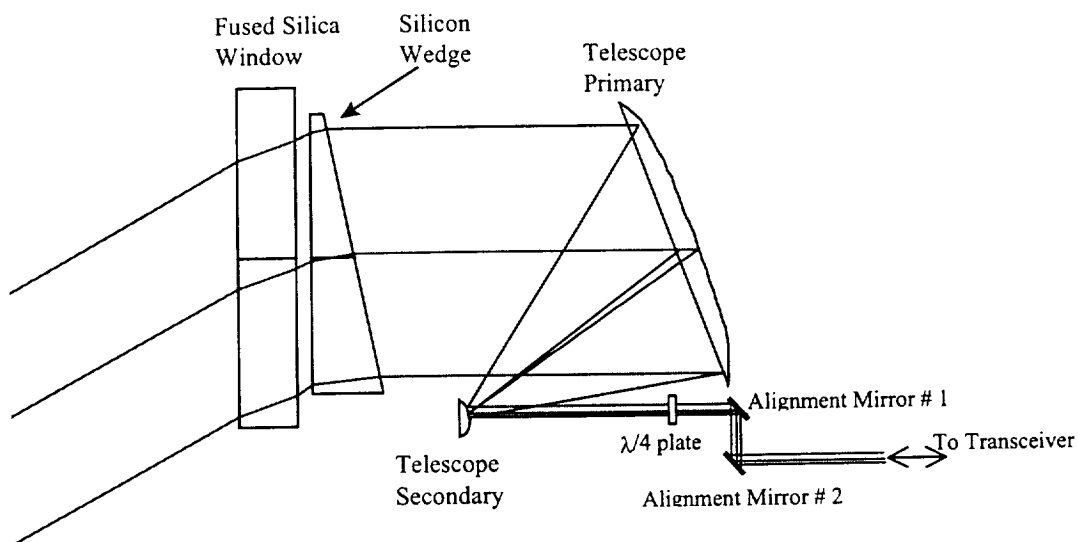


Figure 1. Optical System Schematic

The optical system along with the transceiver system will be housed in a pressurized Hitchhiker canister. The performance, physical and environmental specifications of the optical system are summarized in the table below.

Table 1. SPARCLE System Parameters

Clear Aperture Diameter	22.6 cm
Beam Expansion Ratio	25:1
Scan Angle (half angle)	30 degrees
Field Of View	80 $\mu$ rad
Maximum Conical Scan Rate	45 degrees/sec
Wavefront Quality	1/10 wave RMS
Optical Transmission	64%
Polarization	Less than 10% ellipticity
Beam Pointing Stability	4 $\mu$ rad/3 msec
Beam Pointing Error	28 $\mu$ rad in nadir and azimuth
Maximum Permitted Envelope	38 (dia.) x 43 (height) cm
Survivability Temperature	-40°C to 60°C
Operating Temperature	0°C to 25°C
Internal Pressure	0.5 atm

### BEAM EXPANDING TELESCOPE

The telescope design is based on an earlier system that was designed and built to address the major design issues associated with a space-based coherent lidar such as size, mass, wavefront quality, polarization purity, and very low optical backscatter<sup>1-3</sup>. By utilizing the lessons learned from the alignment and characterization of the first telescope, the optical and opto-mechanical designs were modified to further improve its robustness and to better comply with the specific environmental constraints associated with

SPARCLE mission.. The design changes also address the issues concerning the telescope assembly procedures and its integration with the lidar transceiver. For the most part, the design improvements take advantage of relaxed telescope constraints resulting from the selection of step-stare scanning over continuous scanning. The step-stare scanning reduced the telescope required field-of-view from 3 mrad to 40  $\mu$ rad and eliminated the need for a back-relief space that would have been necessary for accommodating the signal beam derotator and misalignment angle compensator. These changes in the requirements allowed for the elimination of the telescope refractive lens which in turn allowed for the use a smaller secondary mirror and lighter support structure.

The telescope consists of two off-axis parabolic mirrors in a Mersenne configuration as shown in figure 2. The off-axis configuration eliminates any central obscuration which will degrade beam quality due to diffraction effects. This configuration also reduces direct backscattering into the lidar system receiver optical path. The size and mass constraints for any space-based coherent lidar dictate that the system be considerably more compact than conventional configurations. The telescope fits within an envelope with dimensions 38X32X33 cm and weighs about 20 kg. To achieve such a compact package, a fast optical design was employed which led to more stringent fabrication and alignment tolerances<sup>4</sup>. To maintain the critical relative alignment between the primary and secondary mirrors over a relatively large operational temperature range and eliminate any misalignment due to differential thermal expansion, the telescope mirrors and its support structure are all made of the same aluminum material. This telescope system is considered athermal since the changes in the optical properties of the mirrors (radius of curvature, thickness, etc.) with temperature are perfectly balanced by the expansion or contraction of the structural supports such that the system maintains its alignment.

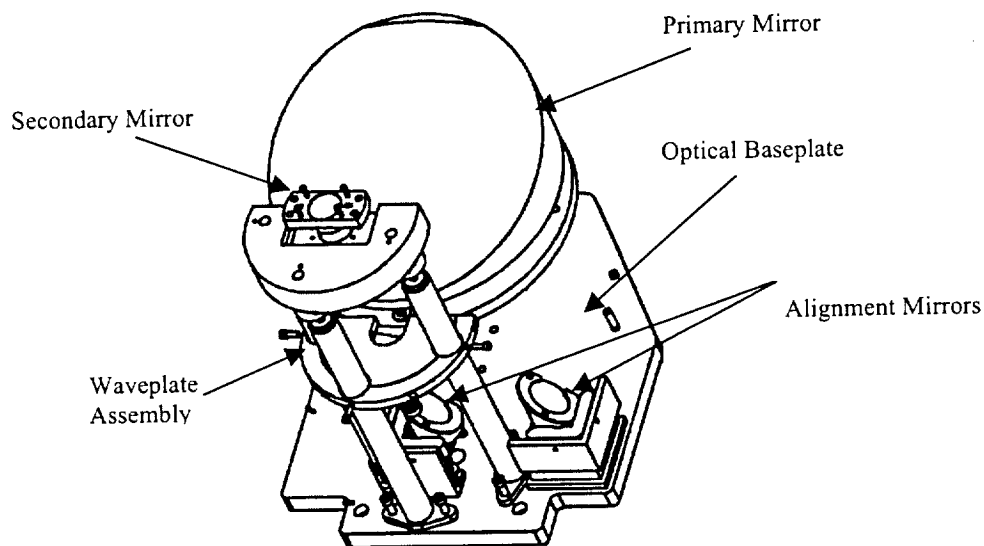


Figure 2. Beam Expanding Telescope

To achieve a minimum acceptable performance from the telescope, a high level of surface figure accuracy on the mirrors must be achieved. Selection of aluminum for the mirror base material coupled with the aspheric surface geometry required of the mirrors has necessitated using high precision single point diamond turning fabrication techniques. However, the level of surface roughness that can be obtained from a diamond turned surface is too high for coherent lidar application that requires a very low scattering and back reflection by the optics. Therefore, the mirrors are plated by a thin layer of nickel, using an

electroless plating technique, before finish diamond machining. The nickel-plated mirrors are then post-polished to reduce their surface roughness to an acceptable level. Finally, the mirrors are coated with gold to achieve a high surface reflectivity approaching 99%.

### OPTICAL WEDGE SCANNER

The lidar scanning is achieved by a 24.7 cm rotating silicon wedge that provides a 30 degree deflection angle. Selection of silicon as the wedge material was mainly driven by its many desirable optical and physical properties and the fact that sufficiently large silicon crystals with a single phase domain could be grown and polished. Because of the high index of refraction of silicon ( $n=3.45$ ), the required deflection angle can be achieved by a relatively small wedge angle of 11.7 degrees which limits the mass of the wedge to about 4 kg. The optical wedge mass was one of the critical considerations, since it directly affects the power drawn by the scanner motor which results in more heat. One of the critical issues associated with the optical wedge that needed to be addressed was its sensitivity to the radial temperature profile that will be generated by the hot scanner motor and the wedge cold surroundings. Radial temperature variations in the wedge can produce a wavefront error due its non-symmetrical shape and its high  $dn/dT$  (change in index of refraction with temperature) value. To improve the thermal properties of the optical wedge, a multilayer coating is designed that can effectively reject any radiation in the solar and far-infrared regions of spectrum while efficiently transmitting the lidar beam at 2-micron wavelength. In this way, the wedge can be thermally decoupled from the surrounding environment, allowed to reach thermal equilibrium quicker, and thereby minimize the impact of  $dn/dT$  by reducing thermal gradients within the wedge.

### OPTICAL WINDOW

The lidar instrument is environmentally isolated by a 5 cm thick, 32 cm diameter optical window made of fused silica. The main design considerations associated with the optical window are: (1) wavefront distortion due to the window substrate deformation under differential pressure condition in space; (2) depolarization due to stress-induced birefringence; (3) wavefront distortion due to any spatial temperature variation that may be present within the window material; and (4) Rejection of solar radiation for better thermal environment inside the canister. The optical window has a multilayer coating for high transmission at 2-micron wavelength and high reflection over the visible region of the spectrum.

This work was supported by NASA Marshall Space Flight Center through a cooperative agreement with The University of Alabama in Huntsville at the Center for Applied Optics.

### REFERENCES

1. Feng, A. Ahmad and F. Amzajerdian, "Design and analysis of a spaceborne lidar telescope," Proc. SPIE Vol. 2540, pp. 68-77, 1995.
2. A. Ahmad, F. Amzajerdian, C. Feng and Y. Li, "Design and fabrication of a compact lidar telescope," Proc. SPIE Vol. 2832, pp. 34-42, 1996.
3. Li, Ye; Blackwell, Timothy S.; Geary, Joseph M.; Amzajerdian, Farzin; Spiers, Gary D.; Peters, Bruce R.; Chambers, Diana, "Characterization of an optical subsystem for 2-um coherent lidars," Proc. SPIE Vol. 3479, p. 122-129.
4. Peters, Bruce R.; Blackwell, Timothy S.; Li, Ye; Geary, Joseph M.; Amzajerdian, Farzin; Bailey, Deborah, "Optomechanical design of a multi-axis stage for the SPARCLE telescope," Proc. SPIE Vol. 3429, p. 48-55.

## Considerations for Designing a Space Based Coherent Doppler Lidar

Gary D. Spiers  
Center for Applied Optics  
University of Alabama in Huntsville  
Huntsville  
AL 35899  
Gary.Spiers@msfc.nasa.gov  
(256) 544 5787

Michael J. Kavaya  
Mail Code SD60  
Global Hydrology and Climate Center  
NASA Marshall Space Flight Center  
Huntsville  
AL 35812  
Michael.Kavaya@msfc.nasa.gov  
(256) 922 5803

**Introduction**

An orbiting coherent Doppler lidar for measuring winds is required to provide two basic pieces of data to the user community. The first is the line of sight wind velocity and the second is knowledge of the position at which the measurement was made. In order to provide this information in regions of interest the instrument is also required to have a certain backscatter sensitivity level. This paper outlines some of the considerations necessary in designing a coherent Doppler lidar for this purpose.

**Line of sight velocity accuracy**

A lidar instrument measures wind velocity by measuring a frequency difference between the transmitted laser beam and the return signal. This frequency difference is due to the transmitted frequency being Doppler shifted by the line of sight velocity seen by the instrument. The line of sight velocity is comprised of velocity components due to the satellite velocity, the earth's rotational velocity and the velocity of the target.

The magnitude of the combined line of sight velocity is given by:

$$\begin{aligned} \text{los\_vel} := & \text{htrgtv} \cos(-\text{trgta} + \text{az} + \text{orblat}(\text{lat}, \text{inc})) \sin(\text{nadalt}(\text{orbh}, \text{n}, \text{alt}, \text{lat})) \\ & + \text{vtrgtv} \cos(\text{nadalt}(\text{orbh}, \text{n}, \text{alt}, \text{lat})) + \text{hsatv} \cos(\text{az}) \sin(\text{n}) + \text{vsatv} \cos(\text{n}) \\ & + \text{Vlat}(\text{lat}) \sin(\text{orblat}(\text{lat}, \text{inc}) + \text{az}) \sin(\text{nadalt}(\text{orbh}, \text{n}, \text{alt}, \text{lat})) \end{aligned} \quad (1)$$

where the first and second terms are the line of sight components of the target velocity with respect to the local WGS84 [1,2] earth ellipsoid surface. The third and fourth terms are the line of sight components of the spacecraft horizontal and vertical velocities. The final term is the component of the earth's rotational velocity along the line of sight. Table 1 lists the parameters and functions called out in equation (1) and table 2 lists the sensitivity of the

Symbol	Parameter
htrgtv	target horizontal velocity
vtrgtv	target vertical velocity
trgta	angle of the target velocity with respect to the local meridian
az	azimuth angle with respect to the spacecraft velocity vector
lat	latitude of the spacecraft
inc	orbit inclination angle
orbh	orbit height

n	instrument nadir angle
alt	altitude of the target with respect to the local WGS84 ellipsoid surface
hsatv	local horizontal component of the spacecraft velocity
vsatv	local vertical component of the spacecraft velocity
orblat(lat,inc)	the angle of the satellite velocity vector to the local meridian
nadalt(orbh,n,alt,lat)	The nadir angle the line of sight makes with the target with respect to the local WGS84 ellipsoid surface.
vlat(lat)	The earth's rotational velocity at a latitude, lat

Table 1) 'Base' parameters.

'base' parameters to error for an instrument at a nominal orbit height of 300 km and an orbit inclination of 52 deg with a nadir angle at the spacecraft of 30 deg.

Parameter	Maximum Error Rate	Error required to give 1 m/s los error
Azimuth angle	68 (m/s)/deg	256 $\mu$ radians
Nadir angle	118 (m/s)/deg	125 $\mu$ radians
Orbit height	0.31 (m/s)/km	3.22 km
Latitude	24 (m/s)/deg	725 $\mu$ radians
Orbit inclination	3.7 (m/s)/deg	4.7 mradians
Target altitude	0.02 (m/s)/km	50 km
Satellite local horiz. velocity	0.5 (m/s)/(m/s)	2 (m/s)
Satellite local vert. velocity	0.87 (m/s)/(m/s)	1.15 (m/s)

Table 2) LOS velocity sensitivities for a 300 km, 52 deg inclination orbit

Note that the error due to each of the parameters is generally a complex function of other parameters (typically azimuth and/or latitude) and the values in table (2) represent a worst case analysis for each parameter. It should be noted that the sensitivities above are valid for any instrument, regardless of measurement technique, that is intended to measure wind velocities on a single shot basis.

In addition to the line of sight velocity sensitivities listed above there will be sensitivities associated with the measurement technique itself and with atmospheric refraction. Both of these effects are dependent on the actual design and wavelength of the lidar under consideration. At the 2  $\mu$ m wavelength frequently considered for a space-based coherent lidar the large Doppler shifts due to the line of sight component of the spacecraft velocity result in a large frequency offset of the return signal from the outgoing frequency. This offset is greater than the bandwidths typically required for obtaining a high quantum efficiency from currently available detectors. This is overcome by tuning either the local oscillator or the transmitted outgoing pulse to offset for the spacecraft induced Doppler shift and hence the bandwidth requirement on the detector [3]. A consequence of this scheme is an increase in the number of frequencies that must be measured compared to a typical ground or aircraft based coherent lidar. The velocity measurement accuracy due to the receiver portion of the instrument including the effect of the velocity algorithm used is  $\sim 0.5 - 1$  m/s for a 2  $\mu$ m system for good ( $>10$  coherent photoelectrons) signal conditions.

Atmospheric refraction produces 'bending' of the lidar beam as it travels down through the atmosphere and this creates a change in the nadir angle at the target. For a 2  $\mu$ m lidar at a 300 km orbit with a 30 deg nadir angle this effect causes a 150 – 200  $\mu$ radian reduction in the nadir angle at the target with the actual value dependent on local atmospheric conditions. This will contribute a 1.3 – 1.7 m/s line of sight velocity error if not correctly accounted for.

#### Target position

This can be broken down into two issues, the first is knowledge of the instrument position with respect to some known global coordinate system, typically WGS84 [1,2]. The second is knowledge of the measurement location with respect to the instrument.

Knowledge of the measurement location with respect to the instrument is dictated by knowledge of the azimuth and nadir angles of the instrument. Errors in the azimuth or nadir angle cause the line of sight to describe a cone about the 'true' or 'ideal' value. The position of the measurement relative to the instrument is simply:

$$Z_{lvlh} := \frac{1}{2} c t_{rtrp} \cos(n) \quad (2)$$

in the vertical and

$$R_{lvlh} := \frac{1}{2} c t_{rtrp} \sin(n) \quad (3)$$

is the radial distance, neglecting the effect of refraction, from the sub-instrument point to the target location,  $c$  and  $t_{rtrp}$  are the velocity of light and the round trip time of flight respectively. We must constrain the azimuthal direction such that the circumferential distance from the 'true position' can be determined. This distance is simply  $(R_{lvlh} \times \text{daz})$  where  $\text{daz}$  is the error in azimuth angle. This provides the target position in a local coordinate frame that can then be transformed to obtain the target position with respect to WGS84 if the position of the instrument with respect to WGS84 is known.

Parameter	Error Rate	Error required to give 1m error
Instrument vertical position	1 m/m	1 m
Nadir angle	44 m / 200 $\mu\text{rad}$	4.55 $\mu\text{rad}$
Round trip time	40 m / 300 ns	7.5 ns

Table 3) Vertical position assignment sensitivity

Parameter	Error Rate	Error required to give 1m error
Instrument horizontal position	1 m/m	1 m
Nadir angle	40 m / 100 $\mu\text{rad}$	2.5 $\mu\text{rad}$
Round trip time	24 m / 300 ns	12.5 ns
Azimuth angle	24 m / 100 $\mu\text{rad}$	4.17 $\mu\text{rad}$

Table 4) Horizontal position assignment sensitivity

#### Instrument position and attitude

The method by which the instrument obtains its attitude and position relative to WGS84 will be dependent on the platform and instrument configuration. One technique is to use an INS/GPS to provide both attitude and position. The performance of an INS/GPS on orbit is typically degraded over that achievable on the ground. In order to meet the error budgets required by a Doppler lidar they must be operated in 'military' or PPS mode. One problem with an instrument dedicated INS/GPS is that unlike a launch vehicle the unit is not powered on through launch and so it must be initialised once on orbit. The lidar can be used to both perform this function as well as track and correct for drift in the INS attitude solution [4].

#### Instrument sensitivity

The calculation of coherent Doppler lidar sensitivity has been extensively discussed in the literature [5] and this paper will only mention issues pertaining to deployment from a space platform. In order to optimise the sensitivity of a coherent lidar it is desired to have good wavefront matching of the local oscillator signal and the return signal. A 300 km altitude, 30 deg nadir angle instrument has a round trip time of flight of the optical pulse from the lidar to the ground and back of ~2.3 milliseconds. During this time the transmit/receive optical axes must remain aligned with respect to each other and any jitter of the lidar during the round trip time will therefore contribute to a loss in sensitivity. Contributors to this misalignment that are not typically of concern for a ground or airborne system are platform attitude drift and nadir tipping due to rotation about the earth's center. A platform attitude drift of ~0.04 deg/sec will contribute ~1.6  $\mu\text{radians}$  of misalignment between the transmit/receive beams while nadir tipping will



contribute  $\sim 2.7$   $\mu$ radians of misalignment. For a 25 cm aperture instrument a total angular offset of  $\sim 7$   $\mu$ radians will result in a 3 dB reduction in SNR.

Finally it should be noted that the Doppler shift due to the component of the spacecraft platform velocity seen by the lidar is a function of the scanner azimuth angle (equation (1)). The bandwidth of the return signal that results from this can result in an azimuthally dependent atmospheric extinction and hence an azimuthally dependent sensitivity.

### Summary

An overview of some of the issues specific to designing a space based coherent Doppler lidar have been presented and examples for an instrument with a 25 cm aperture in a 300 km, 52 degree inclination orbit orbit altitude presented.

### Acknowledgements

Funding for this work has been provided by Dr. Ramesh K. Kakar, NASA Code Y and by the NASA NMP EO-2 SPARCLE program.

### References

- [1] MIL-STD-240, "Department of Defence World Geodetic System (WGS)", 11 January 1994.
- [2] DMATR 8350.2, "Department of Defence World Geodetic System 1984, Its Definition and Relationships with Local Geodetic Systems", Second Edition 1 September 1991.
- [3] G. D. Spiers, "Analyses of Coherent Lidar Wind Measurement Missions", Final Report on Contract No. NAS8-38609, Delivery Order No. 128, Report Date 8/28/96.
- [4] G.D. Emmitt, T. Miller and G.D. Spiers, "Pointing Knowledge for SPARCLE and Space-based Doppler Wind Lidars in General", Tenth Biennial Coherent Laser Radar Technology and Applications Conference, Mount Hood, 28<sup>th</sup> June – 2<sup>nd</sup> July 1999.
- [5] See for example R.G. Frehlich and M.J. Kavaya, "Coherent laser radar performance for general atmospheric refractive turbulence", Appl. Opt. 30, 5325, December 1991.

# Performance Analysis for the Space Readiness Coherent Lidar Experiment

Gary D. Spiers  
Center for Applied Optics  
University of Alabama in Huntsville  
Huntsville  
AL 35899  
Gary.Spiers@msfc.nasa.gov  
(256) 544 5787

## Introduction

The primary function of SPARCLE is to validate the ability of coherent Doppler lidar to accurately measure atmospheric winds. The requirements for SPARCLE are listed in table (1).

Line of sight velocity accuracy	Wind Measurement Accuracy $\sigma_{LOS} < 2$ m/s, 1 m/s of which is attributable to instrument error or uncertainty and the rest to platform pointing and alignment. Assumes single shot LOS, in regions of high SNR and low wind turbulence and shear.
Vertical position accuracy	The accuracy of the height assignment of the wind data above the GPS reference ellipsoid shall have an RMS error $< 50$ meters.
Horizontal position accuracy	The accuracy of the horizontal location of the wind data shall have a RMS error $< 500$ meters.
Aerosol backscatter sensitivity ( $\beta_{50}$ , single shot)	$5 \times 10^{-7} \text{ m}^{-1} \text{ sr}^{-1}$ (goal) $5 \times 10^{-6} \text{ m}^{-1} \text{ sr}^{-1}$ (acceptable)

Table 1) Key SPARCLE performance requirements [1]

There are a number of issues that must be considered when assessing the anticipated performance of a space based coherent lidar. These are shown schematically in figure (1).

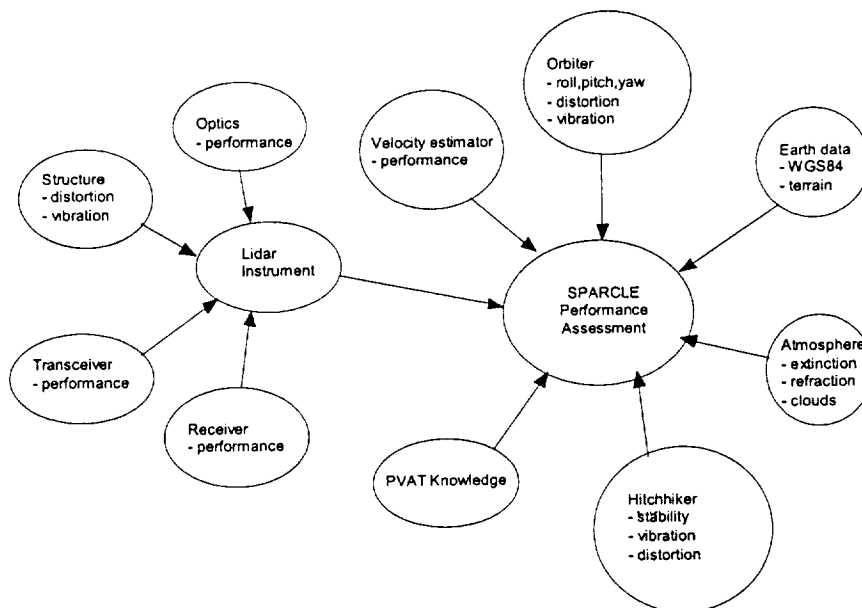


Figure 1) Contributors to the performance of SPARCLE.

## Methodology

Performance of the instrument is evaluated through a combination of tools. These include error budgets for each of the major requirements, a Monte Carlo simulation that includes the statistics of the processes involved and individual tools for evaluating specific contributors (see for example [4]).

## Line of Sight Velocity Accuracy

The line of sight velocity accuracy consists of two requirements, one attributable to the lidar instrument and one attributable to the combination of the lidar instrument and platform. Knowledge of the instrument's attitude (nadir and azimuth angle) is crucial to obtaining the required line of sight velocity accuracy [2].

There are a number of key problems associated with obtaining the attitude of an instrument on a Hitchhiker [5] platform. Timely attitude data is not available through the Hitchhiker interface and the Hitchhiker platform is not a precision pointing platform. Therefore SPARCLE can not rely on pre-launch alignment of the SPARCLE instrument with respect to a known attitude determination system in order to meet the 2 m/s line of sight velocity error requirement. To meet the requirement SPARCLE provides its own attitude knowledge system that uses the ground return signal of the lidar to initialise the INS portion of an integrated INS/GPS [3]. This also removes the need for absolute calibration of the lidar instrument nadir and azimuth angles prior to launch, placing repeatable rather than absolute nadir and azimuth requirements on the lidar hardware.

The lidar instrument portion of the line of sight velocity accuracy requirement has contributions from the measurement of the master oscillator/local oscillator offset, slave oscillator/master oscillator offset and return signal frequencies. Additional contributions come from local oscillator errors associated with frequency drift during the round trip time and assumptions used in the tuning algorithm. In combination these errors associated with frequency measurement contribute  $\sim 0.75$  m/s to the line of sight velocity accuracy. The nadir and azimuth portion of the line of sight velocity accuracy budgeted to the instrument contribute a further  $\sim 0.33$  m/s to the line of sight error to give a total line of sight velocity error of  $\sim 0.82$  m/s.

Instrument position and orbit inclination knowledge errors (if not corrected in post processing) contribute to an incorrect determination of both the ground velocity and the nadir angle at the ground. These errors contribute  $\sim 0.37$  m/s to the line of sight velocity accuracy whilst the accuracy of determining the instrument velocity contributes an additional  $\sim 0.1$  m/s to the line of sight velocity accuracy error. The final contribution to the line of sight velocity accuracy comes from a combination of the ability to correctly initialise the INS using the lidar, the subsequent drift and resolution of the INS gyroscopes and change, due to thermal or vibration environments, of the INS position with respect to the lidar. These contribute a further  $\sim 0.89$  m/s to give an RSS total for the combined instrument and platform of  $\sim 1.3$  m/s.

## Position

The GPS portion of the INS/GPS provides the location of the instrument with respect to WGS84 [6,7] to better than 20 m. The time of flight to the ground in combination with knowledge of the azimuth and nadir angles provides the location of the target with respect to the instrument to within 50 m in the horizontal and  $\sim 30$  m in the vertical.

## Backscatter Sensitivity

Table (2) shows the budgeted allowances for the backscatter sensitivity.

Wavelength	2.0512 $\mu\text{m}$	Pulse energy	100 mJ
Pulse length	0.17 $\mu\text{m}$	Receiver efficiency	0.25
Clear aperture diameter	0.226 m	Transmit beam 1/e2 diameter	0.185 m
One way optics transmission	0.64	Wavefront aberration	0.69
Polarisation efficiency	0.9	Truncated/untruncated correction	0.59
Misalignment efficiency	0.64	Range to target	384 km
Target altitude	1 km	Nadir angle at target (spherical earth)	31.56 deg.
Vertical resolution of processed data	250 m	One way atmospheric transmission	0.84
Horizontal wind velocity search space	$\pm 10$ m/s		
Single shot velocity estimator	Capon, $b_0=75.36$ , $\alpha=1.08$ , $\gamma=17.45$ , $\chi=0.568$ , $g_0=18.25$ , $\epsilon=1.8$ , $\delta=0.765$ , $\mu=0.301$		

Table 2) Parameters used in determining the SPARCLE backscatter sensitivity.

It should be noted that the details of the science requirement for SPARCLE specified the backscatter in terms of certain approximations (e.g. spherical earth) rather than 'real world' values and this is reflected in Table (2). At this time it is too early in the program to have data available that validates the parameter allocation indicated in Table (2) however to date none of the relevant subsystems that these requirements flow down to has indicated a problem in meeting their requirements. For the conditions listed in table (2) SPARCLE has a sensitivity ( $\beta_{50}$ , single shot) of  $2.7 \times 10^{-6} \text{ m}^{-1} \text{ sr}^{-1}$  or  $5.3 \times 10^{-6} \text{ m}^{-1} \text{ sr}^{-1}$  if 3 dB of margin for unexplained loss is included. Note that the margin is not required within the specification for backscatter sensitivity in the SPARCLE science requirements.

One of the important issues related to performance is the misalignment efficiency. Table (3) identifies key contributors to the misalignment efficiency. In addition to the usual lidar contributors such as laser beam pointing jitter, optical subsystem jitter due to vibration and scanner stability there will be misalignment contributions due to nadir angle tipping and due to changes in the attitude of the shuttle during the round trip time. Shuttle attitude drift rates can be controlled through requirements placed on the orbiter in the SPARCLE payload integration plan.

Laser jitter (pulse to pulse at telescope output)	1 $\mu$ radian
STS attitude drift (<0.04 deg/sec)	1.6 $\mu$ radians
Nadir tipping during the round trip time	2.7 $\mu$ radians
Optical subsystem jitter	3 $\mu$ radians
Scanner stability	4 $\mu$ radians
RSS Total	6 $\mu$ radians

Table 3) Round trip pointing jitter budget

One of the important issues in validating this budget is related to on-orbit vibration affecting the optical subsystem jitter. The Hitchhiker platform is not a precision pointing platform and lacks information about its local vibration environment. A lot of accelerometer data has been collected during microgravity experiments on the orbiters but there is insufficient data to reliably translate this experiment specific acceleration data into rates of attitude change, which is what we require. Fortunately the magnitude of the accelerometer data implies (with considerable assumptions) that the on orbit vibration environment will contribute negligibly to this misalignment but it is unlikely that this can be absolutely verified prior to launch.

### Summary

At this stage in the development of the SPARCLE instrument it is expected to have a backscatter sensitivity of  $2.7 \times 10^{-6} \text{ m}^{-1} \text{ sr}^{-1}$ , a final line of sight velocity accuracy of  $\sim 1.3 \text{ m/s}$  and be capable of locating the measurement with respect to WGS84 to within 50 m in the horizontal and 30 m in the vertical.

### Acknowledgements

This work was conducted in support of the NASA NMP EO-2 SPARCLE mission.

### References

- [1] "Space Readiness Coherent Lidar Experiment (SPARCLE) Mission and Science Requirements Document", MSFC-RQMT-2828, NASA Marshall Space Flight Center, 1998.
- [2] G.D. Spiers and M.J. Kavaya, "Considerations for Designing a Space Based Coherent Doppler Lidar", Tenth Biennial Coherent Laser Radar Technology and Applications Conference, Mount Hood, 28<sup>th</sup> June – 2<sup>nd</sup> July 1999.
- [3] G.D. Emmitt, T. Miller and G.D. Spiers, "Pointing Knowledge for SPARCLE and Space-based Doppler Wind Lidars in General", Tenth Biennial Coherent Laser Radar Technology and Applications Conference, Mount Hood, 28<sup>th</sup> June – 2<sup>nd</sup> July 1999.
- [4] G.D. Spiers, "The Effect of Optical Aberrations On The Performance Of A Coherent Doppler Lidar", Tenth Biennial Coherent Laser Radar Technology and Applications Conference, Mount Hood, 28<sup>th</sup> June – 2<sup>nd</sup> July 1999.
- [5] "Hitchhiker Customer Accommodations & Requirements Specifications", HHG-730-1503-07, NASA Goddard Space Flight Center, 1994.
- [6] MIL-STD-240, "Department of Defence World Geodetic System (WGS)", 11 January 1994.
- [7] DMATR 8350.2, "Department of Defence World Geodetic System 1984, Its Definition and Relationships with Local Geodetic Systems", Second Edition 1 September 1991.

## **Primary mirror manufacturing considerations for a space based coherent lidar**

Timothy S Blackwell, Ye Li, Bruce R Peters, Farzin Amzajerian

The University of Alabama in Huntsville  
Center for Applied Optics  
Huntsville Alabama  
Tim.Blackwell@msfc.nasa.gov  
256-890-6030

Jeff Klingmann, Keith Carlisle, Anthony Demiris, James H. Hamilton

Precision Systems and Manufacturing Group  
Lawrence Livermore National Laboratory  
P.O. Box 808, L-537  
Livermore, CA 94551

### **ABSTRACT**

The measurement of winds from a space borne platform is of significant scientific importance to both weather prediction and climate research. One of the key technologies embodied in coherent detection of winds from space is the use of large aperture, compact, lightweight, high-quality wavefront, photon-efficient optics. This paper discusses the optical design, The mechanical design, material preference, diamond turning issues, polishing requirements, and coating selections for the primary mirror of a 25X afocal beam expander intended for use in space-based coherent lidar systems.

Performance requirements levied on a lidar optical system are primarily driven by operational signal to noise budgets, but other factors such as the thermal and launch load environments also factor into the optics design. Therefore, the sensitivity of any coherent lidar is generally limited by the quality of its optical system. Aberrations generated by the optics from manufacturing errors, optical misalignment, or operational thermal activity will substantially affect measurement accuracy's especially when used at the ranges expected from space platforms. The stringent optical performance requirements coupled with demanding physical and environmental constraints have created the need for a design with unique optical and robust mechanical design characteristics. This paper will survey various manufacturing considerations when producing a 25cm diameter f/0.9; 150mm off axis parabola which is associated with the 2-micron SPace Readiness Coherent Lidar Experiment (SPARCLE). This mirror has a final figure of better than 1/4 wave p-v at HeNe and surface roughness of better than 15 angstroms RMS.

### **KEY WORDS**

Lidar, laser radar, afocal telescope, off axis parabolas, diamond turning, space telescopes, large optics

## INTRODUCTION

Accurate global wind fields are the single most important measurement remaining in the continuing effort to validate technology areas that could lead to fundamental advances in our understanding of how atmospheric winds affect our climate and weather. SPARCLE is NASA's first demonstration of a coherent Doppler wind lidar in space. SPARCLE is to be flown aboard a space shuttle in the middle part of 2001 as a stepping stone towards the development and deployment of a long-life-time operational instrument to be introduced in the later part of the next decade. SPARCLE is an ambitious project, which intends to evaluate the suitability of coherent lidar for wind measurements, and to demonstrate the maturity of the technology for space based applications. In anticipation of a space shuttle technology demonstration mission, we designed and fabricated a 25-cm prototype compact afocal telescope. The telescope was designed for operation at 2-micron wavelength in accordance with NASA's plan for the development and deployment of an eye-safe solid state coherent lidar. SPARCLE is to be placed in a hitchhiker canister inside the payload-bay of the space shuttle. For the SPARCLE telescope, having a relatively large aperture and a very long operating range (350 km), the optical performance requirements became very stringent. In addition to strict performance requirements, the physical and environment constraints associated with this instrument further press the limit of optical fabrication technologies, especially in the area of large off-axis optics. These imposed constraints, combined with the optical performance requirements, created many challenges in the design, fabrication, assembly, and testing of this optical system. When one considers that the rigorous optical requirements of the SPARCLE mission must be achieved to acquire valuable data, we find that the most sensitive element in the optical system is the primary mirror. Smaller secondary mirrors although vitally important, are routinely manufactured to these kinds of tolerances, therefore we will concentrate on the more demanding technology issues of producing the primary mirror.

Design trade studies such as operational wavelength, atmospheric transmission, transmitted laser power, pointing accuracy and instrument sensitivity collectively determine the overall system requirements. Optical system requirements are additionally influenced by practical matters such as optical throughput, size and weight constraints, as well as ease of manufacture, alignment, and testing. Optical transmission efficiency is a factor because the instrument must be as sensitive as possible to weak backscattering from atmospheric aerosols.

The packaging constraints for this particular mission dictate that the system be more compact than standard configurations which leads to a faster optical system with tighter alignment tolerances. The optical design selected to meet these objectives uses two optical elements, a parabolic primary mirror and a parabolic secondary mirror. Both were designed to be compact, as light as possible, and maintain optical throughput with high wavefront quality. Due to the mirror material choice, its large size and rigorous wavefront requirements, opto-mechanical designs incorporated many of the lessons learned throughout the precision machining industry. The large optics diamond turning machine LODTM, located at Lawrence Livermore National Laboratories LLNL in Livermore California, provided the necessary accuracy to meet the demanding challenges set forth in the optical prescription. The Diamond turning machine DTM-3, also at LLNL was used to produce the initial figure in the optical surface. The mirrors were then electroless nickel-plated by NASA in the plating laboratories at MSFC and the final optical figuring and minimization of the surface roughness was achieved on LODTM. Post polishing was accomplished by zone-polishing techniques developed in industry and mastered by Space Optics Research Labs (SORL) in Boston Massachusetts. The Gold coating is an advanced proprietary process, which has been developed by Epner technologies in Brooklyn New York. Metrology on the primary mirror was done by UAH at MSFC in Huntsville Alabama.

## OPTICAL DESIGN

The telescope optics are based on a prototype system that was designed and built to address major design issues associated with a space-based coherent lidar. By utilizing the lessons learned from manufacture, alignment, and characterization of the prototype telescope, optical designs were modified to further improve its robustness and to better comply with the specific thermal environment associated with the SPARCLE mission. Our design changes also address issues concerning the telescope assembly procedures and its integration with the lidar transceiver. Various configurations for the telescope have been evaluated against the performance requirements, and a Galilean type of telescope has been selected.

The telescope consists of an off-axis parabolic primary mirror and a rotationally symmetric parabolic secondary mirror arranged in the Mersenne configuration as shown in figure 1. The off-axis configuration eliminates any central obscuration, which will degrade beam quality due to diffraction effects especially at these sensing ranges. This configuration also reduces direct backscattering into the lidar system receiver optical path.

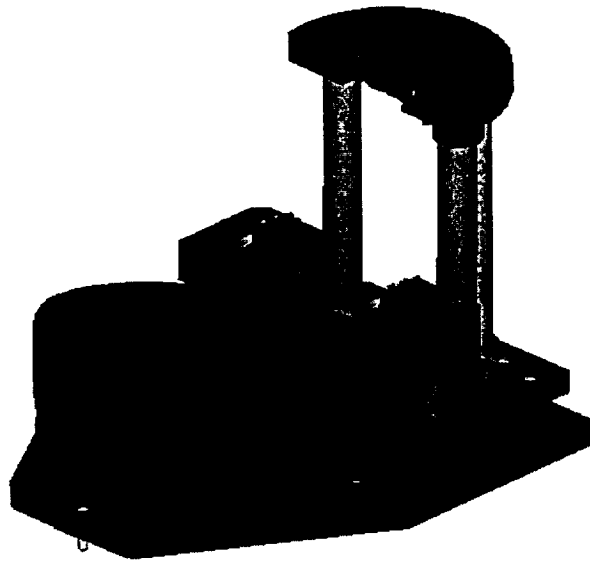


**Figure 1.** The SPARCLE telescope Mersenne configuration as designed showing the primary mirror the secondary mirror and the interface mirrors to the transceiver.

The diffraction limited SPARCLE beam expander was designed and modeled by using ZEMAX optical software. Prototype data verified the Zemax model by using SYNOPSIS optical software to analyze interference data. Data were taken using a two-micron Twyman Green interferometer at MSFC.

The flight telescope is designed to have a full field of view of 80 micro-radians, an angular magnification of 25x, and a primary mirror aperture of 25 cm. The optical spacing between the primary and secondary mirror is 22.5 cm with the primary mirror operating at F#/0.9 and a de-center of 15 cm. In addition, a small flat optical surface with a width of 7 mm was designed on the outer radial edge of the primary mirror as a reference for testing and system assembly.

The point spread function (PSF) size was obtained by using an ideal lens to focus the collimated output rays down to a point. The PSF was contained within a diffraction limited Airy disc with a Strehl ratio of 93% and RMS wavefront error of 1/25 wave at the operating wavelength. Table 1 below provides a list of the primary mirror specifications for the flight telescope.

Tolerance and sensitivity analysis is a very important factor when designing a working optical system. These parametric sensitivities have been analyzed to determine the telescope optical performance during fabrication steps and for final assembly. The analyses assume a fixed focal point in space. However, the accepted focal point is surrounded by a volumetric tolerance

Conic constant of primary mirror:	+/- 0.0003
Radius curvature of primary mirror:	+/- 10.0 $\mu\text{m}$
Total irregularity of each mirror:	0.5 fringes
y - tilt of primary mirror:	0.01° ( 170 $\mu\text{rad}$ )
x - tilt of primary mirror:	0.01 °
x and y de-center of primary mirror:	10 $\mu\text{m}$
Focal length:	9.227 inches
Final diameter:	10.236 inches
Off-axis distance:	0.787 inches to vertex edge
Surface accuracy:	¼ P-V over 95% of clear aperture at 633 nm wavelength

Table 1. Primary mirror optical prescription

## MECHANICAL DESIGN

Opto-mechanical design and analysis is a very critical step in the development of an optical system. The objective of a good optical design is to ensure that the elements are mounted securely and with minimal distortions. To maintain the critical relative alignment between the primary and secondary mirrors over a relatively large operational temperature range and eliminate any misalignment due to differential thermal expansion, the telescope mirrors and its support structure are made of the same aluminum material. Design of the mounting and support structure for the primary mirror must also be considered. The requirements for this structure are that it be stable enough to maintain alignment during launch environment and that it be compact enough to be accommodated within the packaging constraints. The mechanical design for this telescope consists of a post-type support structure where the mirror is mounted directly to a backing plate. This telescope system is considered athermal since the changes in the optical properties of the mirrors with temperature are perfectly balanced by the expansion or contraction of the structural supports such that the system maintains its alignment. The size and mass constraints dictate that the system be considerably more compact than conventional configurations. The telescope fits within an envelope with dimensions 38X32X33 cm and weighs about 20 kg.

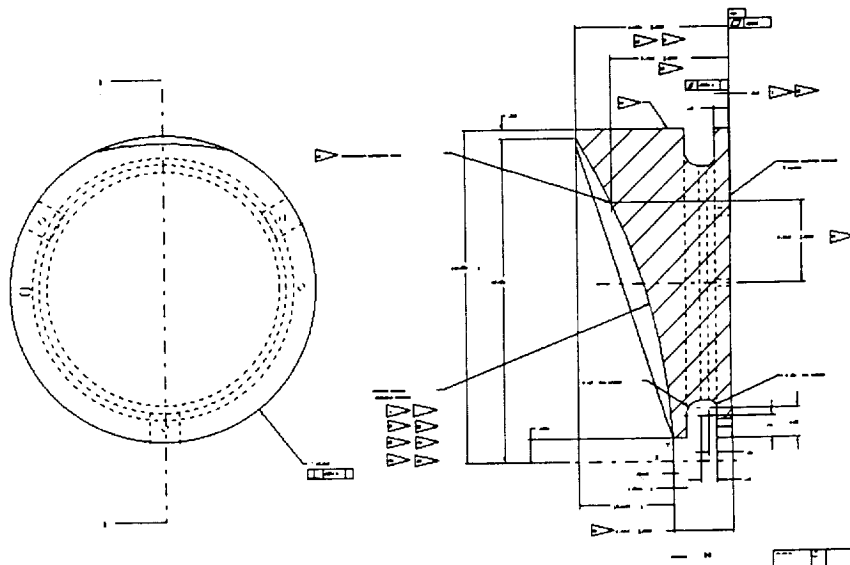


**Figure two.** The primary mirror mechanical drawing. The three mounting pads and locator holes are shown on the left and the parabola and the stress reducing ring for mounting is shown on the right.

## MATERIAL PREFERENCES

The typical approach is to select materials for the optical system that have very high microyield strength but, these materials are also very expensive to fabricate. The optical system is going to need to operate over a temperature range that is not abnormally large for most applications, but the wavefront quality for SPARCLE must be maintained throughout a 0-25°C static temperature range with less than 2.0°C differential. Therefore, an athermal system is most desirable. For SPARCLE, the optical elements and the supporting structure are fabricated from the same aluminum material.

To achieve athermal operation with a low weight and a reasonable fabrication approach is to use metal mirrors manufactured using single point diamond turning technology. The structural efficiency of Aluminum, the quotient of the material's elastic modulus and the material's density, is more than adequate at 102.1 compared to other candidate materials.



Furthermore, the optical surface of this mirror is overcoated with electroless nickel, this is done because the nickel is harder and readily accepts diamond turning and polishing. It is desirable to have the coefficient of thermal expansion of the nickel coating (8.4 ppm/°F) closely match the CTE of the bulk mirror material. The CTE of Aluminum is 13.1 ppm/°F. Because of its relative ease to machine, its availability, its good structural efficiency, the metal of choice was Aluminum 6061 T 651.

## NICKEL PLATING

The plating process must not result in excessive residual shear stress between the electroless nickel and the aluminum. It is possible to see as much as 15 ksi combined internal and thermal stress depending on the thickness of the plated layer and the plating rates. When electroless nickel-plating aluminum mirrors, the phosphorous content requirements are eleven percent and the bath pH remains around 4.6. The temperature of the plating bath is held constant at 190C with a uniformly distributed high flow rate constantly refreshing the plating optic with a uniform coating of nickel phosphorous. The plating rate usually runs twenty hours for a uniform 0.006" layer. This coated layer has a Rockwell hardness of about 52, however the nickel is still compliant for post-polishing activities. Following plating, the mirrors are thermally cycled to release any residual hydrogen that may have been trapped during the plating process. Thermal cycling should take the mirrors from room temperature to 121C and back to room temperature in an eight-hour time span. It is imperative that any mounting pads or reference surfaces on the optic that are being used for the diamond turning process are well protected and receive no plating. These pads are registration surfaces for mounting to the diamond turning machines and should not be damaged in the plating process or when handling the mirrors. Even minor damage to the pads will result in poor optical figure on the final mirrored surface.

## DIAMOND TURNING

When diamond turning optical elements such as the primary mirror for SPARCLE, several aspects must be considered in the design phase of the blank. Mass of the diamond turning surround, spindle rotation rate, tool feed rate and mirror-fastening techniques must also be carefully understood when designing the mirror blank. The rotation rate and balance of the spindle and the feed rate of the diamond tool are of primary importance in generating optical quality elements. Finite element analysis was used to determine the spin rates employed (54RPM) during the diamond turning process. By a better understanding of the dynamics of rotation and how this effects the at-rest shape of the optic, we determine at what point the mirror blank begins to give to the centrifugal forces of rotation. Mirror fastening, which involves attaching to the surround for diamond turning and to mounting the mirror to the telescope support structure during assembly should also be considered. The SPARCLE primary mirror is designed to be mounted on three pads which have been optically finished and which retain a planarity from pad to pad of  $\frac{1}{4}$  wave at HeNe. In some cases 100-micron pitch groves in the pads with about 100-micron depth provide enough surface contact to resist plastic deformation between the pads and the mount. These groves allow for any micron sized particulates to escape into the groves and therefore not interfere with the mounting registration. The SPARCLE primary mirror pads can be seen in figure 3 as well as showing the locator pins and the Rockwell hardness test points on the side of the mirror. Locator pins are used on either side of the mirror to ensure consistent registration for placement of the blank on the different diamond turning machines when transferring the mirror from the initial diamond turning facility to the plating facility and back to the finish diamond turning machine.

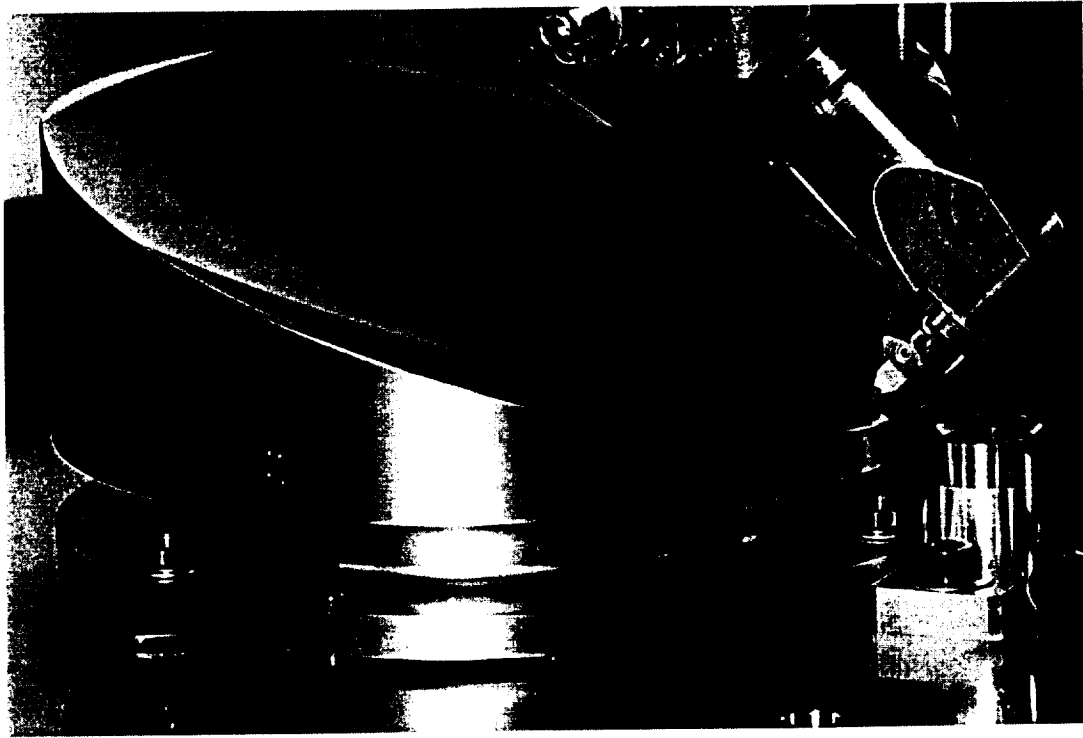


Figure 3. close up of the primary mirror installed on LODTM. Notice the mounting pads and the alignment locator pins. Also notice the small reference optical flat surface at the top of the mirror.

Stresses from mounting the mirrors on precision machinery must not make their way to the optical surfaces. The groove seen in figure 3 at the base of the mirror eliminates any stress transfer to the optic surface from the mounting process. Once again, torque settings for the hardware can be determined by finite element analysis. It has been found that the through holes in the pads for mounting hardware should have beveled ends as opposed to a clean bore. It turns out that mounting, removal, and subsequent remounting of the mirrors on the various machines can result in small welts on the edges of the through holes which can offset the mirrors enough to destroy the registration.

Figure 4 shows the primary mirror data taken as a linear profile through the vertex. The left side is one mirror and the right side is the other mirror. This machine produced a  $\frac{1}{4}$  wave p-v surface with about 120 Å surface roughness. Post polishing of these mirrors will bring the RMS roughness down around 10 to 15 Å surfaces and meet the requirement to produce a figure accuracy of better than  $\frac{1}{4}$  wavelength at HeNe over 90% of the full aperture.

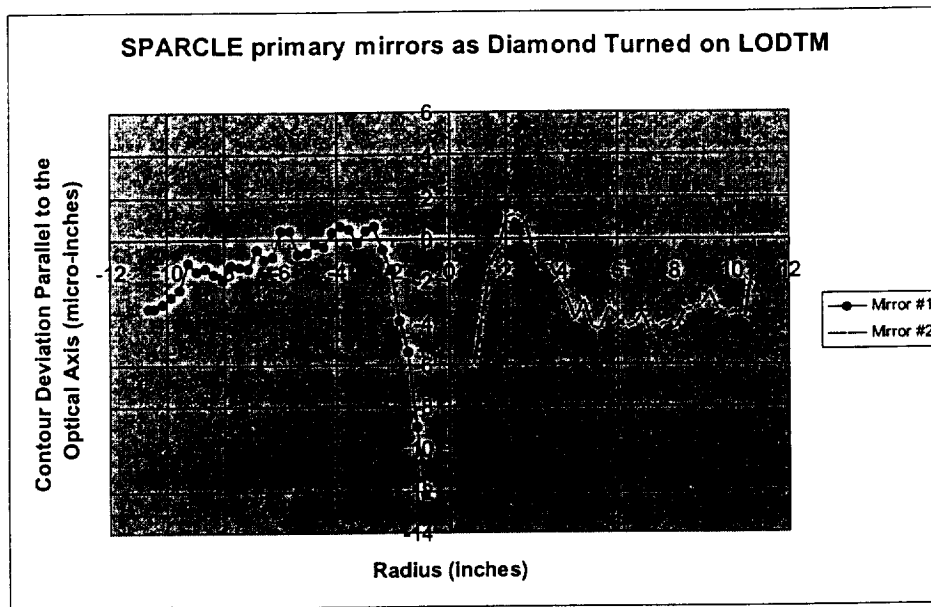


Table two. The SPARCLE primary mirror surface as turned on the LODTM

### POLISHING REQUIREMENTS

The polishing requirements are straightforward and are implemented primarily to reduce the RMS roughness from the 125 or so angstrom level down acceptable levels. The reason that it is desirable to have such small surface roughness is due to the fact that the return signal from atmospheric aerosols is extremely tenuous. Any amount of backscatter from the outgoing laser pulse off of the optical surfaces can be potentially damaging to the sensitive receiver detectors. The requirements for the primary mirror polishing are that the surface figure maintains at least 1/4 wave p-v at HeNe wavelength and that the RMS roughness be better than twenty angstroms. The polishing was achieved using zone polishing techniques where the principal thrust is to initially remove the rough diamond turning grooves, then concentrate on bringing the optic into figure. SORL was qualified to meet and actually exceed the requirements placed on the mirrors. The mirrors have been polished to 15 angstroms RMS roughness and the figure is 1/6 wave p-v at HeNe.

### Gold-Plating

Gold plating requirements are driven by the high reflectivity needed to receive weak signals from aerosols in the atmosphere. The primary mirror optical surface is polished and figured to the required wavefront, leaving optical throughput as the remaining factor to producing an optical system capable of meeting the needs of SPARCLE. The Nickel-plated 6061-T651 Aluminum mirror was gold plated using electrodeposition technologies producing 97% reflectivity at 700 nanometers wavelength and 98.5% reflectivity at 2060 nanometers.

The gold purity is maintained at 99.99% and plates onto the mirror with a knoop hardness of 180. Witness samples are provided with the mirrors for laboratory metrology and coating adhesion tests. The coating is performed by Epner Technology located in Brooklyn New York.

### SUMMARY

The technology issues that are involved in producing world class performance from rigorous requirements such as the optical prescription of the SPARCLE telescope are within the capability already existing in industry provided that the optical designer utilize the manufacturing choices available in industry. Rough machining of the blank material can be performed on standard computer controlled milling machines. Initial figuring of the optical surface is done on any diamond turning

machine, which can produce anywhere from 200 to 500 angstroms RMS roughness. The nickel-plated coating will cover the diamond tool groves with better adherence due to the increased plating area. The final diamond turning can be done with one of two objectives. One, which is the most desirable, is to diamond turn the optic such that the figure and roughness require no post polishing. However the precision required to produce such high quality directly off the diamond turning machine limits the choice of facility. When the option of post polishing is introduced, the need for the diamond turning facility to produce a finished product is relaxed somewhat in terms of RMS roughness and is relaxed as well for producing a figure that is cost prohibitive.

#### ACKNOLOGMENTS

This work was supported by NASA Marshall Space Flight Center through a cooperative agreement with The University of Alabama in Huntsville, at the Center for Applied Optics. The authors wish to acknowledge the support of Darrell Engelhaupt of UAH/CAO for providing his expertise in mirror material testing and the Nickel-plating process. We are also grateful to Roy Young of NASA/MSFC for his hard work as a quality assurance engineer and ensuring compliance under NASA's flight hardware quality standards.

#### REFERENCES

1. Feng, A. Ahmad and F. Amzajerdian, "Design and analysis of a spaceborne lidar telescope," Proc. SPIE Vol. 2540, pp. 68-77, 1995.
2. A. Ahmad, F. Amzajerdian, C. Feng and Y. Li, "Design and fabrication of a compact lidar telescope," Proc. SPIE Vol. 2832, pp. 34-42, 1996.
3. Li, Ye; Blackwell, Timothy S.; Geary, Joseph M.; Amzajerdian, Farzin; Spiers, Gary D.; Peters, Bruce R.; Chambers, Diana," Characterization of an optical subsystem for 2-um coherent lidars," Proc. SPIE Vol. 3479, p. 122-129.
4. Peters, Bruce R.; Blackwell, Timothy S.; Li, Ye; Geary, Joseph M.; Amzajerdian, Farzin; Bailey, Deborah, "Optomechanical design of a multi-axis stage for the SPARCLE telescope," Proc. SPIE Vol. 3429, p. 48-55.
5. F. Amzajerdian, G. D. Spiers, B. R. Peters, Y. Li, T. S. Blackwell, and J. M. Geary, " Design and Operational Characteristics of the Shuttle Coherent Wind Lidar," 19th International Laser Radar Conference, Annapolis, MD, July 6-10, 1998.
6. M. J. Kavaya, G.D. Emmitt, "The Space Readiness Coherent Lidar Experiment (SPARCLE) Space Shuttle Mission," Proc. SPIE Vol. 3380, Conference on Laser Radar Technology and application III, 12<sup>th</sup> Annual International Symposium on Aerospace/Defense Sensing, Simulation, and Controls, AeroSense, Orlando, FL, 1998.
7. A. Ahmad, C. Feng, F. Amzajerdian, Y. Li "Design and Fabrication of a Compact LIDAR Telescope", Proc. SPIE Vol. 2832, Denver, CO August 4-9, 1996.
8. P.J. Reardon, B.R. Peters, F. Amzajerdian, "Thermal Considerations for the SPARCLE Optical System," SPIE Proc. 3707, Orlando, FL., April 6-9, 1999.

## Metrology of optical beam expander for Space Readiness Coherent Lidar Experiment

**Timothy S. Blackwell and Farzin Amzajerdian**

*The University of Alabama in Huntsville  
Center for Applied Optics, Huntsville, Alabama 35899  
256-890-6030 tim.blackwell@msfc.nasa.gov*

**Thomas J. Kester**

*NASA Marshall Space Flight Center, Huntsville, Alabama 35812  
256-544-9204 thomas.kester@msfc.nasa.gov*

**Abstract:** Stringent requirements of this telescope demands testing of its individual elements through each step of fabrication and complete metrology of the integrated telescope both at Helium-Neon and the operational two micron wavelengths.

**Summary:** Performance requirements for the SPARCLE<sup>1</sup> telescope optical quality are driven by factors such as the coherent laser radar signal to noise limit, the thermal operating environment, and the survivability of vibrational launch loads. To meet the signal to noise requirements, the telescope must minimize optical aberrations in order to project the outgoing pulse from space through the troposphere with the best possible beam profile. Studies show that, although all aberrations reduce the lidar performance, small amounts,  $\frac{1}{2}$  wave, of spherical aberration will produce approximately 50% reduction in heterodyne efficiency<sup>2</sup>. In addition to the overall wavefront quality requirements, spatial polarization efficiency and optical transmission are of great concern due to the tenuous return signal from atmospheric aerosols. The thermal environment that the optical system will encounter during the course of a mission places specific demands on the mechanical support structure as well as the optical elements and beam steering elements. Although the telescope is designed to maintain its wavefront quality over a large static temperature range, it must also be capable of performing under thermal gradient conditions. Vibrational launch load survivability implies that the telescope be capable withstanding exposure to a broad band vibration spectrum without suffering plastic deformation resulting in misalignment. We will begin by presenting the optical design requirements with a system overview.

Figure 1 shows an expanded view of the complete telescope. The primary mirror and the secondary mirror reference surfaces seen here are for alignment of the relative tilts between the two elements.



Figure 1. Expanded telescope showing the opto-mechanical support structure.

The assembled telescope is designed as a compact 11x10x15 inch 25x afocal beam expander with a 23cm obscuration-free beam diameter. It is  $\lambda/4$  at 633nm peak-to-valley wavefront, and better than 90%

transmission at the operational wavelength of 2060 nm while maintaining its wavefront quality over the thermal operating range of 0.0C to +25.0C.

The primary mirror<sup>1</sup> mother parabola is f/0.6 with a 23cm diameter off axis section centered 187mm from the vertex. The secondary mirror is a convex paraboloid with a six-millimeter useable aperture having a full 32 millimeter physical aperture and a figure accuracy of  $\lambda/4$  at 633nm peak-to-valley and 99% reflectivity at 2060nm.

Table 1 shows some of the parameters of the assembled telescope and the environments for which it must operate or survive in.

### Telescope Requirements

Beam Expansion Ratio	25:1
Single Pass Wavefront Quality	1/15 <sup>th</sup> wave RMS at 2.0 micron over full clear aperture
Single Pass Optical Transmission	0.85 at 2.0 micron wavelength
Input Clear Aperture Diameter	0.92 centimeter
Output Clear Aperture Diameter	23.3 centimeter
Vibrational Integrity	launch survivability
Maximum Permitted Envelope	38 cm x 43 cm (diameter and height)
Survivability Temperature	-40°C to 60°C
Operating Temperature	0°C to 25°C
Maximum Operating Temperature Gradient	8°C over the operating temperature

Table 1. Telescope optical requirements

Optical performance and mechanical accuracy was monitored during each of the fabrication processes for both the primary mirror and the secondary mirror. Rough machining for each mirror was inspected to insure that the physical dimensioning was compliant with their respective design. The critical measurements made, using a coordinate measurement machine (CMM), were the base optical surface shape and the location and size of the alignment pins. Mounting pads located on the back of the primary mirror and the alignment reference surfaces on both of the mirrors involved continuous monitoring during fabrication to ensure exact optical registration to the mounting surfaces, although not all monitoring was done in-situ. Both of the mirrors were plated with electroless nickel and, after final diamond turning and post polishing, a thin film of gold was deposited on all of the mirrors.

The final primary mirror optical surface, both mirror reference-flat surfaces, and final mounting pad planarity were measured interferometrically using a large aperture ZYGO. Prior to gold plating, the finished optical surface of the secondary mirror was measured using a Talysurf long trace profilometer. RMS surface roughness was measured for both mirrors on a WYKO TOPO-3D. Since two primary mirrors and three secondary mirrors were manufactured, an air spaced assembly of the beam expander was built which allowed us to choose the best matching pair. This resulted in two beam expanders that exceed the operational wavefront requirements. Although a large fabrication database exists for the entire telescope, we will present only the optical metrology data that is relevant to the final product.

Currently, the SPARCLE telescope is undergoing cleaning of each of the individual components as well as all ground support equipment, and preparation for the final assembly process. This telescope is being assembled as flight qualified hardware and all aspects of assembly and qualification are monitored by MSFC quality control. Assembly is scheduled to be complete in the spring and vibrational and thermal testing is scheduled to be complete by early summer this year. Metrology data taken during these exercises will be presented.

The planned assembly requires that datum planes be transferred between the primary mirror, the secondary mirror, and the interface assemblies using the built in optical reference surfaces. Each mirror reference-plane optical surface figure is repeatedly measured during assembly to determine any resulting changes to

the optical performance due to the mountings. This all-reflective telescope design is to be assembled and measured interferometrically at 633nm. Spatial polarization transmission efficiency measurements will be made at the operational design wavelength of 2060nm. Both of the mirrors in the interface assemblies are tested for surface figure prior to and following mounting in their respective subassemblies. Spatial linear polarization efficiencies for 2060nm reflected light will be tested at 45 degrees incidence for each of the interface alignment mirror assemblies.

We will discuss metrology of the each element of the telescope as well as discuss metrology of the telescope during assembly and as a system. We will also discuss the thermal and vibration test results. Figure 2 shows the expected results for the flight telescope. The data is extracted from the air-spaced setup wherein we determined the best possible match of "as fabricated" primary and secondary mirrors. The data does not include performance of the beam steering optics. We see here that the wavefront quality is .426 waves peak-to-valley at the operating wavelength of 2060nm.

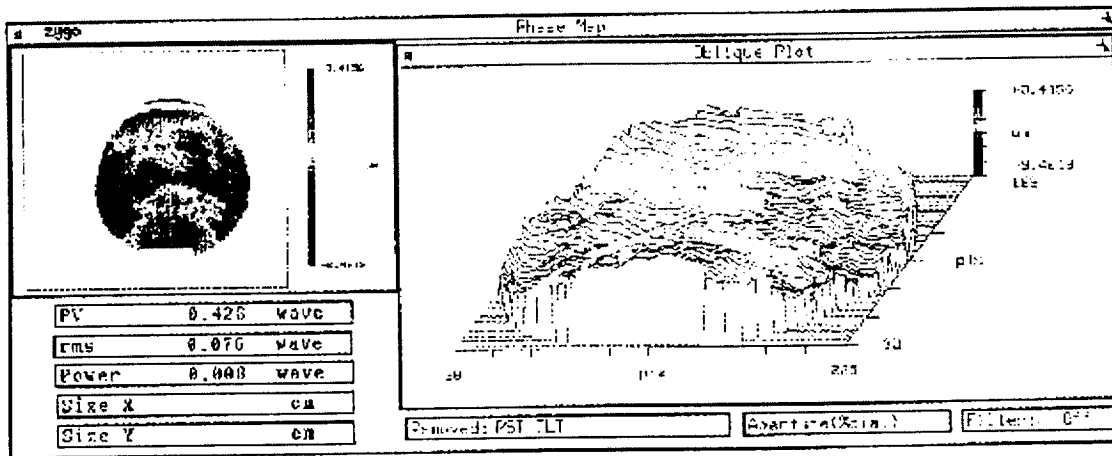


Figure 2. Expected performance of the SPARCLE telescope based on interferometer data taken on preliminary assembly tests.

#### References:

<sup>1</sup>Space Readiness Coherent Lidar Experiment (SPARCLE) mission and science Requirements document MSFC-RQMT-2828 NASA Marshall Space Flight Center, 1998

<sup>2</sup>Gary D. Spiers, *The effect of optical aberrations on the performance of a coherent Doppler lidar*. Proceedings of the Tenth Biennial Coherent Laser Radar Technology and Applications Conference, 1999.

<sup>3</sup>Tim Blackwell et al. *Primary Mirror Manufacturing Considerations for a Space-based Coherent Lidar*. Proc.SPIE Vol. 3757, p.40-47.

## Construction and Space-qualification of a Lidar Telescope

Farzin Amzajerian, Timothy S. Blackwell, Bruce R. Peters, Patrick Reardon

*The University of Alabama in Huntsville, Center for Applied Optics, Huntsville, AL 35899, USA*

Roy Young

*NASA Marshall Space Flight Center, Space Optics Manufacturing Technology Center, Huntsville, AL 35812 USA*

### ABSTRACT

Demanding physical and environmental constraints combined with demand for high optical quality create many challenges in designing, fabricating, and testing a space-based lidar telescope. These challenges are further exaggerated for coherent lidars because of their sensitivity to projected transmitted beam profile at the target plane and aberrations in the return signal phase front. This paper reports the development of a telescope system for the SPACe Readiness Coherent Lidar Experiment (SPARCLE), and discusses its space-qualification testing methodology and results.

### Introduction

Presently, several lidar systems are either being developed or being considered for deployment in space for remote sensing of the earth atmosphere and surface. Any space-based lidar instrument needs to be mechanically rugged and thermally stable to maintain its optical alignment through violent launch vibrations and during operation in the harsh thermal environment of space. These constraints present the designers with a challenging task given the mass and volume restrictions imposed by the launch vehicle and the orbiting spacecraft. The lidar telescope in particular deserves careful consideration, since it is one of the dominating component in establishing the instrument sensitivity and at the same time one of the most alignment sensitive components that consumes a major portion of the total mass and volume budgets. The criticality of the telescope is even more drastic for solid state coherent lidars operating in near infrared wavelength region. In addition to high optical throughput and polarization efficiency required by most lidar systems, solid state coherent lidars require a very high wavefront quality as well. This paper reports the development of a lidar telescope for the SPACe Readiness Coherent Lidar Experiment (SPARCLE). SPARCLE was intended to be the first demonstration of a coherent Doppler wind lidar in space<sup>1</sup>. The development of the lidar telescope for SPARCLE has provided a wealth of experience for design, fabrication, and test of telescopes for future lidar space missions.

### Lidar Telescope Description

The telescope consists of two off-axis parabolic mirrors in a Mersenne configuration as shown in figure 1. The off-axis configuration eliminates any central obscuration, which will degrade beam quality due to diffraction effects. This configuration also reduces direct backscattering into the lidar system receiver optical path. The size and mass constraints for any space-based coherent lidar dictate that the system be considerably more compact than conventional configurations. This telescope fits within an envelope of dimensions 38X32X33 cm and weighs about 20 kg. To achieve such a compact package, a fast optical design was employed which led to very tight fabrication and alignment tolerances<sup>2</sup>. The telescope is designed to have a full field of view of 80 micro-radians, an angular magnification of 25x, and a primary mirror aperture of 25 cm. The optical spacing between the primary and secondary mirror is 22.5 cm de-centered by 15 cm.

To maintain the critical relative alignment between the primary and secondary mirrors over a relatively large operational temperature range and eliminate any misalignment due to differential thermal



expansion, the telescope mirrors and its support structure are all made of the same type of aluminum material. Thus, this telescope system is athermal since the changes in the optical properties of the mirrors (radius of curvature, thickness, etc.) with temperature are perfectly balanced by the expansion or contraction of the structural supports such that the system maintains its alignment.

The telescope mirrors incorporate a number of alignment surfaces and precision pinholes for ease of alignment and integration with the lidar transceiver (Figure 2). The primary mirror has a 7.0mm wide reference surface on the edge of its optical surface and three mounting pads, with optical-grade surfaces, on its back side. All four of the primary's reference surfaces are diamond turned to be parallel to each other and perpendicular to the virtual axis of the mirror's parabola. The combination of these reference surfaces and two precision pinholes establish the exact position and direction of the parabola's axis. The secondary mirror also has reference flat surfaces on the front and back. The primary mirror and the secondary support posts are mounted to an optical baseplate. The top surface of the optical baseplate is diamond turned to generate a large flat optical surface to serve as a datum plane and to further reduce any distortion that can result from attaching the primary mirror and the secondary mirror support posts to the baseplate. The backside of the optical baseplate also has three flat and parallel pads for mounting to the lidar transceiver without distorting the telescope alignment. Location and alignment of the transceiver beam to the telescope is achieved through two mirror tip-tilt-stages and a linear stage on one mirror that together deliver stages 5 degrees of freedom.

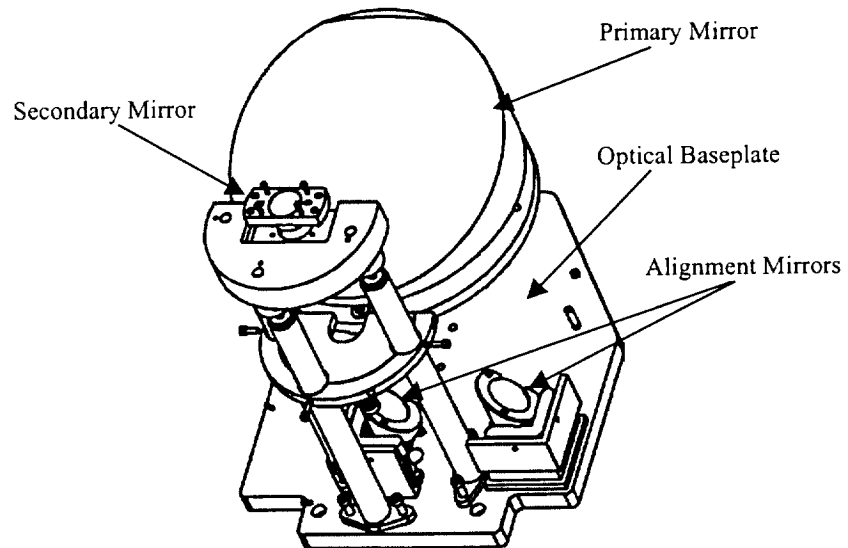


Figure 1. SPARCLE Transmitter/Receiver Telescope.

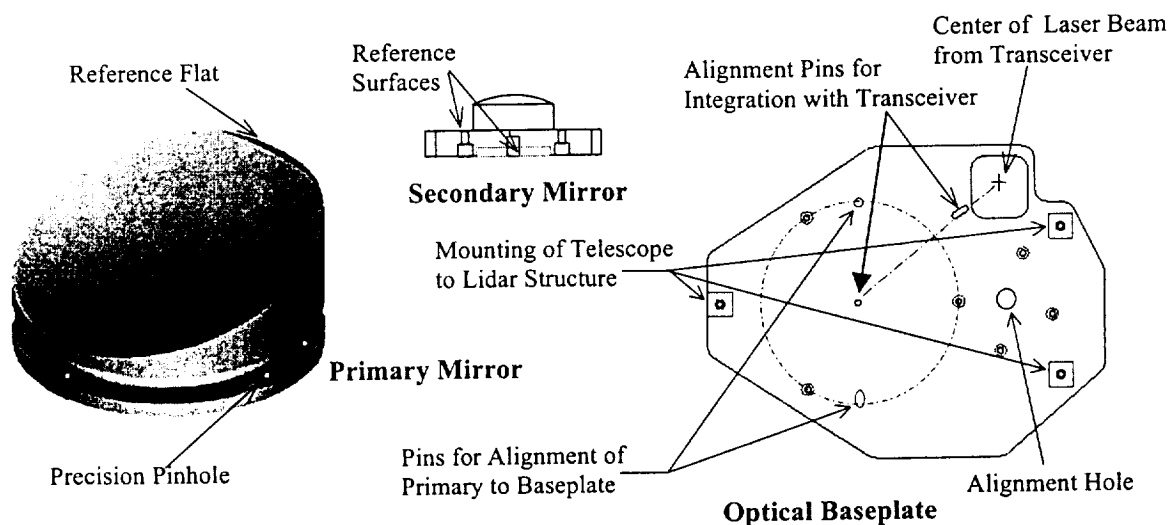


Figure 2. Alignment and reference surfaces of Lidar Telescope Components.

### **Fabrication**

The required wavefront quality necessary for efficient coherent detection necessitated a high level of surface figure accuracy on the mirrors. Selection of aluminum for the mirror base material coupled with the aspheric surface geometry of the mirrors and the required surface figure accuracy dictated the use of high precision single point diamond turning fabrication techniques. However, the level of surface roughness that can be obtained from a diamond turned surface is too high for coherent lidar application that requires a very low scattering and back reflection by the optics. To achieve the required surface roughness, the mirrors were plated by a thin layer of nickel, before finish diamond machining, and then polished to reduce the diamond-turning grooves.

The following summarizes the fabrication process of mirrors that involved several organizations including NASA/Marshall Space Flight Center (MSFC), Lawrence Livermore National Laboratories (LLNL), and the University of Alabama in Huntsville/Center for Applied Optics(UAH/CAO). The mirrors were first rough machined to right dimensions and then stress-relieved along with all the diamond turning fixtures. The mirrors were then diamond turned to generate the optical surfaces to a figure accuracy of about one micron. Next, the mirrors were nickel-plated using an electroless plating technique. The nickel plating of the primary mirror was performed at the NASA/MSFC and the secondary mirror was plated at Speedring, Inc. At this stage the mirrors were prepared for the finish diamond turning. The finish diamond turning of the primary mirror was performed on the Large Optics Diamond Turning Machine (LODTM), at Lawrence Livermore National Laboratories, and the secondary mirror was diamond turned at the NASA/MSFC and the UAH/CAO facilities. The primary mirror was post-polished by Space Optics Research Labs (SORL) using a zone-polishing technique. The diamond turned secondary mirror, due to its small size and symmetric shape, turned out to have a sufficiently small surface roughness, requiring no post-polishing. The mirrors were then coated by a high purity alloy of gold, with a high reflectivity and durability, using a unique process developed by Epner Technologies. Gold-plating increased the surface reflectivity at 2-micron wavelength to more than 98% for a circular polarized beam. The final surface figure accuracy and roughness of the mirrors were measured to be 0.1 micron peak-to-valley and 20 angstroms RMS, respectively.

The mirrors were thermally treated several times over the course of fabrication process to enhance their long-term stability and ensure the desired performance in the thermal environment of space. The internal stresses in the mirror material were released following the rough machining by performing a boiling water-liquid nitrogen treatment. In addition, the mirrors were stabilized by thermally cycling them several times before and after nickel-plating. The last phase of thermal treatment was performed over the specified telescope survivability temperature of -40C to 60C to minimize the risk of any misalignment due to temperature variations on orbit.

### **Assembly and Alignment**

The telescope is currently being assembled under formal NASA space flight hardware quality control. All the telescope components along with all the assembly and alignment fixtures and equipment have been fabricated, tested, and cleaned in compliance with the relevant space quality assurance requirements. The telescope assembly requires that the datum planes be transferred between the primary mirror, the secondary mirror, and the interface assemblies, using the built in optical reference surfaces. This is achieved by a commercial phase-shift interferometer. Each reference surface plane is repeatedly measured during assembly to determine any resulting changes to the optical performance due to the mountings. Operating at 633 nm wavelength, the interferometer allows the alignment of the telescope components to specified tolerances. The telescope need to be aligned and remain aligned in orbit to the following general tolerances:

Mirrors spacing	4.2 $\mu\text{m}$
De-center	5.5 $\mu\text{m}$
Tilt	23 $\mu\text{rad}$

### **Performance and Environmental Testing**

The performance of the telescope will be measured at both 633 nm and 2060 nm wavelengths. The all-reflective design of the telescope allows the use of a commercial interferometer for measuring its wavefront quality. The wavefront quality measurements provide the Zernike coefficients, which define all the contributing low spatial-order aberrations introduced by imperfect fabrication and alignment. The wavefront quality measurements will be repeated at different temperatures from less than 0 to greater than 30 degrees centigrade to demonstrate the telescope performance over its anticipated on-orbit temperature range of 0-25 degrees C. The Zernike coefficients from these measurements will be fed into a variety of computer models for further analyses of the telescope's anticipated behavior in the space environment. The computer models utilized will include the ASAP (Advanced System Analysis Program) optical analysis code to simulate the thermal and vibrational environments of the space for quantifying the impact of the temperature gradients and vibrations present within the instrument canister. Capability of the telescope in withstanding vibrational launch loads will be demonstrated by measuring the telescope wavefront quality before and after exposing it to a series of vibration spectrums. The wavefront quality measurements will be used in the ASAP model to quantify any plastic deformation, which may result from vibrating the telescope, and the resultant misalignment.

In addition to interferometric measurements, the telescope transmission and polarization efficiencies will be measured at the operational wavelength of 2060nm. The measurement setup, using a single-frequency, CW, Tm, Ho:YLF laser, has been developed for quantifying the telescope optical throughput and its polarization states.

Based on the component-level measurements, the telescope is expected to perform to about 1/20 wave RMS at 2-micron in laboratory environment and about 1/15 wave at worse-case thermal scenarios in space. The transmission and polarization efficiencies of the telescope are expected to be about 96% and 95%, respectively.

### **Summary**

Manufacturing transmit/receive telescopes for any space-based lidar instrument require careful consideration of all the competing performance, physical, and environmental requirements. The telescope design, fabrication, integration, and testing are particularly challenging for a coherent lidar instrument because of its sensitivity to the telescope alignment and wavefront quality. The development of SPARCLE telescope provided a valuable opportunity in understanding and addressing the issues associated with a space-based lidar telescope and establishing a process for its space-qualification. SPARCLE telescope has a very good wavefront quality and is capable of operating over a relatively large temperature range while tolerating the presence of considerable temperature gradients across its support structure and primary mirror. This paper describes the unique features of the SPARCLE telescope design, its fabrication methodology, and its performance and space-qualification tests. A number of optical and mechanical models have been developed for specifying the SPARCLE telescope fabrication and alignment tolerances, validating its design in withstanding the vibrational launch loads and operating over the anticipated temperature range. These analytical tools will be also used for analyzing the results of the performance and environmental tests and predicating the telescope performance in orbit.

### **References**

1. M.J. Kavaya, G.D. Emmitt, "The Space Readiness Coherent Lidar Experiment (SPARCLE) Space Shuttle Mission," Proc. SPIE Vol. 3380, p. 2-11, 1998.
2. Y. Li, F. Amzajerdian, B. R. Peters, T. S. Blackwell, and P. Reardon, "Optical Design and Analyses of SPARCLE Telescope," 10<sup>th</sup> Coherent Laser Radar Conference, June 28-July2, 1999, Mount Hood, OR, USA.

## Construction and Space-qualification of a Lidar Telescope

Farzin Amzajerian, Timothy S. Blackwell, Bruce R. Peters, Patrick Reardon

*The University of Alabama in Huntsville, Center for Applied Optics, Huntsville, AL 35899, USA*

Roy Young

*NASA Marshall Space Flight Center, Space Optics Manufacturing Technology Center, Huntsville, AL 35812 USA*

### ABSTRACT

Demanding physical and environmental constraints combined with demand for high optical quality create many challenges in designing, fabricating, and testing a space-based lidar telescope. These challenges are further exaggerated for coherent lidars because of their sensitivity to projected transmitted beam profile at the target plane and aberrations in the return signal phase front. This paper reports the development of a telescope system for the SPACe Readiness Coherent Lidar Experiment (SPARCLE), and discusses its space-qualification testing methodology and results.

# Fabrication, metrology and modeling of the space-based lidar telescope for SPARCLE

B. R. Peters,\* P. J. Reardon, F. Amzajerdian, T. S. Blackwell

Center for Applied Optics  
The University of Alabama in Huntsville  
Huntsville, Alabama 35899

## ABSTRACT

Over the past 7 years, NASA Marshall Space Flight Center (MSFC) through the Global Hydrology and Climate Center (GHCC) has been working; in collaboration with the University of Alabama in Huntsville (UAH) Center for Applied Optics (CAO), and others; towards demonstrating a solid state coherent Doppler lidar instrument for space-based global measurement of atmospheric winds. The Space Readiness Coherent Lidar Experiment (SPARCLE) was selected by NASA's New Millennium Program to demonstrate the feasibility and technology readiness of space-based coherent wind lidar. The CAO was responsible for the design, development, integration, and testing of the SPARCLE optical system. Operating at 2-micron wavelength, SPARCLE system performance is dominated by the optical quality of the transmitter/receiver optical system. The stringent optical performance requirements coupled with the demanding physical and environmental constraints of a space-based instrument necessitate extensive characterization of the telescope optical performance that is critical to predicting the lidar system efficiency and operation in space. Individual components have been measured prior to assembly and compared to the designed specifications. Based on the individual components, the telescope design was optimized to produce a suitable telescope. Once the telescope is completed, it will be tested and evaluated and the data shall be used to anchor computer based models of the optical system. Commercial optical modeling codes were used to evaluate the performance of the telescope under a variety of anticipated on-orbit environments and will eventually be compared to environmental tests conducted in the course of qualifying the telescope for flight. Detailed analysis using the "as built" data will help to reduce uncertainties within the lidar system model and will increase the accuracy of the lidar performance predictions.

**Keywords:** lidar, telescope, optical design, optical modeling, optical testing

## 3. INTRODUCTION

It is the stated goal of NASA's Earth Science Enterprise (ESE) to exploit the unique perspective of space-based remote optical instruments to observe and study large-scale environmental processes. The recent paradigm shift of ESE space flight programs has been away from missions that rely on large, expensive custom spacecraft with single instruments; and towards missions that are smaller, flexible, and more affordable yet while still accomplishing the science goals. In order to fit within the new requirements, the remote sensing instruments onboard must find innovative ways to reduce the size, weight, and power requirements of the sensor package along with realizing substantial reductions in cost.

As outlined in the NASA *Mission To Planet Earth: Capability/Technology Needs Assessment and Investment Plan*, several current optical instruments have a need for a meter-class telescope to support the study of land cover, atmospheric circulation, natural hazards, and lower tropospheric chemistry. Although the instruments proposed to study these science themes are different, they share a common unfulfilled technology need. Coherent Doppler lidar for vector wind measurement,<sup>1</sup> differential absorption lidar (DIAL) for atmospheric monitoring,<sup>2</sup> and Fourier transform infrared (FTIR) spectrometer to monitor concentration of gasses within the atmosphere<sup>3</sup> all incorporate a lightweight meter-class telescope within the instrument. The high quality telescope envisioned for each of these instruments has a 0.5-1.2 meter diameter primary mirror; with general performance parameters on the order of  $\lambda/10$  minimum wave front quality across the whole aperture; alignment stability over temperatures from  $-40^{\circ}$  to  $60^{\circ}\text{C}$ ; and overall optical system weights of  $15\text{ kg/m}^2$  of collection aperture.

---

\* Further corresponding author information -

Dr. Bruce R. Peters: Email: [petersb@email.uah.edu](mailto:petersb@email.uah.edu); WWW: <http://www.uah.edu/cao/>;  
Tel: 256-824-2526; Fax: 256-824-6618.



optical properties of the mirrors (radius of curvature, thickness, etc.) with temperature are perfectly balanced by the expansion or contraction of the structural supports such that the system maintains its alignment.

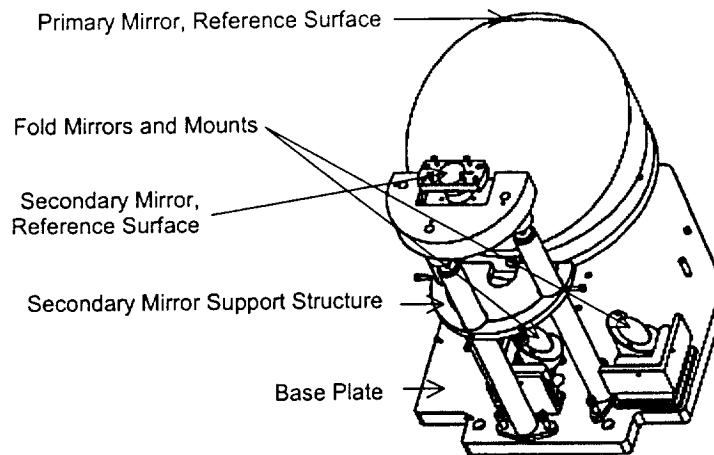


**Figure 1c. SPARCLE optomechanical design.**

The telescope mirrors incorporate a number of alignment surfaces and precision pinholes for ease of alignment and integration with the lidar transceiver. The primary mirror has a 7.0-mm wide reference surface on the edge of its optical surface and three mounting pads, with optical-grade surfaces, on its back side. All four of the primary's reference surfaces are diamond turned to be parallel to each other and perpendicular to the virtual axis of the mirror's parabola. The combination of these reference surfaces and two precision pinholes establish the exact position and direction of the parabola's axis. The secondary mirror also has reference flat surfaces on the front and back. The primary mirror and the secondary support posts are mounted to an optical baseplate. The top surface of the optical baseplate is diamond turned to generate a large flat optical surface to serve as a datum plane and to further reduce any distortion that can result from attaching the primary mirror and the secondary mirror support posts to the baseplate. The backside of the optical baseplate also has three flat and parallel pads for mounting to the lidar transceiver without distorting the telescope alignment. Location and alignment of the transceiver beam to the telescope is achieved through two mirror tip-tilt-stages and a linear stage on one mirror that together deliver 5 degrees of freedom.

#### Allowed Positional Errors

Mirrors spacing	4.2 $\mu\text{m}$
De-center	5.5 $\mu\text{m}$
Tilt	23 $\mu\text{rad}$

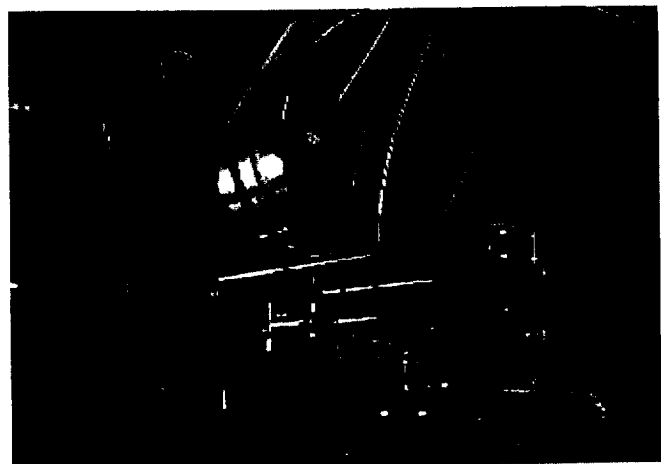
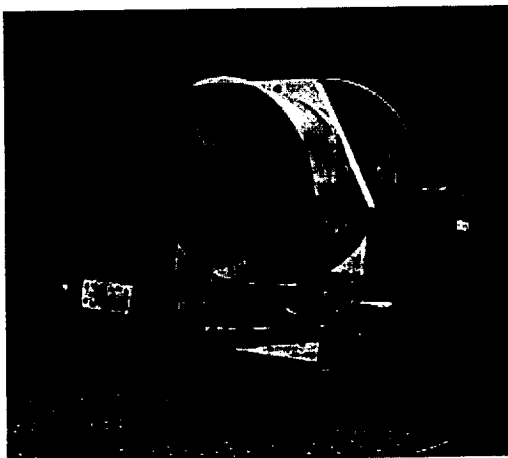


**Figure 2. Assembled engineering model of the SPARCLE telescope.**

The assembled engineering model of the SPARCLE telescope is shown in Figure 2. The telescope is shown mounted to a tip and tilt stage that is not part of the telescope and is only intended to facilitate optical testing.

### 3. FABRICATION AND COMPONENT PERFORMANCE

The required wavefront quality necessary for efficient coherent detection necessitated a high level of surface figure accuracy on the mirrors. Selection of aluminum for the mirror base material coupled with the aspheric surface geometry of the mirrors and the required surface figure accuracy dictated the use of high precision single point diamond turning fabrication techniques. However, the level of surface roughness that can be obtained from a diamond turned surface is too high for coherent lidar application that requires a very low scattering and back reflection by the optics. To achieve the required surface roughness, the mirrors were plated by a thin layer of nickel, before finish diamond machining, and then polished to reduce the diamond-turning grooves.

The following summarizes the fabrication process of mirrors that involved several organizations including NASA/Marshall Space Flight Center (MSFC), Lawrence Livermore National Laboratories (LLNL), and the University of Alabama in Huntsville/Center for Applied Optics(UAH/CAO). The mirrors were first rough machined to right dimensions and then stress-relieved along with all the diamond turning fixtures. The mirrors were then diamond turned to generate the optical surfaces to a figure accuracy of about one micron. Next, the mirrors were nickel-plated using an electroless plating technique. The nickel plating of the primary mirror was performed at the NASA/MSFC and the secondary mirror was plated at Speedring, Inc. At this stage the mirrors were prepared for the finish diamond turning. The finish diamond turning of the primary mirror was performed on the Large Optics Diamond Turning Machine (LODTM), at Lawrence Livermore National Laboratories, and the secondary mirror was diamond turned at the NASA/MSFC and the UAH/CAO facilities. The primary mirror was post-polished by Space Optics Research Labs (SORL) using a zone-polishing technique. The diamond turned secondary mirror, due to its small size and symmetric shape, turned out to have a sufficiently small surface roughness, requiring no post-polishing. The mirrors were then coated by a high purity alloy of gold, with a high reflectivity and durability, using a unique process developed by Epner Technologies Inc.<sup>6</sup> Gold-plating increased the surface reflectivity at 2-micron wavelength to more than 98% for a circular polarized beam. The final surface figure accuracy and roughness of the mirrors were measured to be 0.1 micron peak-to-valley and 20 angstroms RMS, respectively.

An additional facet of the system performance is the magnitude of polarizance induced by the telescope on the transmitted and collected light. The Epner Gold plating was ellipsometrically tested by J.A. Woollam<sup>7</sup> and found to contribute from 0.04 to 2.41 degrees of retardance and from essentially 0% to less than 0.4% diattenuation across the pupil. Thus, incident circularly polarized light exits the telescope as essentially unaffected circularly polarized light, as computed in Synopsys.<sup>8</sup>

The mirrors were thermally treated several times over the course of fabrication process to enhance their long-term stability and ensure the desired performance in the thermal environment of space. The internal stresses in the mirror material were released following the rough machining by performing a boiling water-liquid nitrogen treatment. In addition, the mirrors were stabilized by thermally cycling them several times before and after nickel-plating. The last phase of thermal treatment was performed over the specified telescope survivability temperature of -40C to 60C to minimize the risk of any misalignment due to temperature variations on orbit.

### 4. SYSTEM PERFORMANCE

The performance of the telescope will be measured at both 633 nm and 2060 nm wavelengths. The all-reflective design of the telescope allows the use of a commercial interferometer for measuring its wavefront quality. The wavefront quality measurements provide the Zernike coefficients, which define all the contributing low spatial-order aberrations introduced by imperfect fabrication and alignment. The Zernike coefficients from these measurements have been fed into a variety of computer models for further analyses of the telescope's anticipated behavior in the space environment. The computer models utilized include ASAP (Advanced System Analysis Program) optical analysis code<sup>9</sup> to simulate the thermal and vibrational environments of the space for quantifying the impact of the temperature gradients and vibrations present within the instrument canister (Figure 3).

A series of interferometric measurements of the assembled telescope were taken (Figure 4). Since the telescope is oriented in a horizontal position, measurements were taken with the secondary assembly oriented at the top, right, bottom and left side to allow for the subtraction of gravity induced distortions and bending. Based on this series of measurements, the telescope is



expected to perform to about 1/20 wave RMS at 2-micron in laboratory environment and about 1/15 wave at worse-case thermal scenarios in space.

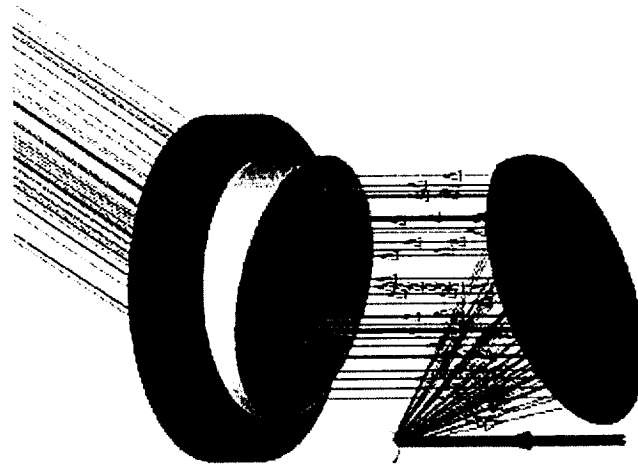


Figure 3. ASAP model of SPARCLE telescope.

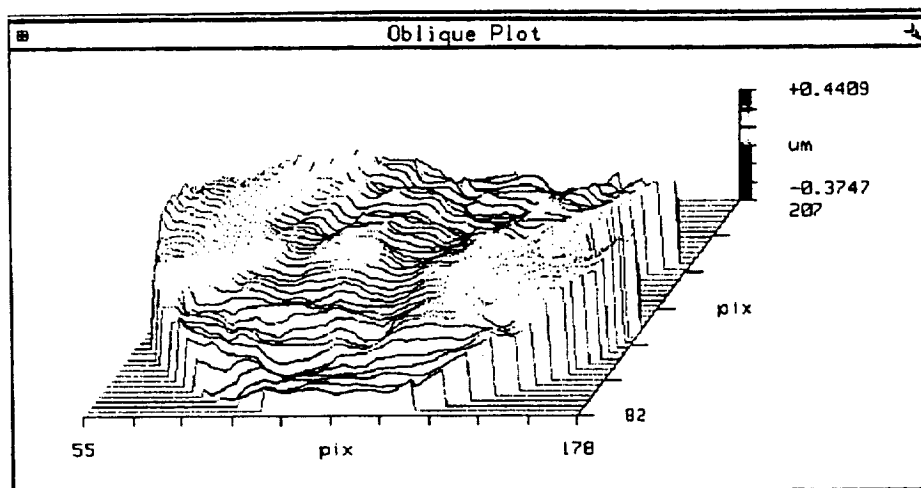


Figure 4. Interferometric measurements.

## 5. ENVIRONMENTAL TESTING

To meet space-qualified requirements, the SPARCLE telescope must undergo both thermal and vibration testing. Both tests are performed at NASA/MSFC with wavefront quality as the final merit function. In this section, we briefly discuss the setups (Figure 5) and current results for the testing of the first engineering model telescope. The testing is ongoing and the results presented here are preliminary in nature.

The telescope thermal tests were performed over its specified operational and survivability temperature ranges of 0 to 25 deg. C and -40 to 60 deg. C, respectively. For the operational thermal test, the telescope was cycled five times over the operational temperature range plus 5 degrees margin at both extremes, and twice from -10 deg. C to +35 deg. C. The telescope performance was continuously monitored by a phase-shift interferometer and its wavefront quality was recorded at 10 degrees intervals. The telescope maintained its alignment well over the whole measurement range. The wavefront quality changes

from -10 deg. C to +35 deg C were less than 0.02 rms wave at 2.05 microns. The telescope was then cycled four times over its survivability temperature range and its wavefront quality was measured displaying no change in its performance.

The telescope is currently being tested for survivability through launch loads. A sine sweep at 1/4g from 5 to 2000 Hz has already been applied in each of the telescope axes to determine its natural frequency. The natural frequency of the telescope was measured to be about 240 Hz along its optical axis (Z-axis) and 140 Hz in X and Y axes that are well beyond the 100 Hz design goal. The telescope is currently being prepared for a random vibration test at space shuttle qualification levels. The telescope will be vibrated along each of its orthogonal axes with a random spectrum having a composite load of 7.0g rms from 20 to 2000 Hz.

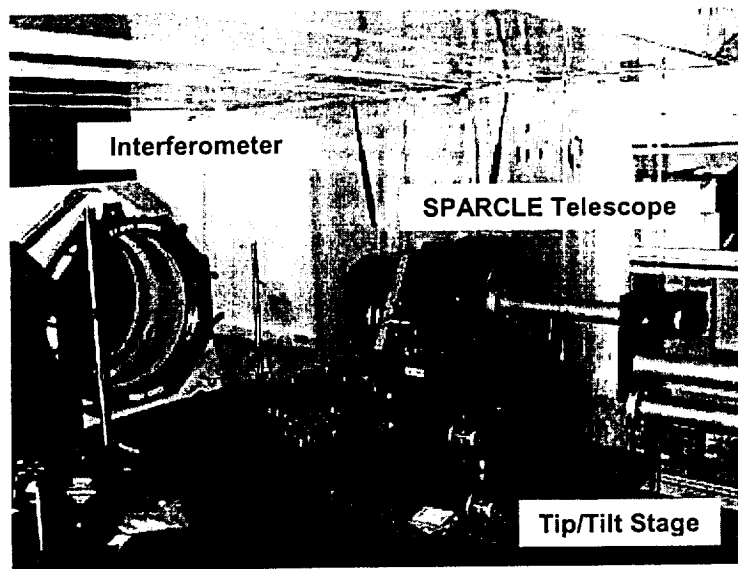


Figure 5. SPARCLE telescope under test.

## 6. CONCLUSION

The manufacturing of the SPARCLE telescope required careful consideration of all the competing performance, physical, and environmental requirements. Its design, fabrication, integration, and testing are particularly challenging for a coherent lidar instrument because of its sensitivity to wavefront quality. The development of SPARCLE telescope provided a valuable opportunity in understanding, baselining, and addressing the issues associated with a space-based lidar telescope and establishing a process for its space-qualification. The engineering model SPARCLE telescope has good wavefront quality and is capable of operating over a relatively large temperature range while tolerating the presence of considerable temperature gradients across its support structure and primary mirror. A number of optical and mechanical models have been developed for specifying the SPARCLE telescope fabrication and alignment tolerances, validating its design in withstanding the vibrational launch loads and operating over the anticipated temperature range. These analytical tools will be further adjusted for analyzing the results of the performance and environmental tests and predicating the telescope performance in orbit.

## 7. ACKNOWLEDGEMENT

This work was supported by NASA Marshall Space Flight Center Global Hydrology and Climate Center through a Cooperative Agreement with The University of Alabama in Huntsville at The Center for Applied Optics.

## 8. REFERENCES

1. M. J. Kavaya, G. D. Spiers, E. S. Lobl, J. Rothermel, and V. W. Keller, "Direct global measurements of tropospheric winds employing a simplified coherent laser radar using fully scalable technology and technique," *Proc. SPIE Vol. 2214, Space Instrumentation and Dual-Use Technologies*, 2214-31, Apr. 6, 1994.
2. H. Edner, K. Fredriksson, A. Sunesson, S. Svanberg, L. Uneus, and W. Wendt, "Mobile remote sensing system for atmospheric monitoring," *Appl. Opt.* 26, 4330-4338 (1987).

3. C. Camy-Peyret, "Ballon-borne infrared Fourier transform spectroscopy for measurement of atmospheric trace species," *Spectr. Acta* **51A**, 1143-1152 (1985).
4. M.J. Kavaya and G.D. Emmitt, "The space readiness coherent lidar experiment (SPARCLE) space shuttle mission," Proc. of the SPIE Laser Radar Technology and Applications III Conference, Vol. 3380 (1998).
5. Y. Li, F. Amzajerdian, B. R. Peters, T. S. Blackwell, and P. Reardon, Optical Design and Analyses of SPARCLE Telescope, 10th Coherent Laser Radar Conference, June 28-July2, 1999, Mount Hood, OR, USA.
6. Herbert Kaplan (Contributing Editor), "Gold Rules the World of Infrared," *Photonics Spectra*, November 1997.
7. J.A. Woollam Co., Inc., Lincoln, NE
8. Synopsys, Optical Systems Design, Inc., East Boothbay, ME
9. ASAP, Breault Research Organization, Inc., Tucson, Arizona.

1. <sup>1</sup> M. J. Kavaya, G. D. Spiers, E. S. Lobl, J. Rothermel, and V. W. Keller, "Direct global measurements of tropospheric winds employing a simplified coherent laser radar using fully scalable technology and technique," Proc. SPIE Vol. 2214, Space Instrumentation and Dual-Use Technologies, 2214-31, Apr. 6, 1994.
2. <sup>2</sup> H. Edner, K. Fredriksson, A. Sunesson, S. Svanberg, L. Uneus, and W. Wendt, "Mobile remote sensing system for atmospheric monitoring," *Appl. Opt.* **26**, 4330-4338 (1987).
3. <sup>3</sup> C. Camy-Peyret, "Ballon-borne infrared Fourier transform spectroscopy for measurement of atmospheric trace species," *Spectr. Acta* **51A**, 1143-1152 (1985).
4. M.J. Kavaya and G.D. Emmitt, "The space readiness coherent lidar experiment (SPARCLE) space shuttle mission," Proc. of the SPIE Laser Radar Technology and Applications III Conference, Vol. 3380 (1998).
- 5 Y. Li, F. Amzajerian, B. R. Peters, T. S. Blackwell, and P. Reardon, Optical Design and Analyses of SPARCLE Telescope, 10th Coherent Laser Radar Conference, June 28-July2, 1999, Mount Hood, OR, USA.
- <sup>6</sup> Herbert Kaplan (Contributing Editor), "Gold Rules the World of Infrared," *Photonics Spectra*, November 1997.

by Herbert Kaplan  
Contributing Editor

<sup>7</sup> J.A. Woollam Co., Inc., Lincoln, NE

<sup>8</sup> Synopsys, Optical Systems Design, Inc., East Boothbay, ME

<sup>9</sup> ASAP, Breault Research Organization, Inc., Tucson, Arizona.